05-4506832 pustaka.upsi.edu.my Perpustakaan Tuanku Bainun Kampus Sultan Abdul Jalil Shah PustakaTBainun ptbupsi

INCORPORATION OF Fe AND gC_3N_4 INTO MESOPOROUS TITANIA NANOPARTICLES FOR PHOTODEGRADATION OF DIBENZOTHIOPHENE

NURUL ADILAH BINTI MOHD NOOR

05-4506832 pustaka.upsi.edu.my Perpustakaan Tuanku Bainun Kampus Sultan Abdul Jalil Shah PustakaTBainun ptbupsi

UNIVERSITI PENDIDIKAN SULTAN IDRIS

2024

05-4506832 pustaka.upsi.edu.my Perpustakaan Tuanku Bainun Kampus Sultan Abdul Jalil Shah PustakaTBainun ptbupsi

05-4506832 pustaka.upsi.edu.my Perpustakaan Tuanku Bainun Kampus Sultan Abdul Jalil Shah PustakaTBainun ptbupsi

INCORPORATION OF Fe AND gC_3N_4 INTO MESOPOROUS TITANIA NANOPARTICLES FOR PHOTODEGRADATION OF DIBENZOTHIOPHENE

NURUL ADILAH BINTI MOHD NOOR

05-4506832 pustaka.upsi.edu.my Perpustakaan Tuanku Bainun Kampus Sultan Abdul Jalil Shah PustakaTBainun ptbupsi

DISSERTATION PRESENTED TO QUALIFY FOR A
MASTERS IN SCIENCE
(RESEARCH MODE)

FACULTY OF SCIENCE AND MATHEMATICS
UNIVERSITI PENDIDIKAN SULTAN IDRIS

2024

05-4506832 pustaka.upsi.edu.my Perpustakaan Tuanku Bainun Kampus Sultan Abdul Jalil Shah PustakaTBainun ptbupsi

05-4506832 pustaka.upsi.edu.my Perpustakaan Tuanku Bainun Kampus Sultan Abdul Jalil Shah PustakaTBainun ptbupsi

UNIVERSITI PENDIDIKAN SULTAN IDRIS
SULTAN IDRIS EDUCATION UNIVERSITY

Please tick (√)

Project Paper	
Masters by Research	/
Master by Mixed Mode	
PhD	

INSTITUTE OF GRADUATE STUDIES

DECLARATION OF ORIGINAL WORK

This declaration is made on the ....1....day of....JULY....20....24....

i. Student's Declaration:

I, NURUL ADILAH BINTI MOHD NOOR, M20182002270, FACULTY OF SCIENCE AND MATHEMATICS (PLEASE INDICATE STUDENT'S NAME, MATRIC NO. AND FACULTY) hereby declare that the work entitled INCORPORATION OF Fe AND gC3N4 INTO MESOPOROUS TITANIA NANOPARTICLES FOR PHOTODEGRADATION OF DIBENZOTHIOPHENE is my original work. I have not copied from any other students' work or from any other sources except where due reference or acknowledgement is made explicitly in the text, nor has any part been written for me by another person.

Signature of the student

ii. Supervisor's Declaration:

I DR. SITI MUNIRAH BINTI SIDIK (SUPERVISOR'S NAME) hereby certifies that the work entitled INCORPORATION OF Fe AND gC3N4 INTO MESOPOROUS TITANIA NANOPARTICLES FOR PHOTODEGRADATION OF DIBENZOTHIOPHENE (TITLE) was prepared by the above named student, and was submitted to the Institute of Graduate Studies as a * ~~partial~~/full fulfillment for the conferment of MASTER OF SCIENCE (CHEMISTRY) (PLEASE INDICATE THE DEGREE), and the aforementioned work, to the best of my knowledge, is the said student's work.

1 JULY 2024
Date

DR SITI MUNIRAH SIDIK
SENIOR LECTURER
DEPARTMENT OF CHEMISTRY,
FACULTY OF SCIENCE AND MATHEMATICS,
UNIVERSITI PENDIDIKAN SULTAN IDRIS,
35900 TANJUNG MALIM, PERAK.
Signature of the Supervisor

05-4506832 pustaka.upsi.edu.my Perpustakaan Tuanku Bainun Kampus Sultan Abdul Jalil Shah PustakaTBainun ptbupsi

INSTITUT PENGAJIAN SISWAZAH /
INSTITUTE OF GRADUATE STUDIES

BORANG PENGESAHAN PENYERAHAN TESIS/DISERTASI/LAPORAN KERTAS PROJEK
DECLARATION OF THESIS/DISSERTATION/PROJECT PAPER FORM

Tajuk / *Title*: INCORPORATION OF Fe AND gC3N4 INTO MESOPOROUS TITANIA NANOPARTICLES FOR PHOTODEGRADATION OF DIBENZOTHIOPHENE

No. Matrik /*Matric's No.*: M20182002270

Saya / *I* : NURUL ADILAH BINTI MOHD NOOR

(Nama pelajar / *Student's Name*)

mengaku membenarkan ~~Tesis~~/Disertasi/~~Laporan Kertas Projek~~ (~~Kedoktoran~~/Sarjana)* ini disimpan di Universiti Pendidikan Sultan Idris (Perpustakaan Tuanku Bainun) dengan syarat-syarat kegunaan seperti berikut:-
acknowledged that Universiti Pendidikan Sultan Idris (Tuanku Bainun Library) reserves the right as follows:-

1. ~~Tesis~~/Disertasi/~~Laporan Kertas Projek~~ ini adalah hak milik UPSI.
   The thesis is the property of Universiti Pendidikan Sultan Idris
2. Perpustakaan Tuanku Bainun dibenarkan membuat salinan untuk tujuan rujukan dan penyelidikan.
   Tuanku Bainun Library has the right to make copies for the purpose of reference and research.
3. Perpustakaan dibenarkan membuat salinan ~~Tesis~~/Disertasi ini sebagai bahan pertukaran antara Institusi Pengajian Tinggi.
   The Library has the right to make copies of the thesis for academic exchange.
4. Sila tandakan (√) bagi pilihan kategori di bawah */ Please tick (√) for category below:-*

☐	**SULIT/*CONFIDENTIAL***	Mengandungi maklumat yang berdarjah keselamatan atau kepentingan Malaysia seperti yang termaktub dalam Akta Rahsia Rasmi 1972. / *Contains confidential information under the Official Secret Act 1972*
☐	**TERHAD/*RESTRICTED***	Mengandungi maklumat terhad yang telah ditentukan oleh organisasi/badan di mana penyelidikan ini dijalankan. / *Contains restircted information as specified by the organization where research was done.*
/	**TIDAK TERHAD / *OPEN ACCESS***	

(Tandatangan Pelajar/ Signature)

DR SITI MUNIRAH SIDIK
SENIOR LECTURER
DEPARTMENT OF CHEMISTRY,
FACULTY OF SCIENCE AND MATHEMATICS,
UNIVERSITI PENDIDIKAN SULTAN IDRIS,
35900 TANJUNG MALIM, PERAK.

(Tandatangan Penyelia / *Signature of Supervisor*)
& (Nama & Cop Rasmi / *Name & Official Stamp*)

Tarikh: 1 JULAI 2024

Catatan: Jika Tesis/Disertasi ini **SULIT** @ **TERHAD**, sila lampirkan surat daripada pihak berkuasa/organisasi berkenaan dengan menyatakan sekali sebab dan tempoh laporan ini perlu dikelaskan sebagai **SULIT** dan **TERHAD**.

Notes: If the thesis is CONFIDENTAL or RESTRICTED, please attach with the letter from the organization with period and reasons for confidentiality or restriction.

05-4506832 pustaka.upsi.edu.my Perpustakaan Tuanku Bainun Kampus Sultan Abdul Jalil Shah PustakaTBainun ptbupsi

ACKNOWLEDGEMENT

Alhamdulillah, all praise to Allah. Peace and blessing to Prophet Muhammad S.A.W., his families and all muslims. A million thanks dedicated to my beloved family for being the strongest support system and give encouragement during my hard time. Special thanks to my supervisors, Dr. Siti Munirah Binti Sidik for the wiseful advices and help during completing this research project and report. I would also like to thank to my co-supervisors, Dr. Mohamad Saufi Bin Rosmi and Dr. Nur Farhana Binti Jaafar for their support and useful comments during completing the study. Without their guidance, patience, ideas and supports, this research project could not have been accomplished. Special appreciation goes to the staffs of Faculty of Science and Mathematics UPSI for their valuable help and cooperation towards me during completing the research work. My gratitude to the Ministry of Higher Education through financial support from Fundamental Research Grant Scheme for Research Acculturation of Early Career Researchers (FRGS-RACER, no. 2019-0164-103-62). Last but not least, I would like to thank to my labmates and coursemates, Muhammad Shaiful Aidil, Ong Suu Wan, Husna Assaedah, Susana Wong and all my friends that have help me during completing this work either directly or indirectly.

05-4506832 pustaka.upsi.edu.my Perpustakaan Tuanku Bainun Kampus Sultan Abdul Jalil Shah PustakaTBainun ptbupsi
05-4506832 pustaka.upsi.edu.my Perpustakaan Tuanku Bainun Kampus Sultan Abdul Jalil Shah PustakaTBainun ptbupsi

05-4506832 pustaka.upsi.edu.my Perpustakaan Tuanku Bainun Kampus Sultan Abdul Jalil Shah PustakaTBainun ptbupsi

ABSTRACT

This study aimed to incorporate Fe and gC_3N_4 into Mesoporous Titania Nanoparticles (MTN) and investigate photodegradation of Dibenzothiophene (DBT). MTN with various aging time (x = 2, 4, 6 and 8 days) were synthesized via sol-gel method before being incorporated with 5wt% Fe (5Fe/MTN-x) and 5wt% gC_3N_4 (5FeMTN-x/5gC_3N_4) using wet-impregnation method. The photocatalysts were characterized using X-ray Diffraction (XRD), Field-Emission Scanning Electron Microscopy (FESEM) with EDX analysis, UV-Visible Diffuse Reflectance Spectroscopy (UV-DRS), Fourier-Transform Infrared Spectroscopy (FTIR), Surface Area Analysis (BET), Photoluminescence Spectroscopy (PL) and Raman Spectroscopy. Photocatalytic performance was evaluated through DBT photodegradation under ultraviolet (UV) light irradiation for 180 min. Parameters such as H_2O_2 volume, DBT concentration and photocatalyst dose were manipulated with prolonging the reaction time to 240 min. The results of XRD showed the formation of MTN with the presence of common peaks at 2θ: 25.34° - 75.00° corresponded to TiO_2 anatase phase. FTIR and BET analyses also confirmed the formation of MTN and successful incorporation of Fe and gC_3N_4 into the hybrid catalysts. UV-DRS and PL results showed the extending of light absorption towards visible light region and lower rate of electron-hole recombination was reached by the addition of Fe and gC_3N_4. The results displayed 5FeMTN-6/5gC_3N_4 owned the highest DBT photodegradation with 38.2% compared to the other photocatalysts. At the optimized conditions, 5FeMTN-6/5gC_3N_4 reached 57.0% at 40 mg/L DBT concentration with 1 g/L photocatalyst dose and 0.01 mL H_2O_2. The presence of Fe and gC_3N_4 enhanced the photocatalytic performance by forming a heterojunction that promoted the generation and inhibit the electron-hole recombination. In conclusion, Fe and gC_3N_4 were successfully incorporate into MTN and reached 57.0% DBT photodegradation at optimized conditions. The implication of this study is this photocatalyst has good potential to be further investigated as a low-cost alternative for DBT removal in fuels.

05-4506832 pustaka.upsi.edu.my Perpustakaan Tuanku Bainun Kampus Sultan Abdul Jalil Shah PustakaTBainun ptbupsi

05-4506832 pustaka.upsi.edu.my Perpustakaan Tuanku Bainun Kampus Sultan Abdul Jalil Shah PustakaTBainun ptbupsi

PENGGABUNGAN Fe DAN gC_3N_4 KE DALAM NANOZARAH TITANIA MESOFORUS UNTUK FOTODEGRADASI DIBENZOTIOFENA

ABSTRAK

Kajian ini bertujuan untuk menggabungkan Fe dan gC_3N_4 ke dalam Nanozarah Titania Mesoforus (MTN) dan mengkaji fotodegradasi Dibenzotiofena (DBT). MTN dengan masa penuaan berbeza (x = 2, 4, 6 dan 8 hari) disintesis melalui kaedah sol-gel sebelum digabungkan bersama 5wt% Fe (5Fe/MTN-x) dan 5wt% gC_3N_4 (5FeMTN-x/5gC_3N_4) menggunakan kaedah penjejalan basah. Sampel fotopemangkin dicirikan menggunakan analisis Pembelauan Sinar-X (XRD), Mikroskopi Pengimbasan Elektron Pancaran Medan (FESEM) dengan analisis EDX, Spektroskopi Resapan Pantulan Ultralembayung (UV-DRS), Spektroskopi Inframerah Fourier Transformasi (FTIR), Analisis Luas Permukaan (BET), Spektroskopi Fotoluminasi (PL) dan Spektroskopi Raman. Prestasi fotopemangkin dinilai melalui fotodegradasi DBT di bawah sinaran ultralembayung (UV) selama 180 min. Parameter seperti isipadu H_2O_2, kepekatan DBT dan dos fotopemangkin telah dimanipulasi dengan memanjangkan masa tindak balas kepada 240 min. Dapatan XRD menunjukkan pembentukan MTN dengan kehadiran puncak biasa pada 2θ: 25.34^o - 75.00^o sepadan dengan fasa *anatase* TiO_2. Analisis FTIR dan BET juga mengesahkan pembentukan MTN dan kejayaan penggabungan Fe dan gC_3N_4 ke dalam pemangkin hibrid. Dapatan UV-DRS dan PL menunjukkan lanjutan penyerapan ke arah kawasan cahaya nampak dan kadar penggabungan semula lubang dan elektron yang lebih rendah dicapai dengan penambahan Fe dan gC_3N_4. Dapatan mempamerkan, 5FeMTN-6/5gC_3N_4 memiliki fotodegradasi DBT tertinggi sebanyak 38.2% berbanding dengan fotopemangkin yang lain. Pada keadaan optimum, 5FeMTN-6/5gC_3N_4 mencapai 57.0% pada 40 mg/L kepekatan DBT dengan 1 g/L dos fotopemangkin dan 0.01 mL H_2O_2. Kehadiran Fe dan gC_3N_4 meningkatkan prestasi fotokatalitik dengan membentuk heterosimpang yang menggalakkan penjanaan dan menghalang penggabungan semula elektron dan lubang. Kesimpulannya, Fe dan gC_3N_4 berjaya digabungkan ke dalam MTN dan mencapai 57.0% fotodegradasi DBT pada keadaan optimum. Implikasi kajian ini ialah fotopemangkin mempunyai potensi yang baik untuk dikaji dengan lebih lanjut sebagai alternatif kos rendah untuk pembuangan DBT dalam bahan api.

05-4506832 pustaka.upsi.edu.my Perpustakaan Tuanku Bainun Kampus Sultan Abdul Jalil Shah PustakaTBainun ptbupsi

05-4506832 pustaka.upsi.edu.my Perpustakaan Tuanku Bainun Kampus Sultan Abdul Jalil Shah PustakaTBainun ptbupsi

CONTENTS

		Page
DECLARATION OF ORIGINAL WORK		ii
DECLARATION OF DISSERTATION		iii
ACKNOWLEDGEMENT		iv
ABSTRACT		v
ABSTRAK		vi
CONTENTS		vii
LIST OF TABLES		xi
LIST OF FIGURES		xii
LIST OF ABBREVIATIONS		xv
APPENDIX LIST		xx
CHAPTER 1 INTRODUCTION		1
1.1	Background Research	1
1.2	Problem statement	4
1.3	Research aim	6
1.4	Research objectives	6
1.5	Scope of study	6
CHAPTER 2 LITERATURE REVIEW		8
2.1	Introduction	8
2.2	Sulfur components	13
2.3	Desulfurization methods for the production of clean fuels	15

05-4506832 pustaka.upsi.edu.my Perpustakaan Tuanku Bainun Kampus Sultan Abdul Jalil Shah PustakaTBainun ptbupsi

05-4506832 pustaka.upsi.edu.my Perpustakaan Tuanku Bainun Kampus Sultan Abdul Jalil Shah PustakaTBainun ptbupsi

2.4 Photocatalysis 19

2.5 Photocatalyst 21

2.6 TiO_2 as a photocatalyst 28

2.7 Modification of TiO_2 photocatalyst 29

2.7.1 TiO_2 synthesize method 30

2.7.1.1 Hydrothermal method 30

2.7.1.2 Electrochemical anodization method 31

2.7.1.3 Electrospinning method 32

2.7.1.4 Sol-gel method 34

2.7.2 TiO_2 synthesize materials 35

2.7.3 Mesoporous structure 37

2.7.4 Addition of metal elements into TiO_2 50

2.7.5 Type of metal elements 51

2.7.5.1 Noble metals 51

2.7.5.2 Transition metals 56

2.7.6 Metal doping method 61

2.7.7 Incorporation of dopant 69

2.8 Addition of Fe and gC_3N_4 into TiO_2 as composite photocatalyst 70

2.9 Addition of hydrogen peroxide (H_2O_2) as oxidizing agent 72

CHAPTER 3 METHODOLOGY 76

3.1 Introduction 76

3.2 Materials 78

3.2.1 Chemicals 78

3.3 Catalyst preparation 79

05-4506832 pustaka.upsi.edu.my Perpustakaan Tuanku Bainun Kampus Sultan Abdul Jalil Shah PustakaTBainun ptbupsi

05-4506832 pustaka.upsi.edu.my Perpustakaan Tuanku Bainun Kampus Sultan Abdul Jalil Shah PustakaTBainun ptbupsi

3.3.1 Synthesize of Mesoporous Titania Nanoparticles (MTN) 79

3.3.2 Synthesize of graphitic carbon nitride (gC_3N_4) 79

3.3.3 Synthesize of MTN-x with addition of 5wt% Fe (5Fe/MTN-x) 80

3.3.4 Synthesize of 5Fe/MTN-x with addition of 5wt% gC_3N_4 (5FeMTN-x/5gC_3N_4) 80

3.4 Catalyst characterization 81

3.4.1 X-ray diffraction (XRD) 81

3.4.2 Surface area analysis (BET) 82

3.4.3 UV-Visible diffuse reflectance spectroscopy (UV-DRS) 83

3.4.4 Field-Emission scanning electron microscopy (FESEM) with EDX analysis 84

3.4.5 Fourier-transform infrared spectroscopy (FTIR) 85

3.4.6 Photoluminescence (PL) 86

3.4.7 Raman spectroscopy 87

3.5 Photodegradation of DBT 87

CHAPTER 4 RESULTS AND DISCUSSION 91

4.1 Effect of Mesoporous Titania Nanoparticles (MTN) aging time 91

4.1.1 Crystallinity 92

4.1.2 Surface morphology with Elemental Analysis 94

4.1.3 Functional group 96

4.1.4 Surface area/pore structure 98

4.1.5 Structural phases 100

4.1.6 DBT degradation 102

4.2 Effect of Fe addition into various MTN 104

05-4506832 pustaka.upsi.edu.my Perpustakaan Tuanku Bainun Kampus Sultan Abdul Jalil Shah PustakaTBainun ptbupsi

05-4506832 pustaka.upsi.edu.my Perpustakaan Tuanku Bainun Kampus Sultan Abdul Jalil Shah PustakaTBainun ptbupsi

4.2.1 Crystallinity 105

4.2.2 Surface morphology with Elemental Analysis 107

4.2.3 Measured band gap 109

4.2.4 Functional group 112

4.2.5 Surface area/pore structure 114

4.2.6 Structural phases 116

4.2.7 DBT degradation 118

4.3 Effect of dopant addition 120

4.3.1 Crystallinity 121

4.3.2 Surface morphology with Elemental Analysis 123

4.3.3 Measured band gap 126

4.3.4 Functional group 129

4.3.5 Surface area/pore structure 131

4.3.6 Photochemical properties 133

4.3.7 Structural phases 135

4.3.8 DBT degradation 136

4.4 Optimization parameters 140

4.4.1 Effect of addition of Hydrogen peroxide (H_2O_2) 141

4.4.2 Effect of catalyst dosage 145

4.4.3 Effect of DBT initial concentration 147

CHAPTER 5 CONCLUSION AND RECOMMENDATIONS 151

REFERENCES 154

APPENDIX 177

05-4506832 pustaka.upsi.edu.my Perpustakaan Tuanku Bainun Kampus Sultan Abdul Jalil Shah PustakaTBainun ptbupsi

05-4506832 pustaka.upsi.edu.my Perpustakaan Tuanku Bainun Kampus Sultan Abdul Jalil Shah PustakaTBainun ptbupsi

LIST OF TABLES

Table No.		Page
2.1	List of catalysts that have been used for PODS of DBT	25
2.2	Summary of modification of bare TiO_2 photocatalyst	44
2.3	Summary of addition of metal elements into TiO_2 photocatalyst	65
3.1	List of Chemicals	78
4.1	Pore structural informations of MTN-2, MTN-4, MTN-6 and MTN-8 photocatalysts	99
4.2	Photodegradation of DBT using MTN-2, MTN-4, MTN-6 and MTN-8 photocatalysts	103
4.3	Pore structural informations of 5Fe/MTN-2, 5Fe/MTN-4, 5Fe/MTN-6 and 5Fe/MTN-8 photocatalysts	115
4.4	Photodegradation of DBT using 5Fe/MTN-2, 5Fe/MTN-4, 5Fe/MTN-6 and 5Fe/MTN-8 photocatalysts	119
4.5	Pore structural informations of MTN-6, 5Fe/MTN-6 and 5FeMTN-6/5gC_3N_4 photocatalysts	132
4.6	Photodegradation of DBT using MTN-6, 5Fe/MTN-6, gC_3N_4 and 5FeMTN-6/5gC_3N_4 photocatalysts	138
4.7	Effect of addition of H_2O_2 for photodegradation of DBT	144
4.8	Effect of catalyst dosage for photodegradation of DBT	146
4.9	Effect of DBT initial concentration for photodegradation of DBT	148
4.10	Optimum conditions for photodegradation of DBT using 5FeMTN-6/5gC_3N_4 under UV light	150

05-4506832 pustaka.upsi.edu.my Perpustakaan Tuanku Bainun Kampus Sultan Abdul Jalil Shah PustakaTBainun ptbupsi

05-4506832 pustaka.upsi.edu.my Perpustakaan Tuanku Bainun Kampus Sultan Abdul Jalil Shah PustakaTBainun ptbupsi

LIST OF FIGURES

No. Figures		Page
2.1	Chemical Structure of DBT	14
2.2	General photocatalytic process of semiconductor Based on Adaptation From Saravanan et al. (2017)	20
2.3	Schematic illustration of synthesizing process of TiO_2 via hydrothermal method	30
2.4	Schematic illustration of electrochemical anodization process with three-electrode measurement system	31
2.5	Schematic illustration of the setup of electrospinning process	33
2.6	Schematic illustration of sol-gel process	34
2.7	Schematic illustration of synthesizing MTN via microwave-assisted method	40
2.8	Schematic illustration of photocatalytic mechanism of MTN via microwave-assisted method Based on Adaptation From Jaafar et al. (2015)	41
2.9	Schematic illustration of synthesizing mesoporous TiO_2 via solvothermal method	42
2.10	Schematic illustration of photodegradation mechanism of doped TiO_2	51
2.11	Plasmon nanoparticles enhanced the photocatalytic activity of semiconductor photocatalyst	52
2.12	Schematic illustration of synthesizing catalyst via wet-impregnation method	63
3.1	Detailed methodology flowchart	77
4.1	XRD patterns of MTN-2, MTN-4, MTN-6 and MTN-8	93
4.2	FESEM images of (a) MTN-2, (b) MTN-4, (c) MTN-6 and (d) MTN-8	94

05-4506832 pustaka.upsi.edu.my Perpustakaan Tuanku Bainun Kampus Sultan Abdul Jalil Shah PustakaTBainun ptbupsi

05-4506832 pustaka.upsi.edu.my Perpustakaan Tuanku Bainun Kampus Sultan Abdul Jalil Shah PustakaTBainun ptbupsi

4.3	EDX dot-mapping images of MTN-4 consist of (a) O, (b) Ti	95
4.4	FTIR spectra of MTN-2, MTN-4, MTN-6 and MTN-8	96
4.5	(a) N_2 adsorption-desorption linear isotherms and (b) pore size distribution of MTN-2, MTN-4, MTN-6 and MTN-8	98
4.6	Raman spectra of MTN-2, MTN-4, MTN-6 and MTN-8	101
4.7	% degradation of DBT for MTN-2, MTN-4, MTN-6 and MTN-8	102
4.8	XRD patterns of 5Fe/MTN-2, 5Fe/MTN-4, 5Fe/MTN-6, 5Fe/MTN-8 and Fe	105
4.9	FESEM images of the samples (a) 5Fe/MTN-2, (b) 5Fe/MTN-4, (c) 5Fe/MTN-6 and (d) 5Fe/MTN-8	107
4.10	EDX dot-mapping images of 5Fe/MTN-6 consist of (a) Ti, (b) O and (c) Fe	108
4.11	UV-DRS spectra of (a) 5Fe/MTN-2, (b) 5Fe/MTN-4, (c) 5Fe/MTN-6 and (d) 5Fe/MTN-8	109
4.12	The band gap of prepared (a) 5Fe/MTN-2, (b) 5Fe/MTN-4, (c) 5Fe/MTN-6 and (d) 5Fe/MTN-8 photocatalysts	111
4.13	FTIR spectra of 5Fe/MTN-2, 5Fe/MTN-4, 5Fe/MTN-6, 5Fe/MTN-8 and Fe	112
4.14	(a) N_2 adsorption-desorption linear isotherms and (b) pore size distribution of 5Fe/MTN-2, 5Fe/MTN-4, 5Fe/MTN-6 and 5Fe/MTN-8	114
4.15	Raman spectra of (a) 5Fe/MTN-2, 5Fe/MTN-4, 5Fe/MTN-6 and 5Fe/MTN-8 (b) Fe	117
4.16	% degradation of DBT for 5Fe/MTN-2, 5Fe/MTN-4, 5Fe/MTN-6 and 5Fe/MTN-8	118
4.17	XRD patterns of Fe, MTN-6, 5Fe/MTN-6, 5FeMTN-6/5gC_3N_4 and gC_3N_4	121
4.18	FESEM images of the samples (a) Fe, (b) gC_3N_4, (c) MTN-6, (d) 5Fe/MTN-6 and (e) 5FeMTN-6/5gC_3N_4	123
4.19	EDX dot-mapping images of 5FeMTN-6/5gC_3N_4 consist of (a) Ti, (b) O, (c) Fe, (d) C and (e) N	125

05-4506832 pustaka.upsi.edu.my Perpustakaan Tuanku Bainun Kampus Sultan Abdul Jalil Shah PustakaTBainun ptbupsi

05-4506832 pustaka.upsi.edu.my Perpustakaan Tuanku Bainun Kampus Sultan Abdul Jalil Shah PustakaTBainun ptbupsi

4.20	UV-DRS spectra of (a) MTN-6, (b) 5Fe/MTN-6 and (c) 5FeMTN-6/5gC_3N_4	126
4.21	The band gap of prepared (a) MTN-6, (b) 5Fe/MTN-6 and (c) 5FeMTN-6/5gC_3N_4 photocatalysts	128
4.22	FTIR spectra of Fe, MTN-6, 5Fe/MTN-6, 5FeMTN-6/5gC_3N_4 and gC_3N_4	129
4.23	(a) N_2 adsorption-desorption linear isotherms and (b) pore size distribution of MTN-6, 5Fe/MTN-6 and 5FeMTN-6/5gC_3N_4	131
4.24	PL spectra of gC_3N_4, MTN-6, 5FeMTN-6/5gC_3N_4 and 5Fe/MTN-6	134
4.25	Raman spectra of (a) MTN-6, 5Fe/MTN-6 and 5FeMTN-6/5gC_3N_4 (b) Fe	135
4.26	(a) UV-Vis absorption spectra of photodegradation of DBT solution (40 mg/L) in the presence of 5FeMTN-6/5gC_3N_4 photocatalyst (b) % degradation of DBT for MTN-6, 5Fe/MTN-6, gC_3N_4 and 5FeMTN-6/5gC_3N_4	137
4.27	Proposed mechanism of heterojunction-type photocatalytic system of TiO_2 incorporated with Fe and gC_3N_4 for photodegradation of DBT Based on Adaptation From Zhu et al. (2018)	139
4.28	% degradation of DBT using 5FeMTN-6/5gC_3N_4 with addition of 0.00, 0.01, 0.03, 0.06 and 0.09 mL of H_2O_2	141
4.29	% degradation of DBT using 5FeMTN-6/5gC_3N_4 with addition of 1, 3, 5, 7 and 9 g/L of catalyst dosage	145
4.30	% degradation of DBT using 5FeMTN-6/5gC_3N_4 with 20, 30, 40, 50 and 60 mg/L concentration of DBT solution	147
4.31	The MS product of $DBTO_2$	149

05-4506832 pustaka.upsi.edu.my Perpustakaan Tuanku Bainun Kampus Sultan Abdul Jalil Shah PustakaTBainun ptbupsi

05-4506832 pustaka.upsi.edu.my Perpustakaan Tuanku Bainun Kampus Sultan Abdul Jalil Shah PustakaTBainun ptbupsi

LIST OF ABBREVIATIONS

ADS	Adsorptive desulfurization
AFM	Atomic Force Microscope
AO	Auto-oxidation
AOPs	Advanced Oxidation Processes
AO7	Acid Orange 7
AO10	Acid Orange 10
$BaSO_4$	Barium sulfate
BDS	Biodesulfurization
BET	Brunnauer-Emmett-Teller
BJH	Barrett-Joyner-Halenda
BPA	Bisphenol A
BT	Benzothiophene
CAL	Calibration volume
CB	Conduction band
CCDs	Charge-coupled devices
CIDs	Charge-injection devices
CM	Conventional sol-gel
2-CP	2-chlorophenol
4-CP	4-chlorophenol
CR	Congo red
Cr(VI)	Hexavalent chromium

05-4506832 pustaka.upsi.edu.my Perpustakaan Tuanku Bainun Kampus Sultan Abdul Jalil Shah PustakaTBainun ptbupsi

05-4506832 pustaka.upsi.edu.my Perpustakaan Tuanku Bainun Kampus Sultan Abdul Jalil Shah PustakaTBainun ptbupsi

$CSTiO_2$	Core-shell TiO_2 nanomaterials
CTAB	Hexadecyltrimethyl-ammonium bromide
CTDs	Charge transfer devices
$Cu_2(OH)_2CO_3$	Copper hydroxycarbonate
	Initial concentration
C_t	Concentration at a specific time
2D	Two-dimensional
3D	Three-dimensional
DBT	Dibenzothiophene
$DBTO_2$	DBT sulfone
2,4-D	2,4-dichlorophenoxyacetic acid
2,4 DNP	2,4 dinitrophenol
2,4-DP	2,4-dichlorophenoxypropionic acid
E	Band gap energy
e^-	Electrons
EDS	Extractive desulfurization
EDX	Energy-Dispersive X-ray
FCC	Fluidized catalytic cracking
FEG	Field emission gun
FESEM	Field-Emission Scanning Electron Microscopy
FTIR	Fourier-Transform Infrared
Fe_2O_3	Iron (III) oxide
GC	Gas Chromatography
GC-MS	Gas Chromatography-Mass Spectrometer
gC_3N_4	Graphitic carbon nitride

05-4506832 pustaka.upsi.edu.my Perpustakaan Tuanku Bainun Kampus Sultan Abdul Jalil Shah PustakaTBainun ptbupsi

05-4506832 pustaka.upsi.edu.my Perpustakaan Tuanku Bainun Kampus Sultan Abdul Jalil Shah PustakaTBainun ptbupsi

h^+	Holes
h	photon energy
HCl	Hydrochloric acid
HDS	Hydrodesulfurization
He-Ne	Helium-Neon
HNO_3	Nitric acid solution
$HO^{\bullet}_2$	Hydroperoxyl radicals
H_2O_2	Hydrogen peroxide
H_2S	Hydrogen sulphide
IR	Infrared
IWI	Incipient wet impregnation
KBr	Potassium bromide
MB	Methylene Blue
MG	Malachite Green
MO	Methyl Orange
MS	Mass spectrometry
MTN	Mesoporous TiO_2 Nanoparticles
MW	Microwave assisted sol-gel
NaOH	Sodium hydroxide
Nd:YAG	Neodymium-Yttrium Aluminium Garnet
Nd: YVO_4	Neodymium-Yttrium Ortho-Vanadate
NH_4F	Ammonium fluoride
NH_4OH	Ammonium hydroxide
4-NP	para-nitrophenol
$O_2^{\bullet-}$	Superoxide radicals

05-4506832 pustaka.upsi.edu.my Perpustakaan Tuanku Bainun Kampus Sultan Abdul Jalil Shah PustakaTBainun ptbupsi

05-4506832 pustaka.upsi.edu.my Perpustakaan Tuanku Bainun Kampus Sultan Abdul Jalil Shah PustakaTBainun ptbupsi

$^{\bullet}OH$	Hydroxyl radicals
ODS	Oxidative desulfurization
OV	Oxygen vacancies
Pc	Phthalocyanine
PL	Photoluminescence
PMT	Photomultiplier Tube
PODS	Photocatalytic Oxidative Desulfurization
PTFE	Polytetrafluoroethylene
PVP	Polyvinylpyrrolidone
RhB	Rhodamine B
RR	Remazol Red
RR198	Reactive Red 198
SDS	Sodium Dodecyl Sulfate
SEM	Scanning Electron Microscopy
SO_x	Sulfur oxides
SPR	Surface Plasmon Resonance
STM	Scanning Tunneling Microscope
TBOT	Titanium (IV) butoxide
TEM	Transmission Electron Microscopy
TiO_2	Titanium oxide
TIOS	Titanium (IV) oxysulfate
TNF	TiO_2 nanofiber
TNR	TiO_2 nanorod
TNT	TiO_2 nanotube
TS	Thiophene

05-4506832 pustaka.upsi.edu.my Perpustakaan Tuanku Bainun Kampus Sultan Abdul Jalil Shah PustakaTBainun ptbupsi

05-4506832 pustaka.upsi.edu.my Perpustakaan Tuanku Bainun Kampus Sultan Abdul Jalil Shah PustakaTBainun ptbupsi

TSD	Ti^{3+} site defects
TTIP	Titanium Tetraisopropoxide
T20	Tween 20
TX100	Triton X100
US	Ultrasound-assisted impregnation
UV	Ultraviolet
UV-DRS	UV-Visible Diffuse Reflectance Spectroscopy
XRD	X-Ray Diffraction
VB	Valence band
WO_3	Tungsten oxide
ZnO	Zinc oxide

05-4506832 pustaka.upsi.edu.my Perpustakaan Tuanku Bainun Kampus Sultan Abdul Jalil Shah PustakaTBainun ptbupsi
05-4506832 pustaka.upsi.edu.my Perpustakaan Tuanku Bainun Kampus Sultan Abdul Jalil Shah PustakaTBainun ptbupsi

05-4506832 pustaka.upsi.edu.my Perpustakaan Tuanku Bainun Kampus Sultan Abdul Jalil Shah PustakaTBainun ptbupsi

APPENDIX LIST

A	UV-Vis Absorption Spectra of DBT Solution at Initial Time
B	Calibration Curve of the Standard DBT in Acetonitrile Solution
C	List of Publications
D	List of Conferences

05-4506832 pustaka.upsi.edu.my Perpustakaan Tuanku Bainun Kampus Sultan Abdul Jalil Shah PustakaTBainun ptbupsi
05-4506832 pustaka.upsi.edu.my Perpustakaan Tuanku Bainun Kampus Sultan Abdul Jalil Shah PustakaTBainun ptbupsi

05-4506832 pustaka.upsi.edu.my Perpustakaan Tuanku Bainun Kampus Sultan Abdul Jalil Shah PustakaTBainun ptbupsi

CHAPTER 1

INTRODUCTION

05-4506832 pustaka.upsi.edu.my Perpustakaan Tuanku Bainun Kampus Sultan Abdul Jalil Shah PustakaTBainun ptbupsi

1.1 Background Research

Desulfurization of fuel oils such as diesel, fluidized catalytic cracking (FCC) gasoline, kerosene, jet fuel and heating oil has become an important topic in oil refining industry. Sulfur compounds in fuel oils were encouraged to be removed as they create problems during refining as well as during their commercial use. During refining, these sulfur compounds can cause corrosion problems in pumping, pipeline and refining equipment and also poisoning some of catalysts used in oil processing (Bhutto et al., 2016). During the commercial use of fuel oils, sulfur compounds has released the sulfur oxides (SO_x) through combustion process which lead to

05-4506832 pustaka.upsi.edu.my Perpustakaan Tuanku Bainun Kampus Sultan Abdul Jalil Shah PustakaTBainun ptbupsi

05-4506832 pustaka.upsi.edu.my Perpustakaan Tuanku Bainun Kampus Sultan Abdul Jalil Shah PustakaTBainun ptbupsi

environmental problems such as acid rain, global warming and atmospheric pollution. Besides, the human health was also exposed to negative impact such as respiratory illness, heart disease and asthma (Hitam, Jalil, & Triwahyono, 2018). With the heightened interest for cleaner air and increased stringent environmental regulations for sulfur concentration in fuel worldwide, the plan to achieve little-to-no sulfur fuels (S-content<10 ppm) has been implementing by many developed and developing countries in order to reduce the negative effects on environment and health (Mandizadeh, Salavati-Niasari, & Sadri, 2017; Bhutto et al., 2016). Therefore, the removal of sulfur in fuel has become the hot topic for many researchers nowadays, as intensive studies were needed to find more economical and viable deep desulfurization technologies.

Hydrodesulfurization (HDS) was the most widely used commercial method for sulfur removal in fuel oils (Bhutto et al., 2016). HDS process was indeed an efficient method in eliminating acyclic and aliphatic sulfur compounds such as thiols, sulfides and disulfides but it was difficult to reduce heterocyclic sulfur compounds such as thiophene (TS), dibenzothiophene (DBT) and its alkylated derivatives due to their steric hindrance (Hitam, Jalil, & Abdulrasheed, 2019). Besides, HDS method employs the use of hydrogen at an elevated pressure (20-100 atm of H_2) and high operating temperature (300-400 ^{o}C) which were very costly option for deep desulfurization (Zeelani, Ashrafi, Dhakad, Gupta, & Pal, 2016; Zaid, Kait, & Mutalib, 2016). Therefore, alternative ultra-deep desulfurization processes such as extractive desulfurization (EDS), adsorptive desulfurization (ADS), biodesulfurization (BDS) and oxidative desulfurization (ODS) were necessary to be developed (Mandizadeh et al., 2017).

05-4506832 pustaka.upsi.edu.my Perpustakaan Tuanku Bainun Kampus Sultan Abdul Jalil Shah PustakaTBainun ptbupsi

05-4506832 pustaka.upsi.edu.my Perpustakaan Tuanku Bainun Kampus Sultan Abdul Jalil Shah PustakaTBainun ptbupsi

Among those various desulfurization techniques, ODS was considered as one of the most encouraging techniques for deep desulfurization due to its mild operating conditions which can be operated under low temperature and ambient pressure, as well as its high ability to oxidize and convert refractory sulfur compound such as DBT without the hydrogen utilization (Ding et al., 2015). In fact, photocatalytic oxidative desulfurization (PODS) has gained attention as the promising technique to improve the performance of ODS, since photocatalysis was one of the advanced oxidation processes (AOPs) that can promote outstanding performance in degrading a wide range of toxic compounds under light irradiation. Besides, photocatalysis also provides other advantages such as easy operation, low-cost, sustainable technology, ability to perform at room temperature, environmental friendliness and capability to transform toxic contaminants into harmless products with high selectivity (Hitam et al., 2019). PODS was assumed to be a potential method to solve this problem since it promotes high catalytic activity, safety, low energy consumption and recycling ability (Zhu et al., 2014). This finding was supported by Miao et al. (2016) which stated that, PODS has been known to be a promising method as it provides a green path to photooxidize sulfur species to highly polar sulfoxides or sulfone product with the presence of ultraviolet (UV) or visible light as the energy source.

In order to improve the PODS activity, some modifications of the existing catalysts have been done by researchers. Generally, the photocatalytic efficiency can be improved by several techniques such as synthesize of high surface area materials, the use of support material, coupling with other semiconductors, formation of a defect structure to improve charge-carrier separation and coupling with organic or inorganic materials (Hitam et al., 2019).

05-4506832 pustaka.upsi.edu.my Perpustakaan Tuanku Bainun Kampus Sultan Abdul Jalil Shah PustakaTBainun ptbupsi

05-4506832 pustaka.upsi.edu.my Perpustakaan Tuanku Bainun Kampus Sultan Abdul Jalil Shah PustakaTBainun ptbupsi

Over the last few decades, various photocatalysts have been developed for PODS and semiconductor-based catalysts such as zinc oxide (ZnO), titanium oxide (TiO_2), tungsten oxide (WO_3), etc were known to exhibit excellent photocatalytic performance (Kang et al., 2019). The presence of photocatalyst in PODS was crucial as it promotes the oxidation of sulfur-containing compounds by enhancing the rate of active species formation and improving the charge transfer. From previous studies, the instantaneous increased of sulfur removal depends on the increasing amount of photocatalyst (Aazam, 2014; Abdelaal & Mohamed, 2014). However, the decreasing in sulfur removal was occurred as the further addition of photocatalyst was beyond the optimum value. It was due to the excess amount of catalyst tends to inhibit the light source and decrease photoelectron productivity which results in reducing the photocatalytic oxidation efficiency (Li et al., 2016). In this perspective, TiO_2 as semiconductor photocatalyst has received considerable attention due to its commercial availability, high chemical stability and excellent catalytic properties (Petronella et al., 2017). This finding was supported by Hosseini and Faghihian (2019) which stated that, TiO_2 was one of various semiconductors that has been widely utilized in photodegradation experiments due to its elevated photocatalytic activity, photochemical stability, affordability and safe to use.

1.2 Problem Statement

TiO_2 has been widely used in the PODS of DBT in fuel due to its promising photoactivity, non-toxicity, chemical stability and low cost (Hitam et al., 2019). However, TiO_2 has several drawbacks that limit its practical application such as has

05-4506832 pustaka.upsi.edu.my Perpustakaan Tuanku Bainun Kampus Sultan Abdul Jalil Shah PustakaTBainun ptbupsi

05-4506832 pustaka.upsi.edu.my Perpustakaan Tuanku Bainun Kampus Sultan Abdul Jalil Shah PustakaTBainun ptbupsi

narrow spectrum utilization due to its wide band gap (3.2 eV) and rapid recombination of electron-hole pairs (Jaafar, Jalil, & Triwahyono, 2017). Modification of TiO_2 into a mesoporous structure was reported successfully increased the stability and photoactivity of the photocatalyst (Zhang et al., 2020). Besides that, the modification of TiO_2 with transition metal and polymeric carbon material can also enhance the photoactivity of the photocatalyst (Sadanandam, Zhang, & Scurrell, 2018; Zaid et al., 2016). Among those various metallic dopants, Fe was considered to be the promising candidate for this research due to the ionic radius of Fe^{3+} (0.69 Å) was nearly similar to Ti^{4+} (0.745 Å), which in turn can help the Fe^{3+} ions to be easily incorporated into TiO_2 crystal lattice. As a result, Fe^{3+} will restrict the recombination of electron-hole pairs by performing as a charge carrier trap, which can significantly enhance the photoactivity (Marami, Farahmandjou, & Khoshnevisan, 2018). In recent years, gC_3N_4 as a well-known polymer has got much attention from researchers due to its advantages such as low cost, electronic characteristics, high chemical and thermal stability, and also an efficient non-metallic photocatalyst (Gahlot, Dappozze, Mishra, & Guillard, 2021; Abedini, Allahyari, & Rahemi, 2021). The incorporation of both Fe and gC_3N_4 can improve the separation of photogenerated electron-hole pairs as it can form heterojunction known as Z-scheme mechanism that allow the reduction and oxidation reactions occurred from different sites of photocatalyst (Zhu, Murugananthan, Gu, & Zhang , 2018). Nevertheless, there was no study has been done to investigate the potential of mesoporous TiO_2 with incorporation of Fe and gC_3N_4 in the degradation of DBT under UV light yet.

05-4506832 pustaka.upsi.edu.my Perpustakaan Tuanku Bainun Kampus Sultan Abdul Jalil Shah PustakaTBainun ptbupsi

05-4506832 pustaka.upsi.edu.my Perpustakaan Tuanku Bainun Kampus Sultan Abdul Jalil Shah PustakaTBainun ptbupsi

1.3 Research aim

The aim of this research was to investigate the photocatalytic efficiency of mesoporous TiO_2 nanoparticles (MTN) with addition of Fe and gC_3N_4 for the photodegradation of DBT in model fuel under UV light irradiation.

1.4 Research Objectives

The objectives of this research are:

1) To synthesize MTN via sol-gel method and modification with Fe and gC_3N_4 via wet-impregnation method.
2) To study the physicochemical properties of prepared photocatalysts.
3) To elucidate the photocatalytic activities of prepared photocatalysts in photodegradation of DBT under UV light.

05-4506832 pustaka.upsi.edu.my Perpustakaan Tuanku Bainun Kampus Sultan Abdul Jalil Shah PustakaTBainun ptbupsi

1.5 Scope of study

In this research, MTN was synthesized via sol-gel method and modified with Fe and gC_3N_4 as a photocatalyst for the photodegradation of DBT in model oil under UV light irradiation. Different aging time (x = 2, 4, 6 and 8 days) were used to prepare the bare MTN-x. Then, 5wt% of Fe was added into MTN-x to form 5Fe/MTN-x before being modified with 5wt% of gC_3N_4 dopant by wet-impregnation method and denoted

05-4506832 pustaka.upsi.edu.my Perpustakaan Tuanku Bainun Kampus Sultan Abdul Jalil Shah PustakaTBainun ptbupsi

05-4506832 pustaka.upsi.edu.my Perpustakaan Tuanku Bainun Kampus Sultan Abdul Jalil Shah PustakaTBainun ptbupsi

as 5FeMTN-x/5gC_3N_4. Then, the physicochemical properties of prepared photocatalysts were characterized using X-ray diffraction (XRD), Surface area analysis (BET), UV-Visible diffuse reflectance spectroscopy (UV-DRS), Field-Emission scanning electron microscopy (FESEM), Fourier-transform infrared spectroscopy (FTIR), Photoluminescence (PL) and Raman spectroscopy. The photocatalytic activity of 5FeMTN-x/5gC_3N_4 was compared with undoped MTN-x and also 5Fe/MTN-x in order to determine the effectiveness of the combination of Fe and gC_3N_4 into MTN for photodegradation of DBT in model oil under UV light. After photocatalytic reaction, the degraded DBT solution was characterized by GC-MS to determine the degradation product.

05-4506832 pustaka.upsi.edu.my Perpustakaan Tuanku Bainun Kampus Sultan Abdul Jalil Shah PustakaTBainun ptbupsi
05-4506832 pustaka.upsi.edu.my Perpustakaan Tuanku Bainun Kampus Sultan Abdul Jalil Shah PustakaTBainun ptbupsi

05-4506832 pustaka.upsi.edu.my Perpustakaan Tuanku Bainun Kampus Sultan Abdul Jalil Shah PustakaTBainun ptbupsi

CHAPTER 2

LITERATURE REVIEW

05-4506832 pustaka.upsi.edu.my Perpustakaan Tuanku Bainun Kampus Sultan Abdul Jalil Shah PustakaTBainun ptbupsi

2.1 Introduction

Several significant problems such as catalyst poisoning in many oil refining processes, corrosion in pumping, pipeline and burners were caused by the existence of sulfur in liquid petroleum fuels. During combustion, liquid fuels that contain high level of sulfur would cause the emission of SO_x which was the main source of environmental pollution and acid rain (Ammar, Kareem, & Ali, 2018). In recent years, deep desulfurization of sulfur in fuels have received much attention and due to the strict environmental regulations, the removal of sulfur have been planned by many developed countries in order to achieve the sulfur content less than 10 ppm (Leng, Sun, Zhang, Yu, & Xu, 2016).

05-4506832 pustaka.upsi.edu.my Perpustakaan Tuanku Bainun Kampus Sultan Abdul Jalil Shah PustakaTBainun ptbupsi

05-4506832 pustaka.upsi.edu.my Perpustakaan Tuanku Bainun Kampus Sultan Abdul Jalil Shah PustakaTBainun ptbupsi

In modern industry, the current desulfurization method being used is HDS (Betiha, Rabie, Ahmed, Abdelrahman, & El-Shahat, 2018). HDS reaction conditions usually takes place in high pressure and high temperature environment in the presence of hydrogen gas. However, the refractory sulfur compounds such as DBT and its derivatives are difficult to be removed by this method as the existence of benzene rings in molecular enhance their aromatic (Wang et al., 2014). Therefore, numerous alternative techniques such as reactive adsorption, BDS, extraction and ODS were being approached to complement the conventional HDS process in order to achieve clean fuels production (Ammar et al., 2018). Among those methods, ODS was considered to be one of the favourable techniques for deep desulfurization of fuels due to its mild reaction conditions such as lower reaction temperature, atmospheric pressure, converting sulfur-bearing molecules to sulfones and removing sulfones from oils by solvent extraction or adsorption (Chen, Liu, Zhang, & Wang, 2017). However, PODS as a new method for sulfur removal was more moderate than traditional chemical oxidation (Wang et al., 2014). This finding was supported by Wu, Li, Liu, Bai, and Yang (2017) which stated that, PODS has gained great interest as one of the promising new method for deep desulfurization of fuels due to its mild reaction conditions and resultant low investment and operating cost. Then, the refractory sulfur compounds was oxidized to highly polar sulfoxides or sulfones through PODS method in which the degradation products can be easily removed from the fuel by solvent extraction or adsorption (Sun, Yu, Wang, Feng, & Li, 2016).

During the past few decades, TiO_2 has been considered to be one of the most effective and suitable photocatalysts in green chemistry technology due to its abundance, non-toxicity, chemical stability and low cost (Pham, Nguyen, Thi, &

05-4506832 pustaka.upsi.edu.my Perpustakaan Tuanku Bainun Kampus Sultan Abdul Jalil Shah PustakaTBainun ptbupsi

05-4506832 pustaka.upsi.edu.my Perpustakaan Tuanku Bainun Kampus Sultan Abdul Jalil Shah PustakaTBainun ptbupsi

Doan, 2018; Chen, Shen, Wang, Xiao, & Luo, 2018). This finding was supported by Yang, Han, and Xue (2014) which stated that TiO_2-based materials has been the most widely used photocatalyst as it promotes chemical stability, non-toxicity and high photocatalytic reactivity. However, TiO_2 has several limitations because of its large band gap (3.0-3.2 eV), in which inhibit its application to some extent (Ma, He, & Liu, 2015; Yang et al., 2014). Therefore, photocatalysis has become one of the most important topics in order to develop the activity of the photocatalysts with high effectiveness and stability (Ma et al., 2015).

Previous study from Anku, Oppong, Shukla, and Govender (2016) has stated that, reducing the large band gap and minimizing the recombination rate of the photogenerated electrons and holes will enhance the photocatalytic activity of TiO_2. Many modification techniques have been done to achieve these goals and the most effective method to enhance the photoactivity of TiO_2 and inhibit the electron-hole recombination rate is by doping the transition metal cations with TiO_2. This finding was supported by Dorraj, Goh, Sairi, Woi, and Basirun (2018); Kalantari, Kalbasi, Sohrabi, and Royaee (2017) which stated that, transition metals such as Mn, Cu, Cr, V, W and Fe cause the visible light absorption ability of TiO_2 to be increased and they can also act as the trapping center to improve the separation of photogenerated electron-hole pairs and in turn will increase the photocatalytic activity of TiO_2. Among various metal ions, Fe was considered to be the most suitable dopant due to its ionic radius that was similar to that Ti^{4+}, and thus, Fe^{3+} ions could be easily incorporated into the TiO_2 lattice. On the other hand, it can act as a shallow trapping in the TiO_2 lattice, as the energy level of Fe^{2+}/Fe^{3+} lies close to that Ti^{3+}/Ti^{4+}, which resulted in suppressing the recombination of electron-hole pairs and extending the

05-4506832 pustaka.upsi.edu.my Perpustakaan Tuanku Bainun Kampus Sultan Abdul Jalil Shah PustakaTBainun ptbupsi

05-4506832 pustaka.upsi.edu.my Perpustakaan Tuanku Bainun Kampus Sultan Abdul Jalil Shah PustakaTBainun ptbupsi

light spectrum absorption ability (Komaraiah et al., 2019; Zou et al., 2017). Previous study from Moradi, Eshaghi, Hosseini, and Ghani (2016) has confirmed the statement, in which the incorporation of Fe into TiO_2 nanoparticles has improved the photocatalytic degradation of Reactive Red 198, since the addition of metal Fe has generated Fe^{3+} ions that can help in the charge separation by being as a charge traps for electron and holes, which in turn will enhance the photocatalytic activity.

In recent years, gC_3N_4 has attracted many researchers' attention as a metal-free visible light photocatalyst that has suitable band gap (2.7 eV), affordable cost and excellent stability for photocatalytic applications (Sadanandam et al., 2018). However, the small surface area and higher electron-hole pair recombination of gC_3N_4 has limited its potential as a photocatalyst to some extent (Gahlot et al., 2021). Therefore, several studies have been done to improve its photocatalytic performance such as by doping with metal/noble metal, non-metal and combination with semiconductor material which can generate large number of active sites for photocatalytic reactions and also increasing its surface area. In particular, the combination of gC_3N_4 with TiO_2 has been widely studied for various photocatalytic applications. For instance, previous study from Lei et al. (2015) has synthesized gC_3N_4/TiO_2 composite for the photodegradation of acid orange 7 (AO7) under UV light irradiation. The enhancement in photocatalytic performace was obtained using the gC_3N_4/TiO_2 as a photocatalyst compared to pure TiO_2 and gC_3N_4 that showed low rate of degradation. The increased in photocatalytic activity under UV light irradiation pronounced the synergistic impact of coupling gC_3N_4 and TiO_2 that enhanced the separation of photogenerated electron-hole charges.

05-4506832 pustaka.upsi.edu.my Perpustakaan Tuanku Bainun Kampus Sultan Abdul Jalil Shah PustakaTBainun ptbupsi

05-4506832 pustaka.upsi.edu.my Perpustakaan Tuanku Bainun Kampus Sultan Abdul Jalil Shah PustakaTBainun ptbupsi

Based on previous study by Li et al. (2014), photocatalytic efficiency of TiO_2 was widely known to be very sensitive to its particle size, crystal phase, crystallinity, pore structure and specific area. Therefore, mesoporous TiO_2 that was first prepared through modified sol-gel process using a phosphate surfactant by David and Jackie in 1995 has gained attention because of its high surface area. This finding was supported by Piumetti et al. (2014) which stated that, MTN has large specific surface area and decreased the internal diffusion resistance to improve the adsorption during catalytic reactions. They also take part in the processes occuring in solar cells, separation/purification, electric and photocatalytic systems and immobilization processes. According to Zou et al. (2017), mesoporous TiO_2 provides some advantages such as high efficiency, high specific surface area, good stability, non-toxicity and ready availability causing it interesting to be widely investigated. Furthermore, due to its mesoporous microstructure, it can enhance the photo-conversion efficiency. In this research, we insist to synthesize MTN using sol-gel method due to its simple process, affordable cost and can be conducted under ambient temperature. Through this method, the modification of physico-chemical and electrochemical properties of MTN can also be carried out to improve its efficiency (Marami et al., 2018).

From the previous published works, it was interesting to explore MTN that was incorporated with Fe and gC_3N_4 as a composite photocatalyst since both of them showed a great potential to improve the photoactivity. Hence, in the present work, the efficiency of photocatalytic behaviour of MTN with the incorporation of 5wt% Fe and 5wt% gC_3N_4 for the photodegradation of DBT in model oil was investigated under UV light irradiation.

05-4506832 pustaka.upsi.edu.my Perpustakaan Tuanku Bainun Kampus Sultan Abdul Jalil Shah PustakaTBainun ptbupsi

05-4506832 pustaka.upsi.edu.my Perpustakaan Tuanku Bainun Kampus Sultan Abdul Jalil Shah PustakaTBainun ptbupsi

2.2 Sulfur components

The rising demand of petroleum causing the huge amount of crude oil need to be transported (Meriem-Benziane, Bou-Said, & Boudouani, 2017). The market price of crude oil can be affected by the most of its important characteristics which were sulfur content and gravity in which low sulfur content of crude oil was specially preffered. Sulfur has the most important effects on refining compared to other heteroelements in crude oil. In fact, high sulfur levels in refinery streams may cause several drawbacks such as deactivate the catalysts that promote required chemical reactions in certain refining processes, produce corrosion in refinery equipment and lead to unwanted air emissions from sulfur compounds that may be subjected to strict legislation controls (Demirbas, Alidrisi, & Balubaid, 2015).

05-4506832 pustaka.upsi.edu.my Perpustakaan Tuanku Bainun Kampus Sultan Abdul Jalil Shah PustakaTBainun ptbupsi

In commercial fuels such as gasoline and diesel oil, the presence of sulfur components enhance to the emission of SO_x, causing air pollution, acid rains, human respiratory malady and threatening the environment (Kalantari, Kalbasi, Sohrabi, & Royaee, 2016). This finding was supported by Singh, Chopra, Mahendra, Kagdiyal, and Saxena (2016) which stated that, harmful effects such as corrosion of engine parts, wear, deposit formation and air pollution were easy to take place when sulfur compounds were present in these fuels (gasoline and diesel). According to Hosseini, Faghihian, and Sanati (2018), one of the main sources of atmospheric pollution produced from the sulfur compounds of transportation fuels. Therefore, strict control on total sulfur in gasoline and diesel which was less than 10 mg/L max as per Euro-V norms has been implemented by number of legislations and several techniques have been adopted for appropriately refineries in order to meet these legislations (Singh et

05-4506832 pustaka.upsi.edu.my Perpustakaan Tuanku Bainun Kampus Sultan Abdul Jalil Shah PustakaTBainun ptbupsi

05-4506832 pustaka.upsi.edu.my Perpustakaan Tuanku Bainun Kampus Sultan Abdul Jalil Shah PustakaTBainun ptbupsi

al., 2016). Kalantari et al. (2016) has also reported that the removal of sulfur content to less than 10 ppm by desulfurization of commercial fuels has largely been considered in order to meet the regulations of environmental protection agencies. Sulfur compounds in fuel can be categorized into four groups which were mercaptans, sulphides, disulphides and thiophenes (Dehghan & Anbia, 2017). The sulfur species in the fuel was commonly being distributed by depending on the origin of the petroleum, type and volume of different stream feeding. However, diesel feeds mostly contain a large number of DBT and alkyl derivatives (Zaid et al., 2016). Figure 2.1 below shows the chemical structure of DBT.

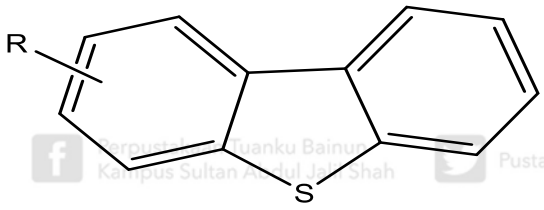


Figure 2.1. Chemical Structure of DBT

In the present work, the sulfur compounds like DBT and its alkyl derivatives were removed in order to obtain the ultra-low sulfur content fuels. However, the poly-aromatic refractory sulfur compounds like DBT and its alkyl derivatives were difficult to be removed by catalytic HDS although this method has been widely used for reducing sulfur content in petroleum fractions. The operation conditions of HDS tend to increase the operation cost (Khayyat & Roselin, 2017). Therefore, alternative desulfurization methods have been approached in order to achieve deep desulfurization and produce the ultra clean fuel (Zhao & Baker, 2015).

05-4506832 pustaka.upsi.edu.my Perpustakaan Tuanku Bainun Kampus Sultan Abdul Jalil Shah PustakaTBainun ptbupsi

05-4506832 pustaka.upsi.edu.my Perpustakaan Tuanku Bainun Kampus Sultan Abdul Jalil Shah PustakaTBainun ptbupsi

2.3 Desulfurization methods for the production of clean fuels.

In oil refining, desulfurization of fuel oils such as diesel, FCC gasoline, kerosene, jet fuel and heating oil was an important practice in order to fulfill the requirement of low-sulfur content fuels. Therefore, economical and viable deep desulfurization technologies have been applied to achieve the requirement specifications (Bhutto et al., 2016).

The current method that was widely employed in industries for sulfur removal was HDS in which sulfur compounds in fuel oils will react with hydrogen in the presence of catalyst to produce hydrogen sulphide (H_2S), which then was removed from the fuel oils (Abro et al., 2014). HDS can effectively remove the aliphatic sulfur compounds such as mercaptanes, sulfides and disulfides from fuels. However, this method was not too effective for the removal of heterocyclic sulfur compounds such as thiophene, benzothiophene, DBT and their derivatives as higher temperature (~400 ^{o}C), higher pressure (~20 MPa) and more active noble catalyst were required for reducing the sulfur contents to a lower level which results in rising the cost and oil loss (Dehghan & Anbia, 2017; Abro et al., 2014). Therefore, alternative methods such as ODS, EDS, ADS and BDS have been considered to overcome the drawbacks of HDS in deep desulfurization (Bhutto et al., 2016).

In EDS, it promotes simple operation and could be carried out at mild conditions. Moreover, the chemical structure of the compounds in fuel oils was maintained and the extracted sulfur compound was reusable as raw materials (Abro et al., 2014). Many types of extractants have been explored such as imidazolidinone,

05-4506832 pustaka.upsi.edu.my Perpustakaan Tuanku Bainun Kampus Sultan Abdul Jalil Shah PustakaTBainun ptbupsi

05-4506832 pustaka.upsi.edu.my Perpustakaan Tuanku Bainun Kampus Sultan Abdul Jalil Shah PustakaTBainun ptbupsi

N,N-dimethylformamide, acetonitrile, methanol and dimethylsulfoxide (Yu et al., 2016; Li, Xiao, Tang, & Zhou, 2016). However, the use of single extraction in EDS was less efficient and multiple extractions were required to get the stipulated sulfur content in fuel oils (Lu, Deng, Ren, & Yang, 2014). Besides, the conventional flammable and volatile organic extractants mentioned above were inefficient and not suitable for environment. Therefore, new extraction agents that were highly efficient, economical and environmental friendly were being widely searched (Yu et al., 2016).

Next, other economically promising technique for the removal of sulfur compounds was ADS. In this method, the removal of sulfur compounds in fuel oils occurred via adsorption on an adsorbent that was typically placed on a non-reactive and porous substrate (Abro et al., 2014). The choice of proper adsorbent was vital as the efficiency of ultradeep desulfurization process depends on the surface chemistry and porosity of the adsorbents (Betiha et al., 2018). Some examples of adsorbent materials being used were metal oxides, clays, activated carbon, silica gel, zirconia, carbon nanotubes and zeolites (Betiha et al., 2018). Among the adsorbents, activated carbon was the mostly to be utilized due to its large surface area and good porosity. The natural raw materials were usually used to produce activated carbon and it was explored that coconut shell-based activated carbon exhibited better results compared to coal- and wood- based activated carbon (Abro et al., 2014). However, the structure, porosity and surface functionality of the common adsorbents were not explicitly defined causing the difficulties in modifying them to meet a specific requirement (Hitam et al., 2019). In addition, this method was still in developing phase in which good absorbents that can selectively and significantly adsorb sulfur compounds without the mixture of hydrocarbons and olefins were being explored by researchers.

05-4506832 pustaka.upsi.edu.my Perpustakaan Tuanku Bainun Kampus Sultan Abdul Jalil Shah PustakaTBainun ptbupsi

05-4506832 pustaka.upsi.edu.my Perpustakaan Tuanku Bainun Kampus Sultan Abdul Jalil Shah PustakaTBainun ptbupsi

Moreover, aromatic sulfur compounds literally contain some similar properties to olefenic, such as the presence of more than two double bonds in which can be easily interact with metal atoms. Besides that, the adsorbents also difficult to be regenerated completely after the adsorption process. Many adsorbents used in previous study also did not show an outstanding adsorption results and proved to be low. For example, only 1-4 mg of sulfur compounds were found to adsorb per g of clay material, which showed that, large amount of adsorbents were needed for conducting this process (Abro et al., 2014).

BDS was another method used for removing sulfur atoms from the organic compounds. In BDS, biological enzymes produced by bacteria and other microorganisms have been used as a biocatalyst, and thus it was considered as green technique. Some microorganisms that have been used for the BDS of fuels are Rhodococcus rhodochrous, Sulfolobus acido-caldarius and Pseudomonas (Betiha et al., 2018). These microorganisms usually consist of natural ability that can consume aromatic sulfur compounds as their energy source and metabolized the organo sulfur compounds via oxidative C-S bond cleavage, reductive C-S bond cleavage or oxidative C-C bond cleavage. Generally, this process was occurred via two pathways and it was known as Kodama pathway. The first subjected was aimed to be against one of the carbon atoms or the 4S pathway as early catalysis was directed against the sulfur axis. Nevertheless, BDS pathways was still in development phase for petroleum fuel since a noteworthy amount of carbon was mineralized making the fuel value to be reduced (Almashjary et al., 2018). In addition, BDS exhibited slow biodegradation and the supply for suitable biocatalyst was very limited. Besides that, the living microbes used were hard to be maintained in terms of logistics of sanitary storage,

05-4506832 pustaka.upsi.edu.my Perpustakaan Tuanku Bainun Kampus Sultan Abdul Jalil Shah PustakaTBainun ptbupsi

05-4506832 pustaka.upsi.edu.my Perpustakaan Tuanku Bainun Kampus Sultan Abdul Jalil Shah PustakaTBainun ptbupsi

handling, shipment, storage and use in the refinery atmosphere since they were very sensitive to nature.

Among those alternative methods, ODS process was one of the promising alternative desulfurization method due to its mild reaction conditions in which the temperature and pressure required were low and selectivity for removing aromatic sulfur compounds was higher compared to the HDS process. Besides that, ODS process also does not require expensive hydrogen (Hossain, Park, & Choi, 2019). This finding was supported by Kalantari et al. (2016), which stated that ODS was considered as one of the most ideal process for deep desulfurization of fuel due to its mild operating conditions, low cost and no requirement for hydrogen. ODS process usually consists of two steps. In first step, sulfur compounds were oxidized into sulfoxides or sulfones by an oxidant. Next in the second step, the formed products were separated from the fuel oils via solvent extraction based on their increased polarity. Then, distillation process was conducted to recover the used solvent (Abro et al., 2014). According to Zhu, Li, and Zhu (2016), in ODS process, the refractory sulfur compound such as DBT can be oxidized to the corresponding sulfone by using oxygen as the oxidant which was favourable due to its abundance in nature and can be conducted under mild pressure conditions. The catalysts being utilized in ODS method usually came from organic and inorganic acids, such as formic, acetic and performic acids. Recently, ionic liquids were also applied in ODS as it became the alternative organic solvents to replace the traditional one. The choice of the oxidant and the extractive solvent play an important role in ODS process as they will influence the efficiency of the sulfur removal. Inappropriate oxidants caused the unwanted side reactions to occur, which in turn decreased the quality and mass of fuel

05-4506832 pustaka.upsi.edu.my Perpustakaan Tuanku Bainun Kampus Sultan Abdul Jalil Shah PustakaTBainun ptbupsi

05-4506832 pustaka.upsi.edu.my Perpustakaan Tuanku Bainun Kampus Sultan Abdul Jalil Shah PustakaTBainun ptbupsi

oils. Then, the choice of solvent that was not suitable for the process might cause the removal of hydrocarbon compounds such as olefins and aromatics from the liquid (Abro et al., 2014).

2.4 Photocatalysis

As one of the AOPs, photocatalysis has been widely applied in the field of green chemistry such as wastewater treatment, exhaust gas treatment and hydrogen production in which catalysts were used to enhance the activity of a reaction with the presence of light absorption (Pham et al., 2018). Besides that, it also known as a promising technology due to its versatility, low-cost and promotes eco-friendly treatment for most of pollutants (Sun et al., 2017). This finding was supported by Saravanan et al. (2015) which stated that, heterogeneous catalytic processes was one of the green technologies that can eliminate toxic chemicals from the environment almost completely even under mild conditions of temperature and pressure due to its broad applicability and high efficiency. In photocatalytic process, the presence of light photons over a semiconductor particle resulted in the formation of several reactive radicals which were important for the oxidation of organic compounds (Fernandes, Gagol, Makos, Khan, & Boczkaj, 2019). According to Zarrabi, Entezari, and Goharshadi (2015), as the effective of ODS technique, the PODS has also gained attention from many researchers due to its low cost and promotes mild operation of conditions. Moreover, PODS can provide a green path by transforming hazardous sulfur species to highly polar sulfoxide or sulfone which were environmentally

05-4506832 pustaka.upsi.edu.my Perpustakaan Tuanku Bainun Kampus Sultan Abdul Jalil Shah PustakaTBainun ptbupsi

05-4506832 pustaka.upsi.edu.my Perpustakaan Tuanku Bainun Kampus Sultan Abdul Jalil Shah PustakaTBainun ptbupsi

friendly substances (Kang et al., 2019; Hitam et al., 2019). In this research, the photocatalytic efficiency of the catalyst was tested via PODS of DBT in a model oil.

Figure 2.2 shows the general photocatalytic process of semiconductor. From the figure below, it can be observed that there was an energy gap between the valence band (VB) and the conduction band (CB). When the photocatalyst was subjected to light irradiation, the electrons (e^-) can be excited from VB to the CB, leaving a hole in the valence band at the same time. The free electrons in the CB reacted with O_2 to produce superoxide radicals ($O_2^{\bullet-}$) which responsible for the pollutant degradation. Then, the holes that present in the VB can react with H_2O to form hydroxyl radicals ($^{\bullet}OH$), which act as an oxidizing agent to oxidize the organic pollutant (Saravanan, Gracia, & Stephen, 2017).

05-4506832 pustaka.upsi.edu.my Perpustakaan Tuanku Bainun Kampus Sultan Abdul Jalil Shah PustakaTBainun ptbupsi

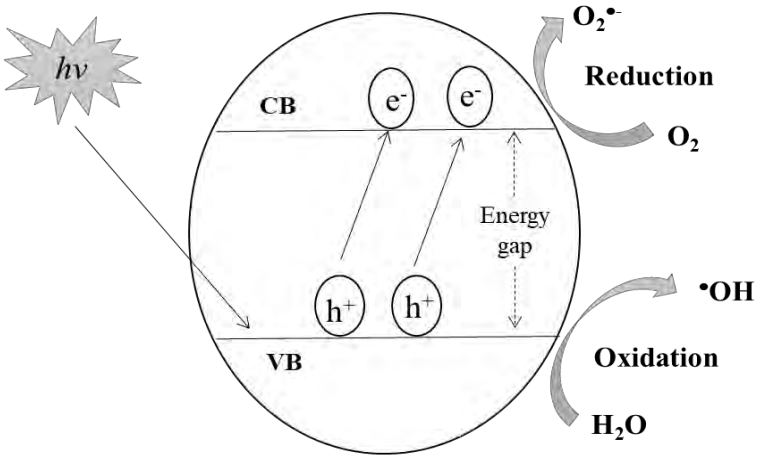


Figure 2.2. General Photocatalytic Process of Semiconductor. Adapted from Saravanan et al., 2017

05-4506832 pustaka.upsi.edu.my Perpustakaan Tuanku Bainun Kampus Sultan Abdul Jalil Shah PustakaTBainun ptbupsi

05-4506832 pustaka.upsi.edu.my Perpustakaan Tuanku Bainun Kampus Sultan Abdul Jalil Shah PustakaTBainun ptbupsi

2.5 Photocatalyst

Nowadays, photocatalysis has been recognized as a potential solution to the growing number of environmental problems due to the development of economy (Chen et al., 2015). According to Geng, Zhang, Li, and Sun (2015), the photocatalyst plays an important role in promoting the efficiency of photocatalytic process. In photocatalytic desulfurization process, the photons from sunlight or other sources can be absorbed by photoactive material known as photocatalyst and relaxation mechanism was utilized to attack sulfur atoms in the petroleum feedstock producing easily separable sulfoxide compositions (Mostafa, El saied, & Morshedy, 2019). In few recent years, PODS has been investigated using heterogenous photocatalyst under suitable light irradiation as a promising type of ODS methods (Kalantari et al., 2016).

05-4506832 pustaka.upsi.edu.my Perpustakaan Tuanku Bainun Kampus Sultan Abdul Jalil Shah PustakaTBainun ptbupsi

Previously, PODS of DBT was widely explored by researchers using different type of photocatalysts. For example, study reported by Zhu et al. (2014) has synthesized amorphous TiO_2 via hydrolysis and calcination method for degradation of DBT under UV light. In this study, the highest removal of DBT was obtained when amorphous TiO_2 was incorporated with ionic liquid and H_2O_2, in which 96.6% of DBT was successfully degraded. In the absence of ionic liquid and H_2O_2, only 1.8% of sulfur removal was obtained, which showed that the synergistic effect of amorphous TiO_2, H_2O_2 and ionic liquid play an important role for the efficiency of photocatalytic activity of DBT degradation. However, the incorporation of amorphous TiO_2 with only H_2O_2 or ionic liquid caused the total removal of DBT obtained to be 4.4% and 18.9%, respectively. This result showed that both of H_2O_2 and ionic liquid were needed to improve the photodesulfurization rate.

05-4506832 pustaka.upsi.edu.my Perpustakaan Tuanku Bainun Kampus Sultan Abdul Jalil Shah PustakaTBainun ptbupsi

05-4506832 pustaka.upsi.edu.my Perpustakaan Tuanku Bainun Kampus Sultan Abdul Jalil Shah PustakaTBainun ptbupsi

Another study from Wang et al. (2012) has reported about the preparation of Nano-TiO_2 in ionic liquid ([Bmim]BF_4) via microwave radiation. The as-prepared TiO_2 was then mixed with DBT in *n*-octane, which act as a model oil for determining the photocatalytic activity of the photocatalyst under UV light. From the result, it can be observed that, the TiO_2 that was microwave-irradiated for 60 min has obtained the highest photocatalytic activity with 88.8% of DBT was successfully removed within 300 min under UV light irradiation. Meanwhile, the TiO_2 that was microwave-irradiated for 20, 40 and 80 min exhibited 43.8%, 70.0% and 75.0% of DBT desulfurization rate, respectively. This indicated that microwave time influenced the physicochemical properties of TiO_2 to improve the efficiency of photocatalytic desulfurization activity.

Then, study reported by Khayyat and Roselin (2017) has synthesized Au nanoparticles doped with TiO_2 (Au/TiO_2) via deposition-precipitation method for photodesulfurization of DBT under UV light irradiation. The photodesulfurization activity was carried out with addition of H_2O_2 as oxidizing agent. From the results obtained, it can be observed that removal of DBT was higher when Au nanoparticles was added into TiO_2 (Au/TiO_2) compared to pure TiO_2, in which 61.0% and 46.0% of DBT was successfully degraded, respectively. The increment in DBT degradation rate was due to the incorporation of Au noble metal into pure TiO_2 that acted as electron traps which in turn will inhibit the recombination of electron and hole pairs. Besides that, Au nanoparticles will also react with H_2O_2 and produce large amount of hydroxyl radicals, that can help to increase the degradation rate of DBT.

05-4506832 pustaka.upsi.edu.my Perpustakaan Tuanku Bainun Kampus Sultan Abdul Jalil Shah PustakaTBainun ptbupsi

05-4506832 pustaka.upsi.edu.my Perpustakaan Tuanku Bainun Kampus Sultan Abdul Jalil Shah PustakaTBainun ptbupsi

Another study by Wang et al. (2014) synthesized TiO_2/gC_3N_4 photocatalyst via two-step method for photodegradation of DBT under irradiation of UV light. From the results, it was observed that 40% of TiO_2/gC_3N_4 exhibited the highest degradation of DBT (98.9%) compared to 40% TiO_2 (79.1%) and pristine gC_3N_4 (1.3%). The photocatalytic performance presented by 40% TiO_2/gC_3N_4 might be due to the synergistic effect between gC_3N_4 and TiO_2 that can perform high separation of photogenerated electron and hole charges, which in turn improved the photodegradation of DBT. Besides, the addition of H_2O_2 as oxidant and suitable metal loading also contributes to the photocatalytic efficiency.

Zhao, Zhang, Wang, Liang, and Li (2009) has synthesized Ti-containing zeolite (Ti/zeolite) as photocatalyst for photodegradation of DBT under UV light. In this study, it was observed that Ti/zeolite exhibited the highest removal of DBT (75.0%) compared to pure TiO_2 (50.0%) with the incorporation of H_2O_2 solution as an oxidant. The highest photocatalytic performance performed by Ti/zeolite could be due to their framework that containing highly dispersed isolated tetrahedral TiO_2 species which will prolong the lifetime of the charge transfer excited state of the photocatalyst and also preventing the agglomeration of TiO_2 from occurred.

Another study reported by Pham, Pham, Nguyen, Tran, and Pham (2018) has synthesized mesoporous Al-MCM-41@Ag/TiO_2 nanocomposite via combining sol-gel and hydrothermal method for photodegradation of DBT under UV light. From this study, it can be observed that Al-MCM-41@Ag/TiO_2 obtained the highest degradation of DBT in which almost 100.0% of DBT was successfully degraded within 120 min at 70 ^{o}C compared to Al-MCM-41@TiO_2 that can only degrade 40% of DBT under the

05-4506832 pustaka.upsi.edu.my Perpustakaan Tuanku Bainun Kampus Sultan Abdul Jalil Shah PustakaTBainun ptbupsi

05-4506832 pustaka.upsi.edu.my Perpustakaan Tuanku Bainun Kampus Sultan Abdul Jalil Shah PustakaTBainun ptbupsi

same conditions. The photocatalytic efficiency showed by Al-MCM-41@Ag/TiO_2 might be due to its strong light absorption ability, in which the presence of Al-MCM-41 will promote high surface area for dispersing the catalytic activity center, thus enhanced the photoactivity. Then, the incorporation of Ag nanoparticles provide electron mobility that facilitate the surface charge transfer to the boundary and increased the separation of photogenerated charges.

Next, previous study reported by Hosseini et al. (2018) has synthesized ZnO/FSM-16 as a photocatalyst for photodegradation of DBT under irradiation of UV light. From the results obtained, it was observed that ZnO/FSM-16 exhibited the highest degradation of DBT (60%) compared to bulk ZnO that only achieved 45% of DBT degradation. The efficient result could be due to the incorporation of catalyst support that help the uniform distribution of ZnO particles on the surface of the support, and thus facilitate the direct interaction between the generated radicals and pollutant molecules. On the other hand, the presence of support also inhibit the recombination of electron and hole charges which in turn will improve the photodegradation performance. In this study, it also proved that the degradation efficiency was influenced by the surface area of photocatalysts, in which ZnO/FSM-16 exhibited larger surface area than ZnO. The surface area obtained for both ZnO/FSM-16 and ZnO photocatalysts were 823.15 m^2/g and 79.13 m^2/g, respectively. However, the optimization of ZnO loading from 3-25% played an important role to improve the degradation rate of DBT. It was observed that 20% of ZnO loading into FSM-16 exhibited the highest degradation activity in which 80% of DBT removal was successfully obtained.

05-4506832 pustaka.upsi.edu.my Perpustakaan Tuanku Bainun Kampus Sultan Abdul Jalil Shah PustakaTBainun ptbupsi

05-4506832 pustaka.upsi.edu.my Perpustakaan Tuanku Bainun Kampus Sultan Abdul Jalil Shah PustakaTBainun ptbupsi

All the previous reported photocatalysts used for PODS of DBT in model oil mentioned above were summarized in Table 2.1.

Table 2.1

List of Catalysts that have been used for PODS of DBT

No.	Catalyst	Pollutant	Reaction condition	Photocatalytic performance (%)	Findings
1	Amorphous TiO_2	DBT	-UV light -H_2O_2: 2:1 -[Bmim]BF_4: 1 mL -Temp.: 30 ^oC -Time: 120 min	Amorphous TiO_2: 96.6	Zhu et al. (2014)
2	Nano-TiO_2	DBT	-UV light -[Bmim]BF_4: 10 mL -Microwave-irradiated time: 20, 40, 60 and 80 min -Time: 300 min	TiO_2 1 (20 min): 43.8 TiO_2 2 (40 min): 70.0 TiO_2 3 (60 min): 88.8 TiO_2 4 (80 min): 75.0 P25: 45.2	Wang et al. (2012)
3	Au/TiO_2	DBT	-UV light -Conc.: 1, 1.5, 2, 2.5 and 3 at% of Au -H_2O_2: 3:1 -Time: 180 min	TiO_2: 46.0 2.5 at% Au/TiO_2: 61.0	Khayyat and Roselin (2017)

(continue)

05-4506832 pustaka.upsi.edu.my Perpustakaan Tuanku Bainun Kampus Sultan Abdul Jalil Shah PustakaTBainun ptbupsi

05-4506832 pustaka.upsi.edu.my Perpustakaan Tuanku Bainun Kampus Sultan Abdul Jalil Shah PustakaTBainun ptbupsi

Table 2.1 *(continued)*

No.	Catalyst	Pollutant	Reaction condition	Photocatalytic performance (%)	Findings
4	TiO_2/gC_3N_4	DBT	-UV light -Conc.: 40% of TiO_2 -Temp.: 30 ^oC - H_2O_2: 6:1 -Time: 120 min	gC_3N_4: 1.3 40% TiO_2: 79.1 40% TiO_2/gC_3N_4: 98.9	Wang et al. (2014)
5	Ti/zeolite	DBT	-UV light -Catalyst amount: 0.1 g -H_2O_2: 3 mL -Time: 160 min	TiO_2: 50.0 Ti/zeolite: 75.0	Zhao et al. (2009)
6	Al-MCM-41@Ag/TiO_2	DBT	-UV light -Catalyst dosage: 0.1 g/L -Temp.: 30-70 ^oC -Time: 120 min	Al-MCM-41@TiO_2 (70 ^oC): 40.0 Al-MCM-41@Ag/TiO_2 (70 ^oC): 100.0	Pham et al. (2018)
7	ZnO/FSM-16	DBT	-UV light -Loading.: 3, 5, 10, 15, 20 and 25% of ZnO -Catalyst dosage: 0.05-0.4 g/L -Time: 550 min	Bulk ZnO: 45.0 ZnO/FSM-16 (3%): 25.0 ZnO/FSM-16 (5%): 40.0 ZnO/FSM-16 (10%): 60.0	Hosseini et al. (2018)

(continue)

05-4506832 pustaka.upsi.edu.my Perpustakaan Tuanku Bainun Kampus Sultan Abdul Jalil Shah PustakaTBainun ptbupsi

05-4506832 pustaka.upsi.edu.my Perpustakaan Tuanku Bainun Kampus Sultan Abdul Jalil Shah PustakaTBainun ptbupsi

Table 2.1 *(continued)*

No.	Catalyst	Pollutant	Reaction condition	Photocatalytic performance (%)	Findings
				ZnO/FSM-16 (15%): 72.0 ZnO/FSM-16 (20%): 80.0 ZnO/FSM-16 (25%): 75.0	

Based on Table 2.1 above, it clarifies that the incorporation of metal doping and catalyst support can increase the number of active sites on the photocatalyst surface and the exposed surface area. However, the degradation rate decreases when the amount of catalyst loading increases above the optimum value and it was due to the interception of light by the suspension (Chanu, Singh, Singh, & Devi, 2019; Hassena, 2016). Besides that, further addition of catalyst loading beyond the optimum value will cause the agglomeration of catalyst particles to occur and in turn will decrease the degradation rate of catalyst as more of its surface become unavailable for photo absorption (Hassena, 2016). This finding was supported by El-Yazeed and Ahmed (2019) which stated that the photodegradation was decreased as the increasing addition of WO_3 particles cause the agglomeration on TiO_2 surface.

05-4506832 pustaka.upsi.edu.my Perpustakaan Tuanku Bainun Kampus Sultan Abdul Jalil Shah PustakaTBainun ptbupsi

05-4506832 pustaka.upsi.edu.my Perpustakaan Tuanku Bainun Kampus Sultan Abdul Jalil Shah PustakaTBainun ptbupsi

2.6 TiO_2 as a photocatalyst

To the best of our knowledge, the most frequently used photocatalyst for the treatment of pollutants was TiO_2 due to its well-known efficiency and near-universal applications (Reddy et al., 2016). This finding was supported by Noor, Sidik, Rosmi, Hitam, and Jaafar (2022); Khalid, Majid, Tahir, Niaz, and Khalid (2017) which stated that, the interest in TiO_2 as an ideal photocatalyst for various environmental applications was mainly due to its natural abundance, chemical stability, non-toxicity and high oxidative power of its photogenerated holes.

For example, a research reported by Abdennouri et al. (2016) has synthesized TiO_2 and titanium pillared purified clay which were prepared via sol-gel method and ion exchange reaction, respectively. These catalysts were used for the photodegradation of selected pesticides consisted of 2,4-dichlorophenoxyacetic acid (2,4-D) and 2,4-dichlorophenoxypropionic acid (2,4-DP) as models of target pollutants. The results showed that the pesticides were efficiently degraded by these photocatalysts under UV irradiation in which TiO_2 exhibited higher photocatalytic activity than the pillared clay samples. Besides, another study reported by synthesized TiO_2 nanotube (TNT) and TiO_2 nanofiber (TNF) coatings for the photodegradation of methylene blue (MB) with the irradiation of UV light. The findings showed TNF coatings exhibited more excellent photoactivity than TNT coatings. These studies have proven that TiO_2 was one of the most well-known and promising semiconducting elements for decomposing organic compounds (Szczepanik, 2017).

05-4506832 pustaka.upsi.edu.my Perpustakaan Tuanku Bainun Kampus Sultan Abdul Jalil Shah PustakaTBainun ptbupsi

05-4506832 pustaka.upsi.edu.my Perpustakaan Tuanku Bainun Kampus Sultan Abdul Jalil Shah PustakaTBainun ptbupsi

However, due to its wide band gap (3.2 eV) and low separation of electron-hole pairs making TiO_2 only responds to UV irradiation which limit its practical use to some extent (Azami et al., 2020; Hitam et al., 2018; Mohamed et al., 2017). This finding was supported by Parangi and Mishra (2019) which stated that pure TiO_2 exhibited low light absorption capacity and low charge separation adaptability that caused the limitations to occur under normal conditions. Therefore, great effort towards the improvement of its photoactivity has been done extensively (Hitam et al., 2018). In the improvement of the photocatalytic activity of TiO_2, different modification approaches like modifying the structure, surface and morphological properties, increase the external surface area and generating the structure defects have been applied extensively (Anandan, Sivasankar, & Lana-Villarreal, 2014). On the other hand, different synthesize methods and materials used to synthesize TiO_2 photocatalyst could also help in the improvement of its photocatalytic performance.

2.7 Modification of TiO_2 photocatalyst

Researchers have studied numerous ways to improve the photocatalytic efficiency and there has been extensive efforts in the modification of the photocatalysts. Many efforts on the modification of bare TiO_2 has been focused on the exploration of different synthesize method, different synthesize materials, use of mesoporous structure, addition of metal and incorporation of dopant.

05-4506832 pustaka.upsi.edu.my Perpustakaan Tuanku Bainun Kampus Sultan Abdul Jalil Shah PustakaTBainun ptbupsi

05-4506832 pustaka.upsi.edu.my Perpustakaan Tuanku Bainun Kampus Sultan Abdul Jalil Shah PustakaTBainun ptbupsi

2.7.1 TiO_2 synthesize method

Extensive literature analysis has shown that the efficiency of photodecomposition of organic compounds by using TiO_2 was affected by the synthesize method. There were various synthesize methods like hydrothermal, sol-gel, electrochemical anodization and electrospinning have been applied to synthesize the TiO_2-based photocatalyst.

2.7.1.1 Hydrothermal method

Hydrothermal method was a heterogeneous reaction that usually conducted in autoclaves with or without Teflon liners in the presence of aqueous solutions under a temperature or pressure that was closely monitored. The aqueous solvents were usually used under high temperature (between 100 ^{o}C-1000 ^{o}C) and pressure (between 1 atm-10 000 atm) that help to enhance the interaction of precursors during synthesize process (Kumar & Pandey, 2018). Figure 2.3 shows the proposed schematic illustration of the synthesizing process of TiO_2 via hydrothermal method described by Subramaniam et al. (2017).

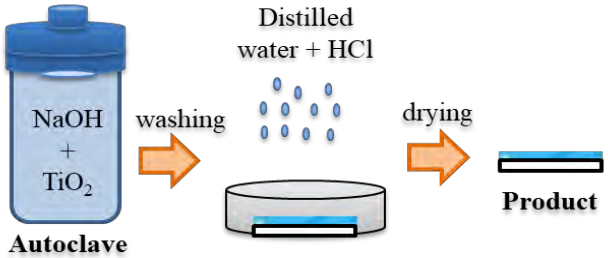


Figure 2.3. Schematic Illustration of Synthesizing Process of TiO_2 via Hydrothermal Method

05-4506832 pustaka.upsi.edu.my Perpustakaan Tuanku Bainun Kampus Sultan Abdul Jalil Shah PustakaTBainun ptbupsi

05-4506832 pustaka.upsi.edu.my Perpustakaan Tuanku Bainun Kampus Sultan Abdul Jalil Shah PustakaTBainun ptbupsi

From the study, Subramaniam and co-workers was successfully synthesized TiO_2 in the form of nanotubes (TNT) that having surface area ranged from 20 m^2/g to 200 m^2/g. From the results obtained, 90% removal of MB was achieved by TNT24 within 120 min under UV irradiation which was two times better than the commercial TiO_2 nanoparticle as only 50% of MB was removed within the same duration of time. The higher degradation of MB was achieved by TNT. This was due to the higher effective surface areas and tubular structure of TNT.

2.7.1.2 Electrochemical anodization method

Another method reported to successfully synthesize TiO_2 was electrochemical anodization method. This method usually uses one from the three electrode configurations which were, a working electrode, a counter electrode and a reference electrode in an aqueous electrolyte to fabricate one dimension TiO_2 nanostructures. The schematic illustration of the system was shown in Figure 2.4.

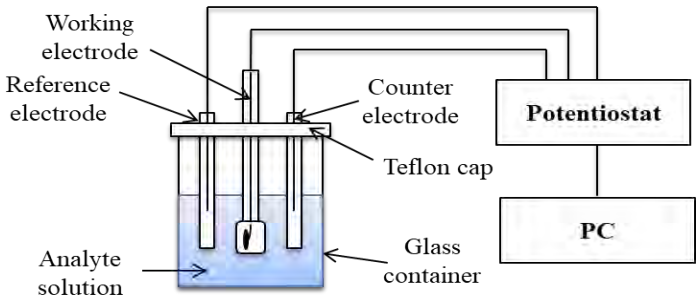


Figure 2.4. Schematic Illustration of Electrochemical Anodization Process with Three-Electrode Measurement System

05-4506832 pustaka.upsi.edu.my Perpustakaan Tuanku Bainun Kampus Sultan Abdul Jalil Shah PustakaTBainun ptbupsi

05-4506832 pustaka.upsi.edu.my Perpustakaan Tuanku Bainun Kampus Sultan Abdul Jalil Shah PustakaTBainun ptbupsi

Arfanis et al. (2017) was successfully synthesized a TNT film by using this method. Then, Nasr, Eid, Habchi, Miele, and Bechelany (2018) managed to produce a highly ordered and oriented TNT and TiO_2 nanorod (TNR) arrays. In this study, the desired length of TNTs was obtained by varying the anodization time from 30 min to 120 min among different samples. The as-synthesized photocatalyst formed a higher amount of photocatalytic active sites and exhibited efficient adsorption of the contaminants since they had an open porous structure with higher surface area. The excellent photocatalytic activity was shown by TNT films with a length of 10 μm for both emerging contaminants caffeine (51%) and salicylic acid (50%), respectively under UV light irradiation. From the observed band gap, it also showed that the longer nanotube films exhibited narrower band gap than the shortest one, thus enhanced the light absorption in the UV region.

05-4506832 pustaka.upsi.edu.my Perpustakaan Tuanku Bainun Kampus Sultan Abdul Jalil Shah PustakaTBainun ptbupsi

2.7.1.3 Electrospinning method

Electrospinning method has been widely used to produce nanofibers with various functions from a variety of polymers, sol-gels, ceramics and composites due to its versatile and cost-effective technique. In this technique, high voltage was applied to give the ejection of a viscous liquid jet via a spinneret for the direct movement of charged molecules. The setup of electrospinning usually involves three major components: high voltage power supply, syringe pump and collector (Nasr et al., 2018). Figure 2.5 illustrates the setup of electrospinning process.

05-4506832 pustaka.upsi.edu.my Perpustakaan Tuanku Bainun Kampus Sultan Abdul Jalil Shah PustakaTBainun ptbupsi

05-4506832 pustaka.upsi.edu.my Perpustakaan Tuanku Bainun Kampus Sultan Abdul Jalil Shah PustakaTBainun ptbupsi

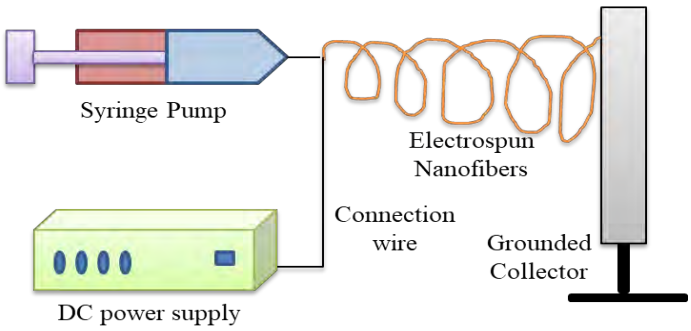


Figure 2.5. Schematic Illustration of the Setup of Electrospinning Process

Nasr et al. (2017) reported on a study of synthesizing TNF using electrospinning technique. In this study, it was discovered that the synthesized photocatalyst has exhibited 19.66 m^2/g of surface area and 16.4 nm of grain size. The degradation rate of methyl orange (MO) performed by the catalyst with UV light irradiation was used as a benchmark to measure the efficiency of photocatalytic performance. From the results obtained, the degradation of MO by pure TNF was higher than the commercial TiO_2 P25 in which 65% and 60% of MO has been decomposed, respectively. The excellent result could be attributed to the larger surface area of pure TNF compared to commercial TiO_2 P25 that has enhanced its photodegradation activity. The band gap value observed for pure TNF was 3.2 eV, and thus it performed well under UV irradiation.

05-4506832 pustaka.upsi.edu.my Perpustakaan Tuanku Bainun Kampus Sultan Abdul Jalil Shah PustakaTBainun ptbupsi

05-4506832 pustaka.upsi.edu.my Perpustakaan Tuanku Bainun Kampus Sultan Abdul Jalil Shah PustakaTBainun ptbupsi

2.7.1.4 Sol-gel method

Sol-gel method has also gained researchers attention to prepare nano-materials since it can be done under simple process with lower temperatures. In this method, the formation of a colloidal solution was occurred as it involved hydrolysis of a titanium alkoxide and then followed by condensation. Then, a gel was obtained after applying the heat treatment, in which the process was illustrated in Figure 2.6.

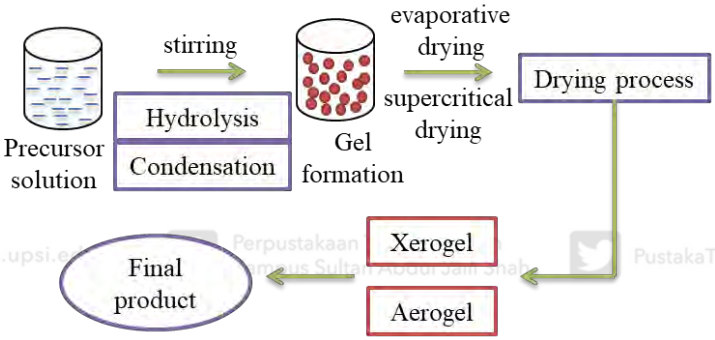


Figure 2.6. Schematic Illustration of Sol-Gel Process

Adding of an acidic or basic such as hydrochloric acid (HCl) or sodium hydroxide (NaOH), respectively, could help to accelerate the reaction (Nasr et al., 2018). Arfanis et al. (2019) reported about the synthesized of novel core-shell TiO_2 nanomaterials ($CSTiO_2$) via one-step smoldering combustion sol-gel method. In this study, caffeine, salicylic acid and hexavalent chromium (Cr(VI)) were degraded below UV illumination to elucidate the efficiency of the photocatalyst. From the results obtained, 65% of caffeine and salicylic acid have been removed in 120 min and 60 min, respectively using $CSTiO_2$ compared to pure TiO_2 that only degraded

05-4506832 pustaka.upsi.edu.my Perpustakaan Tuanku Bainun Kampus Sultan Abdul Jalil Shah PustakaTBainun ptbupsi

05-4506832 pustaka.upsi.edu.my Perpustakaan Tuanku Bainun Kampus Sultan Abdul Jalil Shah PustakaTBainun ptbupsi

30% of the pollutants under the same irradiation time. Meanwhile, for Cr(VI), efficient degradation has been obtained in which the pollutant was almost completely decomposed by the photocatalyst in 10 min. The excellent degradation results were obtained through the addition of urea that has enhanced TiO_2 photocatalytic activity. Besides that, the larger specific surface area of $CSTiO_2$ (175 m^2/g) compared to pure TiO_2 (48.6 m^2/g) also helped to improve the photocatalytic activity as more photoexcited electrons will be formed to inhibit the recombination of charge carriers.

2.7.2 TiO_2 synthesize materials

The efficient performance of photocatalysts also depends on the materials being used during the synthesizing processes. The materials properties can help to produce the photocatalysts with desired structures, morphology, crystallinity and surface area.

The study reported by Subramaniam et al. (2017) stated that the materials used to synthesize TNT were commercial TiO_2 P25 Degussa nanoparticles, NaOH and HCl. In this research, commercial TiO_2 was added at first into NaOH solution and then constantly stirred for 4 h. The suspension was formed during the stirring process and then it underwent hydrothermal treatment by transferring it into a Teflon-lined autoclave container, securely sealed and put in an oven at 180 ^oC. The different reaction times for hydrothermal treatment was done in order to diversify the effective surface areas of TNT. The product formed was treated with HCl solution overnight

05-4506832 pustaka.upsi.edu.my Perpustakaan Tuanku Bainun Kampus Sultan Abdul Jalil Shah PustakaTBainun ptbupsi

05-4506832 pustaka.upsi.edu.my Perpustakaan Tuanku Bainun Kampus Sultan Abdul Jalil Shah PustakaTBainun ptbupsi

before washing using 5 L bottle tap water until the decanter water reached the pH 7. Lastly, the sample formed was filtered, dried at 60 ^{o}C and grounded to fine particles.

Arfanis et al. (2017) synthesized TNT films by using titanium foils, Pt mesh, ethylene glycol, distilled water and ammonium fluoride (NH_4F). First of all, both of the electrodes which were free surfaces of 1.32 cm^2 from 20×20×0.125 mm titanium foils as the anodic electrode and a Pt mesh as the counter electrode were immersed into an organic electrolyte consisting of 98% vol. ethylene glycol, 2% vol. distilled water and 0.3% wt NH_4F. The anodization process was conducted under galvanostatic conditions in a lab-made Teflon cell by using 3.15 mA cm^{-2} with an Autolab PGSTAT-30 potentiostat (Ecochemie).

05-4506832 pustaka.upsi.edu.my Perpustakaan Tuanku Bainun Kampus Sultan Abdul Jalil Shah PustakaTBainun ptbupsi

Another study by Nasr et al. (2017) synthesized pure TNF using titanium tetraisopropoxide (TTIP), polyvinylpyrrolidone (PVP), absolute ethanol and acetic acid. In this study, the viscous solution required for electrospinning was initially prepared. First, TTIP was added into the mixture of 2 mL of acetic acid, 3 mL of ethanol and 0.3 g of PVP. Then, the mixture solution was stirred for 1 h at room temperature to ensure it dissolved well. The homogeneous solution was then transferred into the syringe pump. After applying a DC voltage at 25 kV and 20 cm working distances, the solution was electrospun and a fibrous mesh was formed on the grounded collector. Lastly, the sample was calcined at 500 ^{o}C for 5 h by using tubular furnace.

05-4506832 pustaka.upsi.edu.my Perpustakaan Tuanku Bainun Kampus Sultan Abdul Jalil Shah PustakaTBainun ptbupsi

05-4506832 pustaka.upsi.edu.my Perpustakaan Tuanku Bainun Kampus Sultan Abdul Jalil Shah PustakaTBainun ptbupsi

In other study, Arfanis et al. (2019) synthesized $CSTiO_2$ via one-step smoldering combustion sol-gel method. The materials to synthesize this photocatalyst consisted of titanium (IV) butoxide (TBOT), nitric acid solution (HNO_3), n-propanol and urea. First of all, 7.5 mL of TBOT was mixed together with 50 mL of HNO_3 aqueous solution and was put under vigorous stirring until it completely dissolved. After 4 h of stirring, 15 mL of n-propanol was added and turned the emulsion into transparent solution. The solution was left overnight under stirring to make it become homogenized. In this study, urea acted as the nitrogen source in which 15 g of urea added into the solution. Finally, the viscous product was obtained by gradually drying the solution at 100 ^{o}C and calcined for 2 h at 400 ^{o}C. The sample was grinded to fine powder after using the calcination process and deionized water for the purpose of eliminating the surplus organic species from the surface. The synthesized sample was represented as $CSTiO_2$. From the reported studies, it can be concluded that the synthesize materials being used were important in order to produce the desired structure of TiO_2 photocatalyst.

2.7.3 Mesoporous structure

Excellent results in photodegradation of organic pollutants usually can be achieved with large surface area and high porosity of TiO_2. Recently, ordered mesoporous TiO_2 films and powders has gained researchers attention as a potential photocatalyst due to their large surface area, tunable pore diameter and nano-confined effects (Zhang et al., 2020; Ovodok et al., 2017). According to Zhang et al. (2020), the large surface areas

05-4506832 pustaka.upsi.edu.my Perpustakaan Tuanku Bainun Kampus Sultan Abdul Jalil Shah PustakaTBainun ptbupsi

05-4506832 pustaka.upsi.edu.my Perpustakaan Tuanku Bainun Kampus Sultan Abdul Jalil Shah PustakaTBainun ptbupsi

help to provide a huge number of active sites which promotes the adsorption and reaction of reactants. Besides, the transport of chemicals in the bulk of TiO_2 materials can be facilitated through produced large pore volumes which enable the accessibility of active sites. On the other hand, the use of mesoporous supports or nano-sized materials can also increase the interaction between target reactant and photocatalyst (Reddy, Kavitha, Reddy, & Kim, 2017). Utilization of a certain synthesize techniques have extremely affected the properties of mesoporous TiO_2 (Niu, Wang, Wu, He, & Zhang, 2018). Mesoporous TiO_2 were commonly prepared via sol-gel, solvothermal, hydrothermal and microwave-assisted methods (Niu et al., 2018; Bagheri, Hir, Yousefi, & Hamid, 2015).

Sol-gel method was first introduced by Antonelli and Ying in 1995 to synthesize mesoporous TiO_2. Preparation of mesoporous TiO_2 via sol-gel method has gained attention as the most common and versatile way since it uses low synthesize temperature and also it was easier to be carried out compared to when it was in a solid state. Besides, variety of new mesoporous TiO_2 can be prepared according to appropriate conditions. However, sol-gel process was slower in the time sense as it takes days or weeks to finish the preparation of mesoporous TiO_2. Chowdhury and Naskar (2018) reported that sol-gel technique was applied to synthesize the mesoporous hollow TiO_2 microspheres for photodegradation of 4-chlorophenol (4-CP) under UV irradiation. From the result obtained, 90% of 4-CP has been successfully degraded in 60 min. The outstanding photocatalytic performance could be attributed from inorganic hollow spheres, which was known to promote several advantages like high surface area, low compactness, mechanical and thermal stability and surface permeability. In this work, copper hydroxycarbonate ($Cu_2(OH)_2CO_3$)

05-4506832 pustaka.upsi.edu.my Perpustakaan Tuanku Bainun Kampus Sultan Abdul Jalil Shah PustakaTBainun ptbupsi

05-4506832 pustaka.upsi.edu.my Perpustakaan Tuanku Bainun Kampus Sultan Abdul Jalil Shah PustakaTBainun ptbupsi

microsphere was used as a precursor. The mesoporous TiO_2 hollow microspheres were obtained after calcined at 400 ^oC at a heating rate of 1 ^oC/min and a dwell time of 2 h. From the characterization results, it was evident that the Brunauer-Emmett-Teller (BET) surface area, total pore volume and average pore diameter of the synthesized photocatalyst were 74.52 m^2/g, 0.23 cm^3/g and 12.37 nm, correspondingly. It also showed that, the band gap of the photocatalyst was 3.06 eV, and thus it performed well under UV irradiation.

Hydrothermal method was an environmental friendly technique and usually used for the large scale production of mesoporous TiO_2. Besides, it also does not require any post-calcination treatment, make use of aqueous solutions and facile recovery of the photocatalyst can be done after synthesizing process. This method was typically carried out in an autoclave provided with Teflon liners and a closed system under controlled temperature and pressure (Petronella et al., 2019). From a study reported by Chowdhury, Ghosh, and Naskar (2016), hydrothermal pathway was used to obtain mesoporous anatase TiO_2 in which titanium (IV) oxysulfate (TIOS), urea and sodium dodecyl sulfate (SDS) were used under aqueous medium at 180 ^oC for 24 h. From the characterization results obtained in this study, the surface area, pore volume and pore diameter of mesoporous TiO_2 were 158 $m^{2/}g$, 0.53 cm^3/g and 24.4 nm, correspondingly. In this study, the efficiency of synthesized mesoporous TiO_2 was observed through photodegradation of MB under UV and visible light. From the findings, it indicated the degradation rate of MB under UV was efficient by using the synthesized mesoporous TiO_2 in which 85-86% of MB was removed after 60 min of irradiation. However, less amount of MB was degraded by synthesized mesoporous

05-4506832 pustaka.upsi.edu.my Perpustakaan Tuanku Bainun Kampus Sultan Abdul Jalil Shah PustakaTBainun ptbupsi

05-4506832 pustaka.upsi.edu.my Perpustakaan Tuanku Bainun Kampus Sultan Abdul Jalil Shah PustakaTBainun ptbupsi

TiO_2 under visible light in which only 14-18% of MB was degraded because of the low photoexcitation as it has wide band gap which was 3.18 eV.

Nowadays, synthesize of mesoporous TiO_2 via microwave-assisted method has gained attention among researchers due to its several advantages such as shorter reaction times, volumetric heating ability and can start heating from interior of material body. Besides, this method was frequently applied to obtain smaller particle sizes and high purity materials (Bagheri et al., 2015). Jaafar, Jalil, Triwahyono, and Shamsuddin (2015) reported that MTN had been synthesized via microwave-assisted method by varying the power densities of microwave with 0.12, 0.37 and 0.56 W/g, and represented as T1, T2 and T3, correspondingly. Figure 2.7 illustrates the process of synthesize MTN via microwave-assisted method.

05-4506832 pustaka.upsi.edu.my Perpustakaan Tuanku Bainun Kampus Sultan Abdul Jalil Shah PustakaTBainun ptbupsi

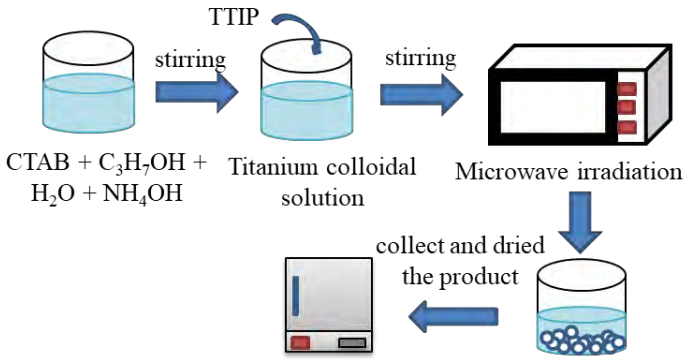


Figure 2.7. Schematic Illustration of Synthesizing MTN via Microwave-Assisted Method

The characterization results illustrated that MTN synthesized with higher power density was obtained larger surface area, high crystallinity, smaller particle size and low band gap. The study reported that the surface areas of T1, T2 and T3 were

05-4506832 pustaka.upsi.edu.my Perpustakaan Tuanku Bainun Kampus Sultan Abdul Jalil Shah PustakaTBainun ptbupsi

05-4506832 pustaka.upsi.edu.my Perpustakaan Tuanku Bainun Kampus Sultan Abdul Jalil Shah PustakaTBainun ptbupsi

152, 161 and 187 m^2/g, respectively, while the particle size was slightly decreased with 13.25, 12.24 and 11.36 nm, respectively, as the microwave power density was increased. The band gap value was also decreased for T3 compared to T1, T2 and commercial TiO_2 which exhibited 3.10 eV, 3.18 eV, 3.12 eV and 3.22 eV, respectively. Then, T1 showed the large total pore volume with 0.44 cm^3/g, followed by T2 and T3 with 0.42 and 0.36 cm^3/g, respectively. In this study, the efficiency of each synthesized MTN was examined through the degradation of 2-chlorophenol (2-CP) under irradiation of visible light and commercial TiO_2 was used as a reference photocatalyst. From the results obtained, the highest degradation was demonstrated by T3 in which 96% of 2-CP was successfully degraded under visible light. Meanwhile, the T2, T1 and commercial TiO_2 showed only 88%, 84% and 69%, respectively. The efficiency of MTN compared to commercial was due to the presence of oxygen vacancies (OV) and Ti^{3+} site defects (TSD) that were formed during the microwave heating. The OV and TSD helped in lowering the band gap and also operated as electron traps inhibiting the electron-hole recombination, and offered good charge carrier migration for the enhancement of photoactivity. Figure 2.8 illustrates the photocatalytic mechanisms of MTN via microwave-assisted method.

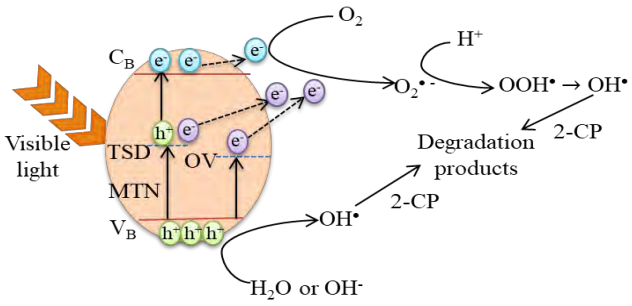


Figure 2.8. Schematic Illustration of Photocatalytic Mechanism of MTN via Microwave-Assisted Method. Adapted from Jaafar et al., 2015

05-4506832 pustaka.upsi.edu.my Perpustakaan Tuanku Bainun Kampus Sultan Abdul Jalil Shah PustakaTBainun ptbupsi

05-4506832 pustaka.upsi.edu.my Perpustakaan Tuanku Bainun Kampus Sultan Abdul Jalil Shah PustakaTBainun ptbupsi

A study from Anjugam Vandarkuzhali et al. (2018) highlighted the synthesized of mesoporous TiO_2 nanospheres by using solvothermal method. Solvothermal synthesize technique was often used to synthesize mesoporous materials with controlled size and high crystallinity as it can be conducted under mild reaction condition. The solvothermal pathway was nearly the same like the hydrothermal analogue apart from the solvent being used which was non-aqueous. The temperature in solvothermal reaction was practically higher than in hydrothermal method since the chosen living solvent used often has a high boiling point (Niu et al., 2018; Byranvand, Nemati Kharat, Fatholahi, & Beiranvand, 2013). Figure 2.9 shows the proposed schematic illustration of the synthesizing process of mesoporous TiO_2 through solvothermal method.

05-4506832 pustaka.upsi.edu.my Perpustakaan Tuanku Bainun Kampus Sultan Abdul Jalil Shah PustakaTBainun ptbupsi

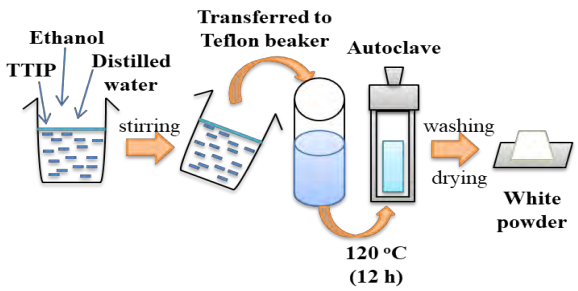


Figure 2.9. Schematic Illustration of Synthesizing Mesoporous TiO_2 via Solvothermal Method

The characterization results demonstrated that the surface area, pore volume and pore size of mesoporous TiO_2 nanospheres were 173 m^2/g, 0.30 cm^3/g and 3.3 nm, respectively, which confirmed that mesoporous had a well-ordered nature. The band gap value observed for mesoporous TiO_2 nanospheres was 3.16 eV. In this study, the efficiency of photocatalytic activity was determined through the

05-4506832 pustaka.upsi.edu.my Perpustakaan Tuanku Bainun Kampus Sultan Abdul Jalil Shah PustakaTBainun ptbupsi

05-4506832 pustaka.upsi.edu.my Perpustakaan Tuanku Bainun Kampus Sultan Abdul Jalil Shah PustakaTBainun ptbupsi

degradation rate of textile dyes, which were congo red (CR), MO, acid orange 10 (AO10) and remazol red (RR) below solar and visible light irradiations. The results show that, the photocatalytic activity of mesoporous TiO_2 nanospheres was more active than TiO_2 P25 Degussa. It was evident when the degradation rate of CR, MO, AO10 and RR were higher by using mesoporous TiO_2 nanospheres in which 62%, 70%, 50% and 72% of degradation has been achieved in 60 min respectively. Meanwhile, TiO_2 P25 Degussa only exhibited 50%, 62%, 42% and 68% of photodegradation, respectively. It clearly indicates that the photocatalytic reaction has been enhanced through the occurrence of anatase phase in the mesoporous TiO_2 structure by utilizing dye-sensitized mechanism that consists of continuous framework build by small particles and mesoporous nature with the large surface area and provide active sites for dye adsorption. A summary of modification of bare TiO_2 photocatalyst was shown in Table 2.2.

05-4506832 pustaka.upsi.edu.my Perpustakaan Tuanku Bainun Kampus Sultan Abdul Jalil Shah PustakaTBainun ptbupsi

05-4506832 pustaka.upsi.edu.my Perpustakaan Tuanku Bainun Kampus Sultan Abdul Jalil Shah PustakaTBainun ptbupsi

Table 2.2

Summary of Modification of Bare TiO_2 Photocatalyst

Photocatalyst	Synthesize method	Synthesize materials	Properties			Band gap	Pollutant	Photocatalytic performance (%)	References
			Particle size	Surface area	Pore volume				
TNT	Hydrothermal	Commercial TiO_2 P25 Degussa nanoparticles, HCl and NaOH	The internal diameter of TNT was in the range from 9.44 nm to 16.90 nm	Surface area of TNT formed from 20 m^2/g to 200 m^2/g	-Pore volume from 0.06 cm^3/g to 0.33 cm^3/g -Pore size from 4.64 nm to 11.61 nm	-	MB	Light source: UV light MB: 90% in 120 min	Subramaniam et al. (2017)
TNT	Electro-chemical anodization	Titanium foils, Pt mesh, ethylene glycol, distilled water	TNT with tube lengths from 1.5 μm to 20 μm	Present open porous structure with large surface area	-	Longer TNT films has narrower band gap	Caffeine and salicylic acid	Light source: UV light Caffeine: 51% in 240 min	Arfanis et al. (2017)

(continue)

05-4506832 pustaka.upsi.edu.my Perpustakaan Tuanku Bainun Kampus Sultan Abdul Jalil Shah PustakaTBainun ptbupsi

05-4506832 pustaka.upsi.edu.my Perpustakaan Tuanku Bainun Kampus Sultan Abdul Jalil Shah PustakaTBainun ptbupsi

Table 2.2 *(continued)*

Photocatalyst	Synthesize method	Synthesize materials	Properties			Band gap	Pollutant	Photocatalytic performance (%)	References
			Particle size	Surface area	Pore volume				
		and NH_4F						Salicylic acid: 50% in 240 min	
TNF	Electro-spinning	TTIP, PVP, absolute ethanol and acetic acid	The grain size of TNF formed was 16.4 nm	Surface area of photocatalyst was 19.66 m^2/g	-	3.20 eV	MO	Light source: UV light MO: 65% in 75 min	Nasr et al. (2017)
$CSTiO_2$	Combustion sol-gel	TBOT, HNO_3, n-propanol and urea	Features an amorphous shell of approximately 1 nm thickness	Surface area of $CSTiO_2$ was 175 m^2/g	-	-	Caffeine, salicylic acid and Cr(VI)	Light source: UV light Caffeine: 65% in 120 min	Arfanis et at. (2019)

(continue)

05-4506832 pustaka.upsi.edu.my Perpustakaan Tuanku Bainun Kampus Sultan Abdul Jalil Shah PustakaTBainun ptbupsi

05-4506832 pustaka.upsi.edu.my Perpustakaan Tuanku Bainun Kampus Sultan Abdul Jalil Shah PustakaTBainun ptbupsi

Table 2.2 *(continued)*

Photocatalyst	Synthesize method	Synthesize materials	Properties			Band gap	Pollutant	Photocatalytic performance (%)	References
			Particle size	Surface area	Pore volume				
								Salicylic acid: 65% in 60 min Cr(VI): 99% in 10 min	
Mesoporous hollow TiO_2 microspheres	Sol-gel	$Cu_2(OH)_2CO_3$, titanium isopropoxide (TIP), ethanol and HCl	Hollow spherical shaped particles of size 2-4 μm	Surface area of photocatalyst was 74.52 m^2/g	-Pore volume of photocatalyst was 0.23 cm^3/g -Pore size of photocatalyst was 12.37 nm	3.06 eV	4-CP	Light source: UV light 4-CP: 90% in 60 min	Chowdhury and Naskar (2018)

(continue)

05-4506832 pustaka.upsi.edu.my Perpustakaan Tuanku Bainun Kampus Sultan Abdul Jalil Shah PustakaTBainun ptbupsi

05-4506832 pustaka.upsi.edu.my Perpustakaan Tuanku Bainun Kampus Sultan Abdul Jalil Shah PustakaTBainun ptbupsi

Table 2.2 *(continued)*

Photocatalyst	Synthesize method	Synthesize materials	Properties			Band gap	Pollutant	Photocatalytic performance (%)	References
			Particle size	Surface area	Pore volume				
Mesoporous anatase TiO_2	Hydrothermal	TIOS, urea, SDS, deionized water and acetone	Aggregation of nanosized particles between 10-20 nm	Surface area of photocatalyst was 158 m^2/g	-Pore volume of photocatalyst was 0.53 cm^3/g -Pore diameter of photocatalyst was 24.4 nm	3.18 eV	MB	Light source: UV light MB: 85-86% in 60 min	Chowdhury et al. (2016)
MTN	Microwave-assisted	TTIP, cetyltrimethyl-ammonium bromide	Particle size of photocatalysts formed from 11.36 nm to	Surface area of photocata-lysts formed from 152	Pore volume of photocatalysts formed from	3.10 eV	2-CP	Light source: Visible light 2-CP: 96% in 360 min	Jaafar et al. (2015)

(continue)

05-4506832 pustaka.upsi.edu.my Perpustakaan Tuanku Bainun Kampus Sultan Abdul Jalil Shah PustakaTBainun ptbupsi

05-4506832 pustaka.upsi.edu.my Perpustakaan Tuanku Bainun Kampus Sultan Abdul Jalil Shah PustakaTBainun ptbupsi

Table 2.2 *(continued)*

Photocatalyst	Synthesize method	Synthesize materials	Properties			Band gap	Pollutant	Photocatalytic performance (%)	References
			Particle size	Surface area	Pore volume				
		(CTAB), propanol, distilled water and ammonium hydroxide (NH_4OH)	13.25 nm	m^2/g to 187 m^2/g	0.36 cm^3/g to 0.44 cm^3/g				
Mesoporous TiO_2 nanospheres	Solvothermal	TIP, ethanol, double-distilled water and distilled water	Average size of the primary particles was around ~5 nm	Surface area of photocatalyst was 173 m^2/g	-Pore volume of photocatalyst was 0.30 cm^3/g	3.16 eV	CR, MO, AO10 and RR	Light source: Solar light and visible light CR: 62% in 60 min	Anjugam Vandarkuzha-li et al. (2018)

(continue)

05-4506832 pustaka.upsi.edu.my Perpustakaan Tuanku Bainun Kampus Sultan Abdul Jalil Shah PustakaTBainun ptbupsi

05-4506832 pustaka.upsi.edu.my Perpustakaan Tuanku Bainun Kampus Sultan Abdul Jalil Shah PustakaTBainun ptbupsi

Table 2.2 *(continued)*

Photocatalyst	Synthesize method	Synthesize materials	Properties			Band gap	Pollutant	Photocatalytic performance (%)	References
			Particle size	Surface area	Pore volume				
					-Pore size of photocatalyst was 3.3 nm			MO: 70% in 60 min AO10: 50% in 60 min RR: 72% in 60 min	

05-4506832 pustaka.upsi.edu.my Perpustakaan Tuanku Bainun Kampus Sultan Abdul Jalil Shah PustakaTBainun ptbupsi

05-4506832 pustaka.upsi.edu.my Perpustakaan Tuanku Bainun Kampus Sultan Abdul Jalil Shah PustakaTBainun ptbupsi

2.7.4 Addition of metal elements into TiO_2

TiO_2 was the well-known promising semiconductor photocatalyst for pollutant degradation (Khalid et al., 2017). However, continuous efforts still has been put on TiO_2 modification to obtain better activity under visible light irradiation in various photocatalytic applications. One of the most common strategies was by doping TiO_2 with metal elements for better separation of photogenerated charges, and in turn will enhance the photocatalytic properties (Khalid et al., 2017; Zhiming, Rui, Xiyu, Lina, & Xiaohuan, 2017). This finding was supported by Yu, Nam, Lee, Kim, and Boo, (2018), which stated that the light absorption efficiency can be boosted by adjusting the large band gap or formation of impurity levels between the conduction band and valence band using the doping method on semiconductor photocatalysis and thus will improve the photosensitive range of a photocatalyst. Another previous study from Camarillo, Rizaldos, Jimenez, Martinez, and Rincon (2019); Mohseni-Salehi, Taheri-Nassaj, and Hosseini-Zori, (2018); Samet et al. (2018) stated the same finding in which chemical modification by metal doping was the most widely adopted strategies that can influence the visible light absorption capability and finally will introduce the cooperative catalysts which can increase the separation between photogenerated electron and hole pairs. Figure 2.10 illustrates the photodegradation mechanism of doped TiO_2.

05-4506832 pustaka.upsi.edu.my Perpustakaan Tuanku Bainun Kampus Sultan Abdul Jalil Shah PustakaTBainun ptbupsi

05-4506832 pustaka.upsi.edu.my Perpustakaan Tuanku Bainun Kampus Sultan Abdul Jalil Shah PustakaTBainun ptbupsi

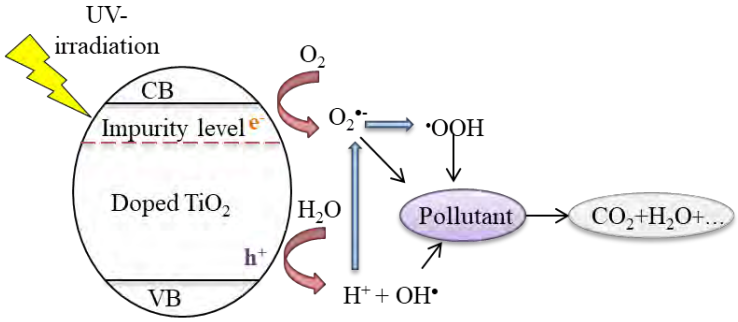


Figure 2.10. Schematic Illustration of Photodegradation Mechanism of Doped TiO_2

2.7.5 Type of metal elements

As demonstrated in literature, the optical absorption and recombination of photogenerated carriers was significantly altered by introducing the crystal lattice of photocatalyst with electronically active secondary species (Humayun, Raziq, Khan, & Luo, 2018). Modifications of TiO_2 photocatalyst with metal elements usually include the use of noble metals (Au, Ag, Pt and Pd) and transition metals (Fe, Co and Ni) (Fang, Xing, & Zhang, 2017).

2.7.5.1 Noble metals

The findings from study by Humayun et al. (2018), the photocatalytic activity of TiO_2 under visible-light irradiation was significantly developed through the effect of surface plasmon resonance (SPR) as plasmonic noble nanoparticles that has lower

05-4506832 pustaka.upsi.edu.my Perpustakaan Tuanku Bainun Kampus Sultan Abdul Jalil Shah PustakaTBainun ptbupsi

05-4506832 pustaka.upsi.edu.my Perpustakaan Tuanku Bainun Kampus Sultan Abdul Jalil Shah PustakaTBainun ptbupsi

band gap was added in the crystal lattice of TiO_2. The SPR effect was increased due to the collective oscillations of electrons on surfaces of noble metal and formed Schottky-barrier which transferred these energetic electrons into the conduction band of the doped semiconductor. The noble metal then will act as electron acceptor, which enhances the separation of photogenerated charges (Humayun et al., 2018; Ribao, Corredor, Rivero, & Ortiz, 2019). Figure 2.11 illustrates the effect of plasmonic nanoparticles towards the photocatalytic efficiency of semiconductor photocatalyst.

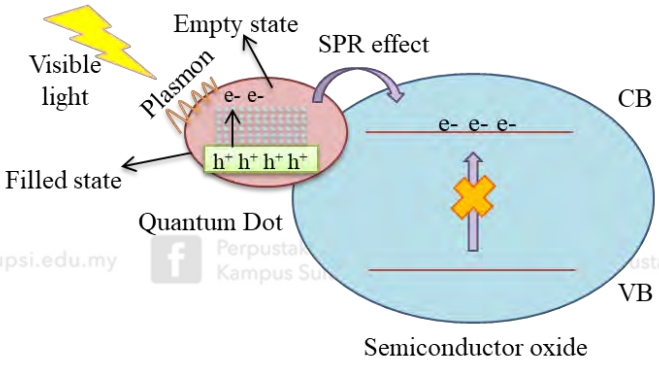


Figure 2.11. Plasmon Nanoparticles Enhanced the Photocatalytic Activity of Semiconductor Photocatalyst

Zhang et al. (2017) studied the performance of synthesized TiO_2 nanotubes (TNT340 and TND340) and Au-modified TiO_2 nanotubes (Au/TNT340 and Au/TND340) towards MO dye under UV irradiation. The pure TiO_2 nanotubes was used as a reference to evaluate the efficiency of Au-uniform doping and Au-non-uniform doping as photocatalysts. From the result obtained, it showed that the photocatalytic activity of Au-uniformly doped TiO_2 nanotubes (Au/TNT340) and Au-non-uniformly doped TiO_2 nanotubes (Au/TND340) were higher than the TNT340

05-4506832 pustaka.upsi.edu.my Perpustakaan Tuanku Bainun Kampus Sultan Abdul Jalil Shah PustakaTBainun ptbupsi

05-4506832 pustaka.upsi.edu.my Perpustakaan Tuanku Bainun Kampus Sultan Abdul Jalil Shah PustakaTBainun ptbupsi

and TND340 within 25 min degradation time. This was proven when the photocatalytic efficiencies of Au/TNT340 and Au/TND340 reached up to 80.6% and 99.2%, respectively compared to TNT340 and TND340 which only exhibited 52.3% and 60%, respectively. As mentioned in literature, this was largely due to the effective separation of charge carriers as the interfaces occurred between the pure stage TiO_2 and Au-doped TiO_2 together with the contribution of 'platinum island' effect that will prevent the recombination of electron/hole pairs and thus, enhanced the photocatalysis. The observed band gap value show that the band gap of TNT340 and TND340 were smaller than the Au/TNT340 and Au/TND340 which were 3.17 eV, 3.18 eV, 3.20 eV and 3.19 eV, correspondingly. The doping of Au caused the blue shift in the absorption band edge of TNT340 and TND340. However, the band gap of Au/TND340 was smaller than the Au/TNT340 which was considered as an evidence for its highest degradation rate. These results clearly indicate that the deposition surface has been the factor of shift direction in the absorption band edge.

Ali et al. (2018) has conducted the synthesize of Ag doped TiO_2 (Ag/TiO_2) nanoparticles via sol-gel technique. From transmission electron microscopy (TEM) micrographs, it has been confirmed that both pure TiO_2 and Ag/TiO_2 nanoparticles catalyst exhibited a non-spherical shape. The synthesized nanoparticles also showed small particle size but well crystalline in nature. The photocatalytic activity of the photocatalysts was assessed by using MB as a target pollutant to be degraded under irradiation of visible light. The findings demonstrated all doped TiO_2 photocatalysts exhibit efficient photocatalytic activity in which MB has been degraded around 72-96% during the course of irradiation compared to undoped TiO_2 which only degrade 30% of MB. The 4.0 mole% Ag-doped TiO_2 ($4\%Ag/TiO_2$) showed the highest

05-4506832 pustaka.upsi.edu.my Perpustakaan Tuanku Bainun Kampus Sultan Abdul Jalil Shah PustakaTBainun ptbupsi

05-4506832 pustaka.upsi.edu.my Perpustakaan Tuanku Bainun Kampus Sultan Abdul Jalil Shah PustakaTBainun ptbupsi

visible-light photocatalytic activity, which can almost degrade 96% of MB within 60 min of irradiation. This result could be due to the combined effect of the dye-sensitized and synergetic action of Ag-doped TiO_2 that enhanced the photocatalytic performance of all doped TiO_2 photocatalyst. From the observed band gap value, it clearly showed that the band gap of 4%Ag/TiO_2 was smaller than the pure TiO_2 which were 2.51 eV and 3.20 eV, respectively. These results match for its efficient result as smaller band gap can improve the photosensitive range towards visible light which enhanced the photocatalytic performance. Therefore, it can be concluded that, Ag was an effective dopant to shift the optical response and enhanced the separation of charge carriers.

Lakshmanareddy, Rao, Cheralathan, Subramaniam, & Shankar (2019) reported the synthesize of Pt/TiO_2 nanotubes via photodeposition (PTP-1.0) and chemical reduction (PTC-1.0) methods for MO dye degradation under solar light irradiation. The TEM images of PTP-1.0 revealed the formation of bigger sized Pt particles which ranges from 4 to 10 nm with agglomeration. On the other hand, the TEM images of PTC-1.0 showed the presence of smaller Pt particles from 1.3 to 2.3 nm. It was believed that the used of capping agent in chemical reduction method help to decrease the size of Pt nanoparticles as the particle size was controlled and prevented from agglomeration to occur. As a result, PTC-1.0 exhibited higher degradation of MO dye than PTP-1.0 which were 94% and 50.5% of degradation rate, respectively, within 30 min of irradiation. The excellent performance of PTC-1.0 could be attributed to the co-existence of Pt^0, Pt^{2+}, Pt^{4+} that benefits the efficient dye decolorization instead of PTP-1.0 catalyst that consisted of only metallic Pt^0 alone. Therefore, it can be concluded that, the charge recombination was inhibited in PTC-

05-4506832 pustaka.upsi.edu.my Perpustakaan Tuanku Bainun Kampus Sultan Abdul Jalil Shah PustakaTBainun ptbupsi

05-4506832 pustaka.upsi.edu.my Perpustakaan Tuanku Bainun Kampus Sultan Abdul Jalil Shah PustakaTBainun ptbupsi

1.0 catalyst since the electrons formed in the conduction band will be exploited by oxidized Pt species for their reduction to Pt^0 while in the case of PTP-1.0, the presence of only Pt^0 causing recombination of charge carriers to occur since the electrons in the conduction band were not scavenged, leading to inhibit dye degradation. In this study, the incorporation of Pt loading with various oxidation state has promoted scavenger effect to occur, thus enhanced the light absorption of TiO_2 towards visible light due to the narrowing band gap.

Sescu et al. (2021) has reported the doping of noble metals (Au and Pd) with TiO_2 by incipient wet impregnation (IWI) and ultrasound-assisted impregnation (US) methods. The result of scanning electron microscopy (SEM) images for the synthesized catalysts showed the similar morphology. However, the lighter image was obtained for the sample doped with Au compared to Pd as it provides better electronic conductor. The photocatalytic activity of the prepared catalysts was assessed through the removal of 2,4 dinitrophenol (2,4 DNP) with irradiation of UV. It was evident from the data obtained that efficient photocatalytic activity was performed by the samples prepared via IWI method, and the highest 2,4 DNP degradation was exhibited by TiO_2-Pd/IWI (70%) compared to TiO_2-Au/IWI (50%) under 120 min of light irradiation. This was due to the contribution of Pd ions that enhanced the formation of charge carriers and inhibited the recombination of e^-/h^+ pairs. This was in line with the band gap value of the photocatalysts, that increased in the pattern of TiO_2-Pd/IWI (2.98 eV) < TiO_2-Au/IWI (3.08 eV) < pure TiO_2 (3.20 eV).

05-4506832 pustaka.upsi.edu.my Perpustakaan Tuanku Bainun Kampus Sultan Abdul Jalil Shah PustakaTBainun ptbupsi

05-4506832 pustaka.upsi.edu.my Perpustakaan Tuanku Bainun Kampus Sultan Abdul Jalil Shah PustakaTBainun ptbupsi

2.7.5.2 Transition metals

Eventhough noble metal dopants showed the outstanding photocatalytic activities, the rareness and high cost of noble metals making non-noble metals to be considered as more ideal co-catalysts for the large-scale application in future (Chen et al., 2019). The effect of transition metals such as cobalt (Co), iron (Fe), copper (Cu), chromium (Cr) and nickel (Ni) have been investigated by researchers to reduce the band gap, inhibit electron and hole recombination rate and apply under visible light (Khaki, Shafeeyan, Raman, & Daud, 2017). The type and amount of transition metals were two crucial things for efficient photocatalytic activity. The separation of electrons and holes can be increased if the amount of metal addition remain at its optimum level. However, the excess amount of metal may distort the catalyst crystallinity and act as a recombination center if they were beyond the optimum value, thus reducing the photocatalytic efficiency (Shayegan, Lee, & Haghighat, 2018).

Blanco-Vega et al. (2017) reported the synthesize of Ni doped TiO_2 (Ni/TiO_2) catalysts via facile and rapid microwave assisted sol-gel (MW) method in which Ni contents were varied from 0.5 to 1.0 wt%, which denoted as 0.5% Ni-TiO_2/MW and 1.0% Ni-TiO_2/MW, respectively. In this study, pure TiO_2/MW and 1.0wt% Ni/TiO_2 prepared by conventional sol-gel method (1.0% Ni-TiO_2/CM) were used for comparative purposes. From SEM micrographs, both doped and undoped TiO_2 distributed spherical nanoparticles which consisted of agglomerates with grain sizes vary from 20-40 nm. The SEM images confirmed the improvement uniformity of particles and decreased in the particle size with the incorporation of Ni^{2+} ions. The narrowing in band gap value was also observed to the photocatalysts with Ni doping

05-4506832 pustaka.upsi.edu.my Perpustakaan Tuanku Bainun Kampus Sultan Abdul Jalil Shah PustakaTBainun ptbupsi

05-4506832 pustaka.upsi.edu.my Perpustakaan Tuanku Bainun Kampus Sultan Abdul Jalil Shah PustakaTBainun ptbupsi

in which 1.0% Ni-TiO_2/MW, 0.5% Ni-TiO_2/MW and 1.0% Ni-TiO_2/CM exhibited 2.72 eV, 2.75 eV and 2.84 eV, correspondingly compared to undoped TiO_2 that perform wide band gap which was 3.08 eV. The photocatalytic activity of the prepared catalysts was assessed by bisphenol A (BPA) degradation under visible light. The findings indicated the highest degradation of BPA was obtained by 1.0% Ni-TiO_2/MW with 93.1% followed by 0.5% Ni-TiO_2/MW and pure TiO_2/MW with 83.1% and 60.1%, respectively, within 120 min. Then, when the 1.0% Ni/TiO_2 prepared by CM and MW methods was compared, only 1.0% Ni-TiO_2/MW showed a complete degradation in 210 min. The excellent performance of 1.0% Ni-TiO_2/MW catalyst could be attributed to lower band gap value, smaller crystallite size and effective separation of photogenerated charges due to the nickel incorporation. These advantages could extend the activation under visible light and thus, enhanced the photocatalytic performance.

05-4506832 pustaka.upsi.edu.my Perpustakaan Tuanku Bainun Kampus Sultan Abdul Jalil Shah PustakaTBainun ptbupsi

Sood, Umar, Mehta, and Kansal (2015) reported the synthesized of Fe doped TiO_2 (Fe/TiO_2) nanoparticles via a novel and facile ultrasonic assisted hydrothermal method. From TEM analysis, it showed that both TiO_2 (bigger) and Fe dopant (smaller) particles appeared in which TiO_2 nanoparticles and Fe dopant formed in grey and dark particles, respectively. The TEM images also revealed the particles with almost spherical shaped ranging from ~10 to 20 nm. The addition of Fe dopant also has reduced the band gap value of photocatalysts, in which Fe/TiO_2 exhibited 2.90 eV which was lower than the synthesized bare TiO_2 (3.20 eV). The reduced band gap will extend the light absorption towards visible light which can advance the photocatalytic performance. The photocatalytic activity of the synthesized nanoparticles was assessed by the removal of para-nitrophenol (4-NP) and MB under visible light

05-4506832 pustaka.upsi.edu.my Perpustakaan Tuanku Bainun Kampus Sultan Abdul Jalil Shah PustakaTBainun ptbupsi

05-4506832 pustaka.upsi.edu.my Perpustakaan Tuanku Bainun Kampus Sultan Abdul Jalil Shah PustakaTBainun ptbupsi

illumination. The result from photodegradation of aqueous solution of 4-NP with the presence of light irradiation indicated that the highest degradation was obtained with 0.05 mol% of Fe dopant, which degrade 92% of 4-NP within 300 min. This outstanding photocatalytic activity can be attributed to the maximum separation of photogenerated charge carriers that occurred with the optimum value of Fe doping content. If Fe content increase more, it might lead the Fe ions to act as recombination centers for the photo-electrons and holes, thus decreasing the photocatalytic efficiency of TiO_2. Then, all the prepared catalysts were further used to degrade the textile dye, MB in order to confirm the versatility of the prepared catalysts under visible light irradiation. From the result obtained, it indicated the 0.075 mol% of Fe dopant exhibited the highest degradation, in which 93% of MB was degraded within 180 min. It was confirmed that this catalyst had high visible light response and maximum decrease in PL intensity which enhanced the separation of photo-electrons and hole-pairs.

Next, Shafei and Sheibani (2019) reported about the synthesize of Cu-doped TiO_2-CNT nanocomposite powder using sol-gel method. In this study, the effect of incorporation of CNT and Cu doping on TiO_2 photocatalyst was observed in detail. The FESEM images of pure TiO_2, TiO_2-10 wt.% CNT nanocomposite (TC) and 1% Cu doped TiO_2-10 wt.% CNT nanocomposite (TCC) was observed before and after calcination. From the results obtained, the FESEM image of TCC and TC samples before calcination were similar as it showed CNT were covered by amorphous TiO_2 while pure TiO_2 sample only showed the different sizes of spherical amorphous TiO_2 particles. However, smaller particle size and the dispersion of CNT in the microstructure was more uniformed in TCC sample compared to TC sample. The

05-4506832 pustaka.upsi.edu.my Perpustakaan Tuanku Bainun Kampus Sultan Abdul Jalil Shah PustakaTBainun ptbupsi

05-4506832 pustaka.upsi.edu.my Perpustakaan Tuanku Bainun Kampus Sultan Abdul Jalil Shah PustakaTBainun ptbupsi

FESEM images of the three samples were then observed after calcination process. From the results, it revealed that pure TiO_2 sample formed spherical TiO_2 particles with the average particle size of 300 nm. Meanwhile, for TC sample, the surface of CNT covered by TiO_2 was observed after calcination was followed by smaller average particle size than pure TiO_2 sample of 200 nm was formed. However, more stable coating of TiO_2 on the CNT was observed in TCC sample after calcination compared to TC sample and this led to the interaction between both components of the composites to be more enhanced. The different morphology observed for TC and TCC samples was due to the addition of Cu doping in the structure of TiO_2 in which Cu^{2+} ions acted as dopants prevented the growth of TiO_2 particles during the process. The incorporation of CNT and Cu doping to TiO_2 also helped in narrowing the band gap value in which TC and TCC samples exhibited 3.05 eV and 2.85 eV, respectively compared to pure TiO_2 that possesses wide band gap which was 3.20 eV. The efficiency of the as-prepared nanocomposites was confirmed via MB degradation under visible light irradiation. The findings indicated the TCC sample displayed the highest degradation of MB which was 81.5% compared to TC and pure TiO_2 samples which were 62% and 5%, respectively, within 60 min of irradiation. This excellent performance could be due to the incorporation of CNT and Cu species into TiO_2 photocatalyst. The close interaction between TiO_2 and CNT in TCC sample prolonged the electron-hole recombination since the interfacial charge transfer was enhanced. Besides, the addition of metallic Cu ions into TiO_2 also helped to inhibit the recombination of electron-hole pairs by acting as electron sink that facilitated the charge separation. The smaller particle size of TCC catalyst also contributed to high photocatalytic performance as it promoted higher surface area than freely grown TiO_2 catalyst in pure TiO_2 sample.

05-4506832 pustaka.upsi.edu.my Perpustakaan Tuanku Bainun Kampus Sultan Abdul Jalil Shah PustakaTBainun ptbupsi

05-4506832 pustaka.upsi.edu.my Perpustakaan Tuanku Bainun Kampus Sultan Abdul Jalil Shah PustakaTBainun ptbupsi

Another study by Biru, Qaderi, Mamat, & Jalil (2021) reported about the synthesize of Cu, Fe, and Ni doped TiO_2 via sol-gel method for photodegradation of MB. FESEM analysis from this study show that the prepared photocatalysts exhibited spherical morphology. The observed band gap value showed an increment when the Cu, Fe and Ni doping was incorporated, but decreased as the amount of metal doping increased. The obtained band gap exhibited from the range of 3.22 eV to 3.42 eV, in which the smallest band gap was displayed by 9 mol% of Ni-doped TiO_2 compared to pure TiO_2. Pure TiO_2 and metal doped TiO_2 photocatalysts were used to determine the efficiency of photocatalytic activity through the degradation of MB under both UV and visible light irradiation. From the result obtained, pure TiO_2 exhibited more than 98% and 97% degradation rates of MB solution within 300 min under UV and visible light irradiation, correspondingly. It showed that the synthesized pure TiO_2 by sol gel method in this study had enhanced the photocatalytic activity compared to the commercial TiO_2 Degussa P25 which can only achieve 45% of activity under visible light within the same irradiation time (Zhang et al., 2015). The addition of transition metals (Cu, Fe and Ni) into TiO_2 had also displayed excellent photocatalytic performance under UV and visible light in which 3, 6 and 9 mol% of metal-doped TiO_2 had been studied. From the results obtained, 3 mol% of Cu and Fe-doped TiO_2 had achieved the highest photocatalytic degradation in which the percentages of MB decolorization was 97.7% and 96.9% under UV light, respectively. Meanwhile, the degradation of MB under visible light using 3 mol% of Cu and Fe-doped TiO_2 was 90% and 84.3%, respectively within 300 min of irradiation. It was proved that 3 mol% was the optimum level of Cu and Fe doping as the degradation results decreased with the increasing amount of metal concentration. However, 3 mol% of Ni-doped TiO_2 showed the highest photoactivity only under UV light in which 97.7%

05-4506832 pustaka.upsi.edu.my Perpustakaan Tuanku Bainun Kampus Sultan Abdul Jalil Shah PustakaTBainun ptbupsi

05-4506832 pustaka.upsi.edu.my Perpustakaan Tuanku Bainun Kampus Sultan Abdul Jalil Shah PustakaTBainun ptbupsi

of MB had been decolorized. The highest degradation rate under visible light was performed by 6 mol% of Ni-doped TiO_2 in which 96.9% of MB decolorization was achieved. The further increased of these metals into TiO_2 will reduce the photocatalytic process as it enhanced the recombination of electron and hole pairs and blocked the active sites of TiO_2 surface from light penetration.

2.7.6 Metal doping method

There were variety of ways to synthesize metal doped TiO_2 photocatalysts. The commonly used synthesize methods include sol-gel, wet-impregnation and hydrothermal methods. In this section, a detailed effect of different methods and conditions of TiO_2 preparation towards its physical and chemical properties will be discussed. These approaches help to imply the good control of preparation conditions which determine the effectiveness of photocatalytic performance.

The most common synthesize method for metal doping was sol-gel technique as it promotes affordable cost, high reliability, good repeatability, ease of setup process, lower temperature utilization and ease of control the physical characteristics and morphology of nanoparticles (Ong, Ng, & Mohammad, 2018). For instance, Altin, Sokmen, and Biyiklioglu (2016) has reported about the synthesize of Co doped TiO_2 with the presence of surfactant Triton X100 (TX100) or Tween 20 (T20) by using sol-gel method. In this study, phthalocyanine (Pc) derivative was used as dye sensitizer to form the photocatalyst with the presence and absence of above

05-4506832 pustaka.upsi.edu.my Perpustakaan Tuanku Bainun Kampus Sultan Abdul Jalil Shah PustakaTBainun ptbupsi

05-4506832 pustaka.upsi.edu.my Perpustakaan Tuanku Bainun Kampus Sultan Abdul Jalil Shah PustakaTBainun ptbupsi

surfactants (Pc/Co-TiO_2). SEM images of the as-synthesized photocatalyst showed the formation of spherical like structures containing aggregated Pc molecules. From TEM image of Pc/Co-TiO_2, the average crystalline grain diameter obtained for the spherical particles were from 5-20 nm due to the agglomeration of Pc. The lighter area was assumed as the organic stage (Pc) while the darker spots on living stage proved the presence of inorganic TiO_2. In this study, the photocatalytic activity was evaluated through the degradation of MO and reduction of Cr(VI) under near visible light irradiation. The result indicated Pc/Co-TiO_2-T20 exhibited the highest photocatalytic activity, in which 60.3% of the MO and 71.3% of the Cr(VI) ions were degraded after 150 min of irradiation. The photocatalytic activity of the prepared catalysts has followed the order: Pc/Co-TiO_2-T20 > Pc/Co-TiO_2-TX100 > Pc/Co-TiO_2 > Co-TiO_2-T20 > Co-TiO_2-TX100 > Co-TiO_2. It can be concluded that, the occurrence of Tween 20 surfactant enhanced the photocatalytic performance of Co-TiO_2 by providing small crystallite size that will increase the surface area of photoactive materials. Besides, the strong absorbance of Pc added into TiO_2 structure caused the extending of catalyst's absorption edge into visible range.

Other than sol-gel method, wet-impregnation method was another option to prepare doped TiO_2. Fe doped TiO_2 (Fe/MT) nanoparticles were synthesized by Rodriguez, Pecchi, Casuscelli, Elias, and Eimer (2019) via wet-impregnation method. SEM images of the prepared photocatalysts demonstrated the wormhole-like mesoporous structure with large portion of intra-aggregated monodispersed nanoparticles that differs in size. As observed, the agglomeration of the nanoparticles was not influenced by the doping of different iron loadings since similar mesostructures were shown by all samples. The observed band gap value in this study

05-4506832 pustaka.upsi.edu.my Perpustakaan Tuanku Bainun Kampus Sultan Abdul Jalil Shah PustakaTBainun ptbupsi

05-4506832 pustaka.upsi.edu.my Perpustakaan Tuanku Bainun Kampus Sultan Abdul Jalil Shah PustakaTBainun ptbupsi

showed a decrement from 3.30 eV to 2.90 eV as the Fe loading was increased, which could stabilize the separation of photogenerated charges and thus, enhanced the photocatalytic activity. However, the surface area was decreased for the photocatalysts with high Fe content which possibly due to the mesopores being partially blocked in the TiO_2 support. The photocatalytic activity of degrading AO7 dye under UV-Vis and visible irradiation were significantly improved with the incorporation of Fe doping in which the dye degradation of around 99% and 54% were achieved, respectively, within 300 min of irradiation. These excellent performances can be attributed to the reducing band gap and high separation of photogenerated charges contributed by Fe^{3+} ions that were finely dispersed on the TiO_2 surface. Figure 2.12 shows the proposed schematic illustration of general wet-impregnation method for synthesizing a catalyst.

05-4506832 pustaka.upsi.edu.my Perpustakaan Tuanku Bainun Kampus Sultan Abdul Jalil Shah PustakaTBainun ptbupsi

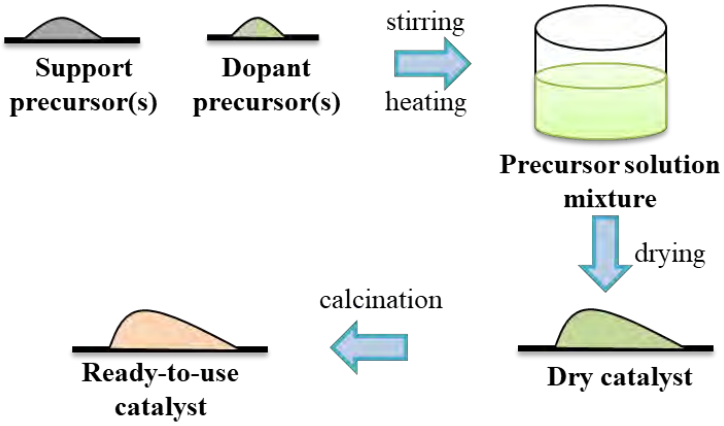


Figure 2.12. Schematic Illustration of Synthesizing Catalyst via Wet-Impregnation Method

05-4506832 pustaka.upsi.edu.my Perpustakaan Tuanku Bainun Kampus Sultan Abdul Jalil Shah PustakaTBainun ptbupsi

05-4506832 pustaka.upsi.edu.my Perpustakaan Tuanku Bainun Kampus Sultan Abdul Jalil Shah PustakaTBainun ptbupsi

Hydrothermal method can also be applied in preparing doped TiO_2. The doping reaction via hydrothermal method was usually conducted in an autoclave with an exact temperature for an amount of time. The solution can be heated to a temperature above its boiling point since the reaction was conducted in an autoclave that able to withstand high pressure for the solution to achieve its vapor pressure (Nasirian, Lin, Bustillo-Lecompte, & Mehrvar, 2018). Kamble, Mahajan, Puri, Shinde, and Garadkar (2018) synthesized Cu doped TiO_2 (Cu/TiO_2) nanoparticles by using hydrothermal method and they observed an increment in photocatalytic activity of doped samples under visible light irradiation in which 85% of malachite green (MG) was degraded by 1.71wt.% Cu/TiO_2 within 180 min of irradiation. Meanwhile, only 53% of MG dye was degraded by using undoped TiO_2 under the same reaction conditions. It was confirmed that the expanding of Cu^{2+} content had caused decreasing in the molecule size and promote the synergistic impact that prolonged the lifetime of photogenerated e^-/h^+ pairs, hence enhanced the photocatalytic performance. The narrower band gap value was obtained as the amount of Cu doping increased in which 1.71wt.% Cu/TiO_2 exhibited the smallest band gap value, 2.34 eV compared to pure TiO_2 that formed 3.18 eV. Meanwhile, the band gap for 0.88wt.% Cu/TiO_2 and 1.52wt.% Cu/TiO_2 showed 2.72 eV and 2.48 eV, respectively. The lower band gap value of 1.71wt.% Cu/TiO_2 could be assumed as an indirect evidence of its efficient degradation rate as metal doping facilitated the separation of photogenerated carriers, thus enhanced the photocatalysis. From TEM micrograph, non-uniform shape and size of particles with agglomeration were obtained within the range of 8-10 nm. The surface area of the photocatalysts also increased with the incorporation of metal doping. A summary of addition of metal elements into TiO_2 was shown in Table 2.3.

05-4506832 pustaka.upsi.edu.my Perpustakaan Tuanku Bainun Kampus Sultan Abdul Jalil Shah PustakaTBainun ptbupsi

05-4506832 pustaka.upsi.edu.my Perpustakaan Tuanku Bainun Kampus Sultan Abdul Jalil Shah PustakaTBainun ptbupsi

Table 2.3

Summary of Addition of Metal Elements into TiO_2 Photocatalyst

Photocatalyst	**Synthesize method**	**Light source**	**Experimental conditions**	**Surface area**	**Band gap**	**Photocatalytic performance**	**References**
Au/TNT	Liquid phase deposition	UV light	Catalyst: 0.5 g/L [MO]: 20 mg/L	-	Undoped TNT: 3.17 eV and 3.18 eV Au-doped: 3.19 eV and 3.20 eV	-99.2% in 25 min	Zhang et al. (2017)
Ag/TiO_2	Sol-gel	Visible light	Catalyst: 1 g/L [MB]: 10 mg/L	-	Undoped TiO_2: 3.20 eV Ag-doped: 2.51 eV	-96% in 60 min	Ali et al. (2018)
Pt/TiO_2	Deposition	Solar light	Catalyst: 2 g/L [MO]: 16.37 mg/L	-	The incorporation of Pt into TiO_2 has reduced the band gap	-94% in 30 min	Lakshmanareddy et al. (2019)

(continue)

05-4506832 pustaka.upsi.edu.my Perpustakaan Tuanku Bainun Kampus Sultan Abdul Jalil Shah PustakaTBainun ptbupsi

05-4506832 pustaka.upsi.edu.my Perpustakaan Tuanku Bainun Kampus Sultan Abdul Jalil Shah PustakaTBainun ptbupsi

Table 2.3 *(continued)*

Photocatalyst	Synthesize method	Light source	Experimental conditions	Surface area	Band gap	Photocatalytic performance	References
Au/TiO_2 and Pd/TiO_2	IWI and US	UV light	Catalyst: 1 g/L [2,4 DNP]: 20 mg/L	Undoped TiO_2: 10.35 m^2/g Au/TiO_2: 10.1 m^2/g Pd/TiO_2: 11.57 m^2/g	Undoped TiO_2: 3.20 eV Au-doped: 3.08 eV Pd-doped: 2.98 eV	-70% in 120 min	Sescu et al. (2021)
Ni/TiO_2	MW	Visible light	Catalyst: 1 g/L [BPA]: 10 mg/L	Undoped TiO_2: 60.3 m^2/g Ni/TiO_2: 83.5 m^2/g	Undoped TiO_2: 3.08 eV Ni-doped: 2.72 eV	-93.1% in 120 min	Blanco-Vega et al. (2017)
Fe/TiO_2	Ultrasonic assisted hydrothermal	Visible light	Catalyst: 0.5 g/L [4-NP]: 10 mg/L [MB]: 10 mg/L	Undoped TiO_2: 50.21 m^2/g Fe/TiO_2: 45.04 m^2/g	Undoped TiO_2: 3.20 eV Fe-doped: 2.90 eV	-92% of 4-NP in 300 min -93% of MB in 180 min	Sood et al. (2015)
Cu/TiO_2-CNT	Sol-gel	Visible light	Catalyst: 0.4 g/L [MB]: 5 mg/L	Undoped TiO_2: 87.3 m^2/g	Undoped TiO_2: 3.20 eV	-81.5% in 60 min	Shafei and Sheibani (2019)

(continue)

05-4506832 pustaka.upsi.edu.my Perpustakaan Tuanku Bainun Kampus Sultan Abdul Jalil Shah PustakaTBainun ptbupsi

05-4506832 pustaka.upsi.edu.my Perpustakaan Tuanku Bainun Kampus Sultan Abdul Jalil Shah PustakaTBainun ptbupsi

Table 2.3 *(continued)*

Photocatalyst	Synthesize method	Light source	Experimental conditions	Surface area	Band gap	Photocatalytic performance	References
				TiO_2-CNT: 121.6 m^2/g Cu/TiO_2-CNT: 187.8 m^2/g	CNT and Cu-doped: 2.85 eV		
(Cu, Fe, Ni)/TiO_2	Sol-gel	UV and Visible light	Catalyst: 1 g/L [MB]: 2.5 mg/L	Undoped TiO_2: 42.08 m^2/g Cu/TiO_2: 31.13 m^2/g Fe/TiO_2: 53.34 m^2/g Ni/TiO_2: 74.12 m^2/g	Undoped TiO_2: 3.24 eV Cu-doped: 3.26 eV Fe-doped: 3.29 eV Ni-doped: 3.22 eV	-98% in 300 min	Biru et al. (2021)
Co/TiO_2 modified with Pc and surfactants	Sol-gel	Near visible light	Catalyst: 2 g/L [MO]: 10 mg/L [Cr (VI)]: 10 mg/L	Pc/Co-TiO_2: 38.620 m^2/g Pc/Co-TiO_2-TX100: 133.937 m^2/g	-	-60.3% of MO in 150 min -71.3% of Cr(VI) in 150 min	Altin et al. (2016)

(continue)

05-4506832 pustaka.upsi.edu.my Perpustakaan Tuanku Bainun Kampus Sultan Abdul Jalil Shah PustakaTBainun ptbupsi

05-4506832 pustaka.upsi.edu.my Perpustakaan Tuanku Bainun Kampus Sultan Abdul Jalil Shah PustakaTBainun ptbupsi

Table 2.3 *(continued)*

Photocatalyst	Synthesize method	Light source	Experimental conditions	Surface area	Band gap	Photocatalytic performance	References
(T20 and TX100)				Pc/Co-TiO_2-T20: 151.978 m^2/g			
Fe/MT	Wet-impregnation	UV and Visible light	Catalyst: 1 g/L [AO7]: 20 mg/L	Undoped TiO_2: 87 m^2/g Fe/MT: 47 m^2/g	Undoped TiO_2: 3.30 eV Fe-doped: 2.90 eV	-99% in 300 min	Rodriguez et al. (2019)
Cu/TiO_2	Hydrothermal	Visible light	Catalyst: No data [MG]: 50 mg/L	Undoped TiO_2: 139.35 m^2/g Cu/TiO_2: 197.84 m^2/g	Undoped TiO_2: 3.18 eV Cu-doped: 2.34 eV	-85% in 180 min	Kamble et al. (2018)

05-4506832 pustaka.upsi.edu.my Perpustakaan Tuanku Bainun Kampus Sultan Abdul Jalil Shah PustakaTBainun ptbupsi

05-4506832 pustaka.upsi.edu.my Perpustakaan Tuanku Bainun Kampus Sultan Abdul Jalil Shah PustakaTBainun ptbupsi

2.7.7 Incorporation of dopant

Various types of photocatalysts for the degradation of organic pollutants have been significantly explored. In recent years, the metal-free and low cost photocatalyst like gC_3N_4 has got much attention from researchers. It has been reported to be a potential candidate for photocatalysis due to its unique structure and electronic properties. According to Huang et al. (2015), gC_3N_4 consist of two-dimensional (2D) network structure with π-conjugated system that can facilitate the charge transfer and a narrow band-gap of 2.7 eV, which beneficial it as a photocatalyst with visible light absorbing ability. However, the weak oxidative ability of photogenerated hole and rapid recombination of charge carriers has limited the photocatalytic activity of gC_3N_4 to some extent (Kesarla et al., 2018; Huang et al., 2015). Therefore, strategy to improve the photocatalytic performace of gC_3N_4 has been intensively done. According to Gahlot et al. (2021), the increment in charge separation can help to improve its photocatalytic performance which can be achieved by modifying it with elemental doping or by coupling it with other semiconductor materials such as ZnO, CeO_2, $ZnWO_4$, CdS and TiO_2. Nevertheless, coupling gC_3N_4 and TiO_2 has got much attention and was widely applied for various photocatalytic applications.

For instance, previous study reported by Wang et al. (2014) has synthesized TiO_2/gC_3N_4 composites for photodegradation of DBT under UV light. The enhancement in photocatalytic performance was obtained using TiO_2/gC_3N_4 as a photocatalyst compared to pure TiO_2 and gC_3N_4 being separately, in which 98.9% of DBT degradation was significantly achieved. Meanwhile, pure TiO_2 and gC_3N_4 only obtained 79.1% and 1.3% of DBT degradation, respectively.

05-4506832 pustaka.upsi.edu.my Perpustakaan Tuanku Bainun Kampus Sultan Abdul Jalil Shah PustakaTBainun ptbupsi

05-4506832 pustaka.upsi.edu.my Perpustakaan Tuanku Bainun Kampus Sultan Abdul Jalil Shah PustakaTBainun ptbupsi

2.8 Addition of Fe and gC_3N_4 into TiO_2 as composite photocatalyst

Besides morphological modification attemps, the implementation of transition metal doping on TiO_2 has been widely used in order to improve the photocatalytic activity of TiO_2. The most popular transition metals used as a dopant were W, Cr, Fe, Co and Mn. The enhancement of photocatalytic activity was achieved as the optical and photo-electrochemical properties of TiO_2 has been modified, in which prolonging the lifetime of electron and holes and extending the light absorption of TiO_2 towards the visible region (Castro, Arconada, & Duran, 2015). This finding was supported by Lutic, Petrovschi, Ignat, Cretescu, and Bulai (2016), which stated that the band gap energy can be shifted from UV to visible region due to the doping with several transition elements (Fe, W, Co, Zn, Ni, Ce), and thus the use of solar energy was possible for the photocatalytic reactions.

05-4506832 pustaka.upsi.edu.my Perpustakaan Tuanku Bainun Kampus Sultan Abdul Jalil Shah PustakaTBainun ptbupsi

Among those various metals, Fe was considered to be the most promising transition metal candidate as dopant since the ionic radius of Fe^{3+} (0.69 Å) and Ti^{4+} (0.745 Å) was almost similar to each other, which in turn can help the Fe^{3+} ions to be easily incorporated into TiO_2 matrix. As a result, Fe^{3+} will restrict the recombination of electron-hole pairs by performing as a charge carrier trap, which can significantly enhance the photoactivity (Sood et al., 2015). From previous study, many researchers have reported about the enhancement in photocatalytic performance after the addition of Fe as a metal dopant. For instance, a study reported by Barkhade and Banerjee (2018) has doped Fe into TiO_2 nanocomposites for the photodegradation of Rhodamine B (RhB). From this study, the photocatalytic activity of Fe doped TiO_2 photocatalyst was efficient compared to pure TiO_2 in which 70% and 7.9% of RhB

05-4506832 pustaka.upsi.edu.my Perpustakaan Tuanku Bainun Kampus Sultan Abdul Jalil Shah PustakaTBainun ptbupsi

05-4506832 pustaka.upsi.edu.my Perpustakaan Tuanku Bainun Kampus Sultan Abdul Jalil Shah PustakaTBainun ptbupsi

has been degraded within 90 min under irradiation of light, respectively. Another study reported by Han, Kambala, Dharmarajan, Liu, and Naidu (2018) has also synthesized Fe^{3+} doped TiO_2 photocatalyst for photodegradation of AO7 with irradiation of different light sources which were UV, visible and solar light. The synthesized photocatalyst performed well under all conditions which proven the efficiency of using Fe as a metal dopant for photodegradation. Similar effect also reported by Eshaghi and Moradi (2018), in which the photoactivity of Fe doped TiO_2 with incorporation of activated carbon has obtained higher degradation rate of Reactive Red 198 (RR198) compared to pure TiO_2.

In recent years, gC_3N_4 was known as a metal-free semiconductor material that has attracted many researchers' attention due to its affordable cost, chemical stability, less toxicity and narrow band-gap of 2.7 eV, which beneficial it as a photocatalyst with visible light absorbing ability (Sadanandam et al., 2018). Although gC_3N_4 has the light absorbing ability towards visible region, the photoactivity of pure gC_3N_4 was still limited to some extent due to its low separation of photogenerated electron and holes and weak light absorption coefficient. In order to solve these issues, various methods have been carried out such as by changing with different precursors, exfoliation, adding co-catalyst, doping with metal/noble metal, non-metal and other semiconductors which can improve the separation of photogenerated carriers and extending the light harvesting ability towards solar light (Huu et al., 2021; Sadanandam et al., 2018). Among the method, the combination of gC_3N_4 with metal and other semiconductor materials was the most widely applied by researchers. For instance, few nanocomposites from previous works such as Ag doped gC_3N_4, NiS_2-modified gC_3N_4, TiO_2 modified with gC_3N_4, ZnO modified with Fe_3O_4/gC_3N_4 and

05-4506832 pustaka.upsi.edu.my Perpustakaan Tuanku Bainun Kampus Sultan Abdul Jalil Shah PustakaTBainun ptbupsi

05-4506832 pustaka.upsi.edu.my Perpustakaan Tuanku Bainun Kampus Sultan Abdul Jalil Shah PustakaTBainun ptbupsi

gC_3N_4 modified with Fe/TiO_2 have been significantly synthesized for photocatalytic applications. In addition, the combination of these photocatalysts will form heterojunction, known as Z-scheme mechanism that can improve the separation of photogenerated charges by allowing the reduction and oxidation reactions occurred from different sites of the photocatalyst (Kesarla et al., 2018). In particular, coupling of gC_3N_4 with TiO_2 has got many attention from researchers for photodegradation of organic pollutants such as degradation of MB (Li, Sun, Xue, Yao, & Zheng, 2016), phenol (Wei et al., 2017), acetaldehyde (Raziq et al., 2015), DBT (Wang et al., 2014) and 2,4 DNP (Zhou et al., 2016). This was due to the ability of gC_3N_4 that can form heterojunction with TiO_2 by generating suitable conduction and valence band levels and close interfacial connection between both of the catalysts (Li et al., 2016).

05-4506832 Perpustakaan Tuanku Bainun Kampus Sultan Abdul Jalil Shah ptbupsi

In the present work, 5wt% of Fe and 5wt% of gC_3N_4 was added into MTN in order to investigate the efficiency of this photocatalyst for the photodegradation of DBT in model oil under UV light irradiation. Although this photocatalyst was still rare for DBT degradation, the great potential showed by this photocatalyst for other photocatalytic applications in previous studies, proving it was worth to be explored.

2.9 Addition of hydrogen peroxide (H_2O_2) as oxidizing agent

In 1939 at I. G. Farbenindustrie, Riedl and Pfleiderer has developed the anthraquinone auto-oxidation (AO) process to produce a H_2O_2 on a massive scale which formed as a clear, colourless liquid and completely miscible with water (Ciriminna, Albanese, Meneguzzo, & Pagliaro, 2016).

05-4506832 pustaka.upsi.edu.my Perpustakaan Tuanku Bainun Kampus Sultan Abdul Jalil Shah PustakaTBainun ptbupsi

05-4506832 pustaka.upsi.edu.my Perpustakaan Tuanku Bainun Kampus Sultan Abdul Jalil Shah PustakaTBainun ptbupsi

Previously, H_2O_2 was widely used as a 'green' oxidant to oxidize and decompose any type of organic substances. It was due to its ability that can exhibited highly reactive hydroxyl radicals ($^{\bullet}OH$) in water that can oxidize and degrade organic substances, especially with the presence of UV light. Fenton's reagent which were the mixture of Fe(II)/Fe(III) and H_2O_2 was commonly used since it can produce large amount of $^{\bullet}OH$ for the degradation of organic substances. However, these reagents required very low pH and formed secondary pollution as the large amount of iron sludge was accumulated at the final process. Therefore, the deposition of Fe onto a solid support in which formed heterogeneous type of Fenton's reagent was widely explored by researchers to avoid the formation of iron sludge which lead to the secondary pollution. The enhancement of photocatalyst's activity for decomposition of organic substances has been successfully achieved when H_2O_2 was utilized with TiO_2 in the presence of UV light irradiation since TiO_2 offered wide band gap energy. Recently, the organic substances was successfully decomposed by the utilization of H_2O_2 with carbon nitride in the presence of visible light source (Saha et al., 2018).

From previous study, H_2O_2 was stated to be the most influenced factor to improve photodegradation rate by producing the $^{\bullet}OH$. The addition of H_2O_2 also reduced the recombination of electron-hole pairs through the consumption of excited electron by H_2O_2 to form $^{\bullet}OH$ as showed in the Eq. (2.1), (Puri, Thakur, Verma, & Barman, 2021).

$$H_2O_2 + e^- \xrightarrow{h\nu} {}^{\bullet}OH + OH^- \quad (2.1)$$

05-4506832 pustaka.upsi.edu.my Perpustakaan Tuanku Bainun Kampus Sultan Abdul Jalil Shah PustakaTBainun ptbupsi

05-4506832 pustaka.upsi.edu.my Perpustakaan Tuanku Bainun Kampus Sultan Abdul Jalil Shah PustakaTBainun ptbupsi

From previous published papers, it was observed that the addition of H_2O_2 solution has significantly enhanced the degradation rate of organic pollutant, which showed the synergistic effect of photocatalyst and H_2O_2. For example, study reported by Mironyuk, Danyliuk, Tatarchuk, Mykytyn, and Kotsyubynsky (2021) has synthesized Fe doped TiO_2 (Fe/TiO_2) nanocatalyst via sol-gel method for photodegradation of CR under UV-A light. From this study, it showed that the CR was almost completely degraded with the addition of 20 mM of H_2O_2 in the CR solution, while only 33.9% of CR degradation rate was obtained within 1 h in the absence of H_2O_2.

Then, another study reported by Keynejad, Nikazar, and Dabir (2017), has utilized TiO_2 as a photocatalyst for desulfurization of diesel under UV light irradiation. From the results obtained, it showed that the total removal of thiol group and sulfur from diesel samples were 88% and 90%, respectively with the addition of 2wt% of H_2O_2. However, the results were totally dropped in the absence of H_2O_2 in which the total thiol group and sulfur removals obtained only about 14% and 0%, respectively. The obtained results proved the efficiency of H_2O_2 as an oxidizing agent that can improve the desulfurization process.

On the other hand, study reported by Khayyat and Roselin (2017) has synthesized Au nanoparticles doped with TiO_2 (Au/TiO_2) as a photocatalyst for the photodegradation of Benzothiophene (BT) and DBT under UV light irradiation. From the results, it can be observed that the degradation rate of DBT and BT increased to 61% and 47%, respectively within 3 h with the incorporation of H_2O_2 solution.

05-4506832 pustaka.upsi.edu.my Perpustakaan Tuanku Bainun Kampus Sultan Abdul Jalil Shah PustakaTBainun ptbupsi

05-4506832 pustaka.upsi.edu.my Perpustakaan Tuanku Bainun Kampus Sultan Abdul Jalil Shah PustakaTBainun ptbupsi

However, in the absence of H_2O_2, the total removal of DBT and BT were only 12.3% and 10%, respectively under the same reaction conditions.

05-4506832 pustaka.upsi.edu.my Perpustakaan Tuanku Bainun Kampus Sultan Abdul Jalil Shah PustakaTBainun ptbupsi
05-4506832 pustaka.upsi.edu.my Perpustakaan Tuanku Bainun Kampus Sultan Abdul Jalil Shah PustakaTBainun ptbupsi

05-4506832 pustaka.upsi.edu.my Perpustakaan Tuanku Bainun Kampus Sultan Abdul Jalil Shah PustakaTBainun ptbupsi

CHAPTER 3

METHODOLOGY

05-4506832 pustaka.upsi.edu.my Perpustakaan Tuanku Bainun Kampus Sultan Abdul Jalil Shah PustakaTBainun ptbupsi

3.1 Introduction

This chapter list the details of materials and methods used in this research. Several characterization techniques were done in order to obtain the correlation between structure and photocatalytic properties of the synthesized photocatalyst. The detailed methodology flowchart of this research was shown in Figure 3.1.

05-4506832 pustaka.upsi.edu.my Perpustakaan Tuanku Bainun Kampus Sultan Abdul Jalil Shah PustakaTBainun ptbupsi

05-4506832 pustaka.upsi.edu.my Perpustakaan Tuanku Bainun Kampus Sultan Abdul Jalil Shah PustakaTBainun ptbupsi

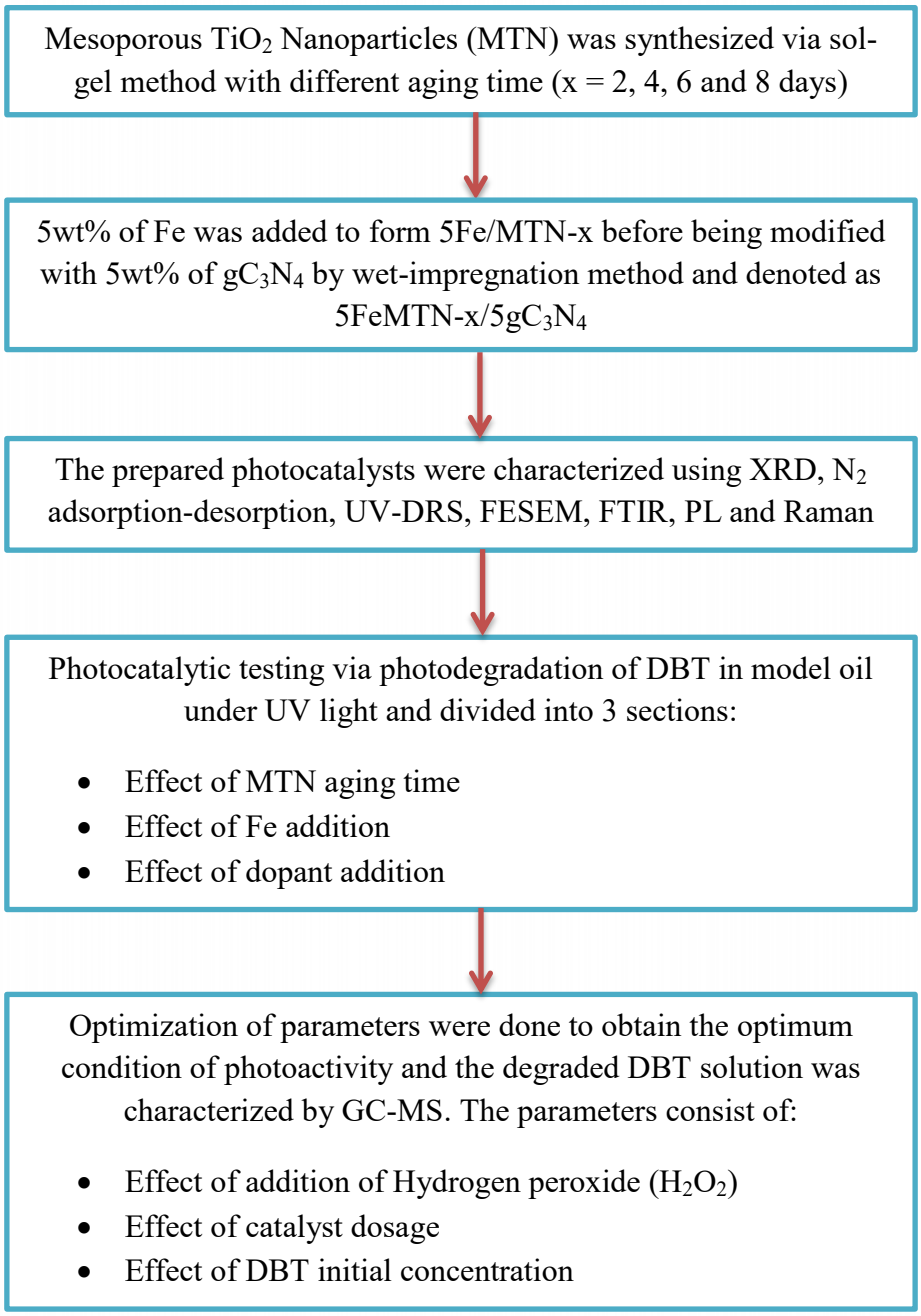


Figure 3.1. Detailed Methodology Flowchart

05-4506832 pustaka.upsi.edu.my Perpustakaan Tuanku Bainun Kampus Sultan Abdul Jalil Shah PustakaTBainun ptbupsi

05-4506832 pustaka.upsi.edu.my Perpustakaan Tuanku Bainun Kampus Sultan Abdul Jalil Shah PustakaTBainun ptbupsi

3.2 Materials

3.2.1 Chemicals

Chemicals used in this research project were analytical grade and received without required further purification. List of chemicals used were as following:

Table 3.1

List of Chemicals

Chemical	Assay	Manufacturer / Source
Hexadecyltrimethyl-ammonium bromide (CTAB)	≥ 98.0%	Sigma-Aldrich
n-Propanol	-	Bendosen
Ammonium hydroxide (NH_4OH)	25.0%	Systerm
Titanium (IV) isopropoxide (TTIP)	97.0%	Sigma-Aldrich
Iron (III) oxide (Fe_2O_3)	≥ 95.0%	-
Urea (CH_4N_2O)	-	Systerm
Dibenzothiophene (DBT) ($C_{12}H_8S$)	98.0%	Sigma-Aldrich
Hydrogen peroxide (H_2O_2)	35.0%	Systerm
Acetonitrile	-	Systerm

05-4506832 pustaka.upsi.edu.my Perpustakaan Tuanku Bainun Kampus Sultan Abdul Jalil Shah PustakaTBainun ptbupsi

05-4506832 pustaka.upsi.edu.my Perpustakaan Tuanku Bainun Kampus Sultan Abdul Jalil Shah PustakaTBainun ptbupsi

3.3 Catalyst preparation

3.3.1 Synthesize of Mesoporous Titania Nanoparticles (MTN)

The MTN was synthesized using sol-gel method. 4.68 g of CTAB surfactant was dissolved in 720 mL distilled water, 120 mL *n*-propanol and 29 mL of 28% ammonia solution. Then, the mixture was stirred continuously for 30 min at 323 K in water bath. After 30 min, the temperature of water bath was increased to 353 K followed with the addition of 5.7 mL TTIP into the mixture. This process was continued for 2 h in water bath to allow the mixture dissolve completely. After 2 h of stirring, the observed white solution was transferred into a container and being placed in the refrigerator for x = 2, 4, 6 and 8 days. After reaching the desired days, the as-synthesized MTN solution was centrifuged at 4000 rpm to collect the gel product and dried overnight in oven at 373 K. Finally, the product was calcined at 823 K for 3 h to remove the impurities. The aging time of MTN with x = 2, 4, 6 and 8 days were denoted as MTN-2, MTN-4, MTN-6 and MTN-8, respectively.

3.3.2 Synthesize of graphitic carbon nitride (gC_3N_4)

Bulk gC_3N_4 was synthesized via thermal polymerization method, using urea as the precursor (Maeda, An, Kuriki, Lu, & Ishitani, 2018). In typical synthesize process, 50 g of urea was placed into an alumina crucible with a cover before being heated in the

05-4506832 pustaka.upsi.edu.my Perpustakaan Tuanku Bainun Kampus Sultan Abdul Jalil Shah PustakaTBainun ptbupsi

05-4506832 pustaka.upsi.edu.my Perpustakaan Tuanku Bainun Kampus Sultan Abdul Jalil Shah PustakaTBainun ptbupsi

muffle furnace. The sample was heated up to 823 K for 3 h at a ramp rate of 275 K/min. After cooling down to room temperature, the sample of yellow powder was observed and noted as gC_3N_4. Then, the obtained product was grounded into fine powder by using a mortar.

3.3.3 Synthesize of MTN-x with addition of 5wt% Fe (5Fe/MTN-x)

The addition of Fe on MTN-x catalyst using 5wt% of Fe was prepared by wet impregnation method. The appropriate amount of MTN and Fe_2O_3 were added into 50 mL of distilled water before being impregnated at 333 K in water bath. The mixture solution was stirred until dry. Then, it was placed in the oven at 373 K overnight for further drying before being calcined using muffle furnace at 823 K for 3 h. The obtained product was denoted as 5Fe/MTN-x.

3.3.4 Synthesize of 5Fe/MTN-x with addition of 5wt% gC_3N_4 (5FeMTN-x/5gC_3N_4)

The modification of 5Fe/MTN-x with 5wt% gC_3N_4 was obtained via wet impregnation method. The appropriate amount of 5Fe/MTN-x and gC_3N_4 were added into 50 mL of distilled water before being impregnated at 333 K in water bath. The mixture solution was stirred until dry. Then, it was placed in the oven at 373 K overnight for further

05-4506832 pustaka.upsi.edu.my Perpustakaan Tuanku Bainun Kampus Sultan Abdul Jalil Shah PustakaTBainun ptbupsi

05-4506832 pustaka.upsi.edu.my Perpustakaan Tuanku Bainun Kampus Sultan Abdul Jalil Shah PustakaTBainun ptbupsi

drying before being subjected to calcination at 823 K for 3 h. The obtained product was denoted as 5FeMTN-x/5gC_3N_4.

3.4 Catalyst characterization

3.4.1 X-ray diffraction (XRD)

In this research, powder X-ray diffractometer (XRD) from model Rigaku miniflex 600c with Cu K radiation (=1.5418) at 2 angle ranging from 20° to 80° was used to determine the crystalline structures of the catalysts (Jaafar et al., 2015). The Joint Committee on Powder Diffraction Standards (JCPDS) library was used to compare the images obtained for determining the crystalline structure (Anandalakshmi, Venugobal, & Ramasamy, 2016).

05-4506832 pustaka.upsi.edu.my Perpustakaan Tuanku Bainun Kampus Sultan Abdul Jalil Shah PustakaTBainun ptbupsi

The particle size of the photocatalyst was estimated using the Debye-Scherrer equation as follows, Eq. (3.1):

$$D \quad \frac{k\lambda}{\beta \cos\theta} \tag{3.1}$$

where D is the particle size, k is the shape factor (k = 0.94), λ is the wavelength of the X-ray radiation (Cu K_α = 0.1542 nm), β is the line width at half-maximum height and θ is

05-4506832 pustaka.upsi.edu.my Perpustakaan Tuanku Bainun Kampus Sultan Abdul Jalil Shah PustakaTBainun ptbupsi

05-4506832 pustaka.upsi.edu.my Perpustakaan Tuanku Bainun Kampus Sultan Abdul Jalil Shah PustakaTBainun ptbupsi

the diffraction angle at the peak maximum. Then, Bragg's law Eq. (3.2) will be used to determine the value of the lattice spacing d(h l) for an XRD peak.

$$d_{(h\ l)} \quad \frac{}{2\sin} \tag{3.2}$$

The peak intensity obtained can help to identify the crystal structure, texture and quantitative phase of the analyzed samples. On the other hand, the sample broadening contributions can be determined through the peak shape (Epp, 2016).

3.4.2 Surface area analysis (BET)

05-4506832 pustaka.upsi.edu.my Perpustakaan Tuanku Bainun Kampus Sultan Abdul Jalil Shah PustakaTBainun ptbupsi

In this research, surface area analysis was performed by using the SA 3100 Surface Analyzer Beckman Coulter, in which can estimate the surface area, isotherm and pore distribution of the photocatalysts (Marfur, Jaafar, & Habibullah, 2019). The adsorption unit was assisted by the specific software on the computer and allowing the interpretation and data fit to the usual adsorption models which were BET and BJH for determining the specific surface areas and pore sizes, respectively (Lutic et al., 2016).

N_2 physisorption analyzer consist of two major components which were the degassing and adsorption stations. First of all, a quartz cell that being used was calibrated for gas adsorption, in which high vacuum (<Pa) at 300 ^{o}C was used to evacuate the cell

05-4506832 pustaka.upsi.edu.my Perpustakaan Tuanku Bainun Kampus Sultan Abdul Jalil Shah PustakaTBainun ptbupsi

05-4506832 pustaka.upsi.edu.my Perpustakaan Tuanku Bainun Kampus Sultan Abdul Jalil Shah PustakaTBainun ptbupsi

within 2 h (degassing) and followed by a complete adsorption cycle in the empty cell at 77 K. Then, 50-150 mg of sample was loaded into the cell before being moved to the degassing station. Purpose of degassing process was to remove the physically adsorbed water and volatiles from the sample which might accumulated during storage. For thermally sensitive solids, the degassing was done at mild temperature and for mechanically fragile porous materials, the stream of inert gas was preferred to be used instead of vacuum using the adsorbate path connected to the degassing station. After degassing process, the cell was transferred to the adsorption path and evacuated. The adsorption cycle was performed by introducing the increment of adsorbate gas into the adsorption station using the calibration volume (CAL). The differences between the measured pressure and that of the empty cell clarify the number of moles of adsorbed nitrogen. During the measurement, the cell was maintained at liquid nitrogen boiling point using a Dewar flask filled with liquid nitrogen (Bardestani et al., 2019).

3.4.3 UV-Visible diffuse reflectance spectroscopy (UV-DRS)

In this research, UV-DRS with model PerkinElmer Lambda 900 was used to measure the optical absorption and band gap of the catalysts. The scanning range was recorded over a range of wavelengths from 300 to 800 nm. The band gap energy of the catalyst samples then were calculated by using Tauc's relation and Kubel a -Munk function, Eq. (3.3):

$$(F(R)h\nu)^{0.5}=A(h\nu-E_g) \quad (3.3)$$

05-4506832 pustaka.upsi.edu.my Perpustakaan Tuanku Bainun Kampus Sultan Abdul Jalil Shah PustakaTBainun ptbupsi

05-4506832 pustaka.upsi.edu.my Perpustakaan Tuanku Bainun Kampus Sultan Abdul Jalil Shah PustakaTBainun ptbupsi

where h , A and E_g represent as photon energy, a constant and optical band gap of the nanoparticles, respectively. F(R) was the Kubelka-Munk function which was approximately proportional to the absorption constant of the material. The determination of light absorption of the samples at different wavelengths were done from the absorption spectra. Then, the values of E_g were estimated from the extrapolation of the linear regions of the plot of $(F(R)h)^{0.5}$ versus h (Rahdar, Aliahmad, & Azizi, 2015).

3.4.4 Field-Emission scanning electron microscopy (FESEM) with EDX analysis

In this research, FESEM with model Hitachi SU 8020 UHR was used to examine the morphologies and element present in the prepared photocatalysts (Kamal et al., 2019). The field emission gun (FEG) that was utilized as the electron source in FESEM consist of single tungsten filament with a pointed sharp tip. The features of this electron source help the formation of electron probe as small as 0.5 nm which exhibited a higher image resolution compared to typical SEM (Abdul Mutalib, Rahman, Othman, Ismail, & Jaafar, 2017).

Energy-Dispersive X-ray (EDX) spectroscopy was widely used for the detection of elemental composition of specimen. In this technique, the elements that have the atomic number higher than boron and at concentration of at least 0.1% can be efficiently detected. Besides that, it can also be applied for the material evaluation and identification, contamination recognition, spot detection of the regions with the diameter up to 10 cm

05-4506832 pustaka.upsi.edu.my Perpustakaan Tuanku Bainun Kampus Sultan Abdul Jalil Shah PustakaTBainun ptbupsi

05-4506832 pustaka.upsi.edu.my Perpustakaan Tuanku Bainun Kampus Sultan Abdul Jalil Shah PustakaTBainun ptbupsi

and quality control monitoring. In this analysis, the characteristic X-rays was produced after the interaction of samples with the electron beam in typical FESEM. The formation of X-ray showed that the interaction between the primary electron beam and nucleus of the sample atoms had been occurred, in which the electron in the nucleus of an atom was excited by primary electron beam before being eliminated from the nucleus and forming an electron hole. Then, the eliminated electron was replaced by the electron from the outer shell of the atom and formed the superfluous X-ray (Abdul Mutalib et al., 2017).

3.4.5 Fourier-transform infrared spectroscopy (FTIR)

In this research, FTIR spectroscopy of PerkinElmer Spectrum 3 was used to identify the chemical functional groups present in the catalysts. The solid sample for FTIR spectroscopy was prepared using the KBr pellet method in which the sample was finely grounded into solid powder. Later, the sample powder was mixed with powdered potassium bromide (KBr) and the mixture was pressing under high pressure at around 12 000 psi for 1-2 min. After the pressing, it can be observed that a very homogeneous KBr pellet was obtained as the common ratio used for the sample powder and KBr was about 1:100. Then, the obtained KBr pellet was carefully inserted into the holder of FTIR instrument. The spectrum of each sample was analyzed and no interfering bands should be appeared in the spectrum if a good pellet was prepared since KBr was transparent down to 400 cm^{-1} (Mohamed et al., 2017). The FTIR spectra for each of the photocatalyst was recorded over a range of wavenumbers from 400 to 4000 cm^{-1} (Jaafar et al., 2015).

05-4506832 pustaka.upsi.edu.my Perpustakaan Tuanku Bainun Kampus Sultan Abdul Jalil Shah PustakaTBainun ptbupsi

05-4506832 pustaka.upsi.edu.my Perpustakaan Tuanku Bainun Kampus Sultan Abdul Jalil Shah PustakaTBainun ptbupsi

In the instrument, a beam of IR irradiation was produced by the emitting from a glowing black-body source. Later, the spectral encoding was generated as the beam passed through into the interferometer. The beams then recombined with different path lengths in the interferometer and forming constructive and destructive interference, known as interferogram. As the beam enters the samples compartment, the certain frequencies of energy will be absorbed by the sample, which showed the unique characteristic of the sample from the interferogram. The received interferogram signal then was measured by detector in energy versus time for all the frequencies concurrently. At the same time, the beam was superimposed as the reference (background) was needed for the instrument operation. Finally, the interferogram will automatically ignored the background spectrum from the sample spectrum and forming only the desirable spectrum by Fourier transformation computer software (Mohamed, Jaafar, Ismail, Othman, & Rahman, 2017).

3.4.6 Photoluminescence (PL)

In this research, PL spectroscopy of PerkinElmer LS 55 was used to determine the electron-hole separation, immigration and recombination rate of the synthesized materials. The PL spectra of the photocatalysts were detected using a 450W Xenon lamp as an excitation source with excitation wavelength of 400 nm (Pham et al., 2018).

05-4506832 pustaka.upsi.edu.my Perpustakaan Tuanku Bainun Kampus Sultan Abdul Jalil Shah PustakaTBainun ptbupsi

05-4506832 pustaka.upsi.edu.my Perpustakaan Tuanku Bainun Kampus Sultan Abdul Jalil Shah PustakaTBainun ptbupsi

First of all, the PL signal passes through a single-grating monochromator will then select a wavelength to transmit to the detector (Perkowitz, 2012). There were various detectors can been used to detect the PL signal such as a photomultiplier tube (PMT), a photodiode and a photoconductor. Among those detectors, a PMT was stated to be the most sensitive detector as it promotes high-speed response (Aoki, 2012).

3.4.7 Raman spectroscopy

In this research, Raman spectroscopy with model of Renishaw inVia Raman Microscope was used to analyze the presence of structural phases and involved vibrational modes of the catalysts (Halim, Coste, Zeroual, Kassiba, & Ouaskit, 2020).

In this spectroscopy, the sample will be irradiated with a monochromatic laser beam which caused the interaction between the sample molecules and the laser, which then developing a scattered light that was used to construct a Raman spectrum.

3.5 Photodegradation of DBT

The photodegradation was performed under constant stirring in a 100 mL glass vessel containing 50 mL of acetonitrile solution of DBT (40 mg/L) as a model oil and specified

05-4506832 pustaka.upsi.edu.my Perpustakaan Tuanku Bainun Kampus Sultan Abdul Jalil Shah PustakaTBainun ptbupsi

05-4506832 pustaka.upsi.edu.my Perpustakaan Tuanku Bainun Kampus Sultan Abdul Jalil Shah PustakaTBainun ptbupsi

amount of catalyst. Before illumination, the suspension was magnetically stirred for 60 min in the dark to attain adsorption-desorption equilibrium between photocatalyst and DBT. Then, the reaction was continued for another 180 min with irradiation of 400W LED UV lamp (395 nm) under continuous stirring. During the reaction, 2 mL of aliquots were sampled every 30 min and centrifuged using micro centrifuge at 13000 rpm for 30 min to separate the liquid phase from solid catalyst before being analyzed by UV-Visible (UV-Vis) spectroscopy. As we know that, UV-Vis spectroscopy was a widely used technique for determining the absorption properties of materials. In this research, UV-Vis spectroscopy of Jasco V-570 was used to determine the absorption of DBT and it was monitored at λ_{max} = 325 nm, as depicted in Appendix A (Abedini et al., 2021).

05-4506832 pustaka.upsi.edu.my Perpustakaan Tuanku Bainun Kampus Sultan Abdul Jalil Shah PustakaTBainun ptbupsi

A calibration curve for determining the degradation of DBT in acetonitrile as model oil was constructed by the following steps. A stock solution of model oil was prepared by transferring specified amount of DBT into 100 mL volumetric flask and followed by the addition of acetonitrile as the solvent to dissolve the DBT and dilute to the mark. Using the volumetric techniques, a series of standard solution was prepared with the range of DBT in acetonitrile solution concentration from 20 to 60 mg/L. From the calibration curve, the concentration of the DBT in acetonitrile solution was determined by the following equation, Eq. (3.4):

$$y = mx + c \tag{3.4}$$

05-4506832 pustaka.upsi.edu.my Perpustakaan Tuanku Bainun Kampus Sultan Abdul Jalil Shah PustakaTBainun ptbupsi

05-4506832 pustaka.upsi.edu.my Perpustakaan Tuanku Bainun Kampus Sultan Abdul Jalil Shah PustakaTBainun ptbupsi

where y is the absorbance value obtained from the UV-Vis spectroscopy, m is the slope of the calibration line and x is the concentration of the DBT in acetonitrile solution, as illustrated in Appendix B. Then, the percentage of DBT degradation at a time, will be calculated as follows:

$$\text{Degradation (\%)} = \left(\frac{-}{} \right) \times 100 \quad (3.5)$$

where was denoted as the initial concentration of DBT before being exposed to irradiation and C_t represents as the concentration of DBT solution at a specific time.

The optimization study for the best catalyst was also carried out based on important parameters, which were addition of H_2O_2 solution, initial DBT concentration and catalyst dosage. The photocatalytic reaction was also prolonging to 240 min in order to improve the percent of DBT degradation. The volumes of H_2O_2 solution were selected (0.01, 0.03, 0.06 and 0.09 mL) and intial concentrations in the range of 20-60 mg/L of DBT were used to determine the optimum condition for photodegradation efficiency. In addition, the chosen catalyst dosages were 1, 3, 5, 7 and 9 g/L. The excess of DBT solution at optimum condition was collected after the photocatalytic reaction. It was separated by high-speed centrifuge and then the upper layer model oil was collected to be analyzed by Gas Chromatography-Mass Spectrometer (GC-MS) with the model from Agilent 7890A/5975C-GC/MSD with the HP-5MS as the GC column to determine the degradation product of DBT (Lu et al., 2020). Both a gas chromatograph and a mass spectrometer were recognized as simple instruments conceptually and the analytical

05-4506832 pustaka.upsi.edu.my Perpustakaan Tuanku Bainun Kampus Sultan Abdul Jalil Shah PustakaTBainun ptbupsi

05-4506832 pustaka.upsi.edu.my Perpustakaan Tuanku Bainun Kampus Sultan Abdul Jalil Shah PustakaTBainun ptbupsi

results produced by these instruments can be easily understood and used. The analytical capabilities of these two instruments were enhanced after being combined as one GC-MS system, in which gas chromatography (GC) was used for the highly competent gas-phase separation of components in complex mixtures while mass spectrometry (MS) was responsible for the identification of the components and also the unknowns. In GC-MS system, the potential showed in the enormous amount of data generated were came from a highly advanced computer programs. Many techniques of data manipulation can be conducted with the presence of computer, which can enhance the quality of analytical results (Karasek & Clement, 2012).

GC-MS system comprises of five parts which were sample introduction, ionization, mass analysis, ion detection and data handling. The sample introduction was generated from the open capillary chromatographic column, either directly or via an open split coupling. Then, electron ionization or chemical ionization was usually utilized to perform the ionization of the analytes. The produced ions then were separated based on their m/z ratio in the mass analyzer. The detection of ions was largely performed using an electron multiplier. Generally, analyte ionization, mass analysis and ion detection were carried out in high-vacuum system. In most benchtop GC-MS systems, the vacuum systems were included with one pumped chamber, evacuated via small turbomolecular pump and supported by a mechanical fore pump. On the other hand, large systems and modern research-grade mass spectrometers usually involve two different pumped vacuum chambers, separated through a baffle containing a slit which were ion source housing and analyzer region (Niessen, 2001).

05-4506832 pustaka.upsi.edu.my Perpustakaan Tuanku Bainun Kampus Sultan Abdul Jalil Shah PustakaTBainun ptbupsi

05-4506832 pustaka.upsi.edu.my Perpustakaan Tuanku Bainun Kampus Sultan Abdul Jalil Shah PustakaTBainun ptbupsi

CHAPTER 4

RESULTS AND DISCUSSION

05-4506832 pustaka.upsi.edu.my Perpustakaan Tuanku Bainun Kampus Sultan Abdul Jalil Shah PustakaTBainun ptbupsi

4.1 Effect of Mesoporous Titania Nanoparticles (MTN) aging time

In this section, we discussed about the MTN which successfully synthesized via sol-gel method. This method was applied by varying the aging time of the bare MTN to study the effect towards the photocatalytic activity. The MTN was aging for x = 2, 4, 6 and 8 days and were denoted as MTN-2, MTN-4, MTN-6 and MTN-8, respectively.

05-4506832 pustaka.upsi.edu.my Perpustakaan Tuanku Bainun Kampus Sultan Abdul Jalil Shah PustakaTBainun ptbupsi

05-4506832 pustaka.upsi.edu.my Perpustakaan Tuanku Bainun Kampus Sultan Abdul Jalil Shah PustakaTBainun ptbupsi

4.1.1 Crystallinity

The crystalline structure and phase information of all the samples were evaluated through XRD characterization. Figure 4.1 shows the XRD patterns of MTN prepared by sol-gel method under various aging time. A series of XRD peaks referring to the common peaks of TiO_2 anatase phase were detected for MTN 2,4,6 and 8 (JCPDS card No. 00-064-0863) at 25.37°, 36.97°, 37.94°, 38.66°, 48.04°, 53.89°, 55.06°, 62.69°, 68.76°, 70.29° and 75.05°, which corresponded to (101), (103), (004), (112), (200), (105), (211), (204), (116), (220) and (215) planes, respectively (Lavand, Bhatu, & Malghe, 2019). From the results, it can be observed that the peaks for all catalyst appeared in similar pattern. The particle sizes of the synthesized catalyst were determined based on the major peak at $2\theta =$ 25.37° using the Eq. (3.1).

05-4506832 pustaka.upsi.edu.my Perpustakaan Tuanku Bainun Kampus Sultan Abdul Jalil Shah PustakaTBainun ptbupsi

The calculated particle sizes of MTN-2, 4, 6 and 8 were 15.13, 18.32, 21.77 and 18.08 nm, respectively. The obtained results proved that the average particle sizes of the catalysts have increased with the increasing aging time and MTN-2 showed the smallest size compared to other samples (Yazici, Comakli, Yetim, Yetim, & Celik, 2016). The result agreed with the study reported by Li, Yang, and Zhu (2017) which stated that prolonging aging time will cause the sol to continue react chemically and agglomerated to form larger sol particles. Other than that, the crystal seed had more available time to grow with the increasing of aging time. However, when the aging time was reached to 8 days, the particle size has decreased. It can be concluded that the crystal growth was

05-4506832 pustaka.upsi.edu.my Perpustakaan Tuanku Bainun Kampus Sultan Abdul Jalil Shah PustakaTBainun ptbupsi

05-4506832 pustaka.upsi.edu.my Perpustakaan Tuanku Bainun Kampus Sultan Abdul Jalil Shah PustakaTBainun ptbupsi

influenced by the MTN viscosity obtained no longer than 6 days. By increasing the aging time to 8 days, the viscosity tend to increase due to the evaporation of water molecules which encouraged the polycondensation of O-Ti-O and transformation into crystal phase to be interrupted and thus, harm the crystal phase system (Fajriati, Mudasir, & Wahyuni , 2017). Therefore, the particle size of MTN-8 was smaller than other photocatalysts. The results clearly indicate that the aging time play a crucial role in controlling the particle size (Arabkhani & Abedini-Khorrami, 2019). From the XRD results, it confirmed the successful formation of MTN photocatalysts.

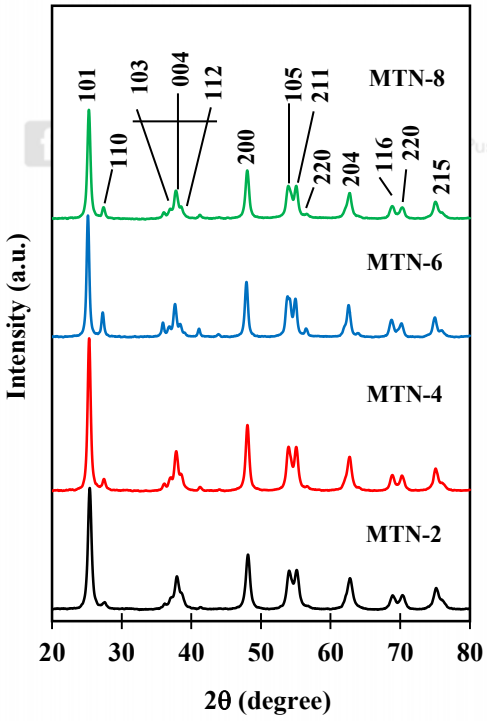


Figure 4.1. XRD Patterns of MTN-2, MTN-4, MTN-6 and MTN-8

05-4506832 pustaka.upsi.edu.my Perpustakaan Tuanku Bainun Kampus Sultan Abdul Jalil Shah PustakaTBainun ptbupsi

05-4506832 pustaka.upsi.edu.my Perpustakaan Tuanku Bainun Kampus Sultan Abdul Jalil Shah PustakaTBainun ptbupsi

4.1.2 Surface morphology with Elemental Analysis

The morphology of the synthesized photocatalysts were studied by FESEM. Figure 4.2 shows the FESEM images of MTN-2, MTN-4, MTN-6 and MTN-8.

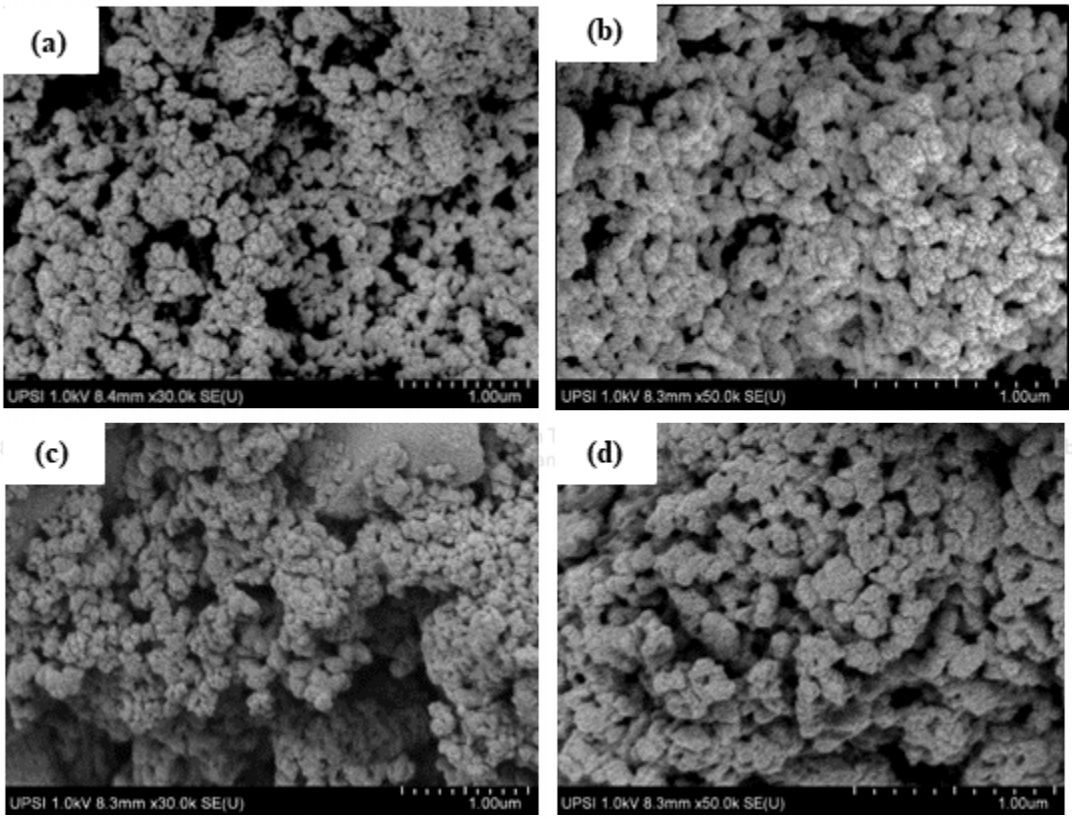


Figure 4.2. FESEM Images of (a) MTN-2, (b) MTN-4, (c) MTN-6 and (d) MTN-8

It can be seen that all samples formed spherical nanoparticles that interconnect with each other to form disordered mesoporous network structure (Mani, Rajendran, Nalajala, Mathew, & Gopinath, 2021). As can be seen from the FESEM images, the mesoporous structure were probably increased from the further aging time of 2 to 8 days.

05-4506832 pustaka.upsi.edu.my Perpustakaan Tuanku Bainun Kampus Sultan Abdul Jalil Shah PustakaTBainun ptbupsi

05-4506832 pustaka.upsi.edu.my Perpustakaan Tuanku Bainun Kampus Sultan Abdul Jalil Shah PustakaTBainun ptbupsi

The formation of larger TiO_2 nanoparticles resulted from further hydrolysis and condensation of titanium precursors, which were then slowly aggregated to one another (Govindaraj, Pandian, Ramasamy, & Mukhopadhyay, 2014). The results obtained were in accordance to the XRD results, as the particle size has significantly increased from Day 2 onward.

The elemental composition of bare MTN sample was determined with EDX technique. The EDX dot-mapping images of MTN-4 was shown in Figure 4.3 and the coloured spots were used to display the elements present in the photocatalyst. From the mapping images, it confirmed the uniform distribution of O and Ti elements in the MTN-4 sample.

05-4506832 pustaka.upsi.edu.my Perpustakaan Tuanku Bainun Kampus Sultan Abdul Jalil Shah PustakaTBainun ptbupsi

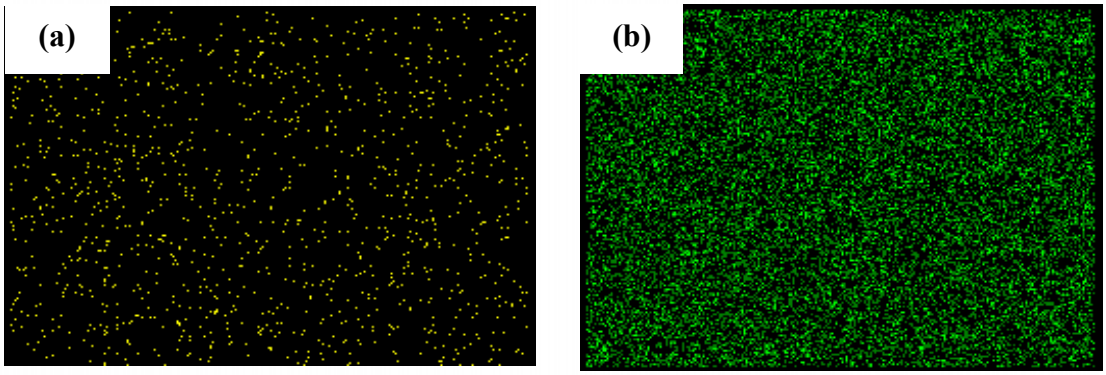


Figure 4.3. EDX Dot-Mapping Images of MTN-4 consist of (a) O, (b) Ti

05-4506832 pustaka.upsi.edu.my Perpustakaan Tuanku Bainun Kampus Sultan Abdul Jalil Shah PustakaTBainun ptbupsi

05-4506832 pustaka.upsi.edu.my Perpustakaan Tuanku Bainun Kampus Sultan Abdul Jalil Shah PustakaTBainun ptbupsi

4.1.3 Functional group

The FTIR analysis was then performed between the region of 4000 and 400 cm^{-1} and the spectra were shown in Figure 4.4.

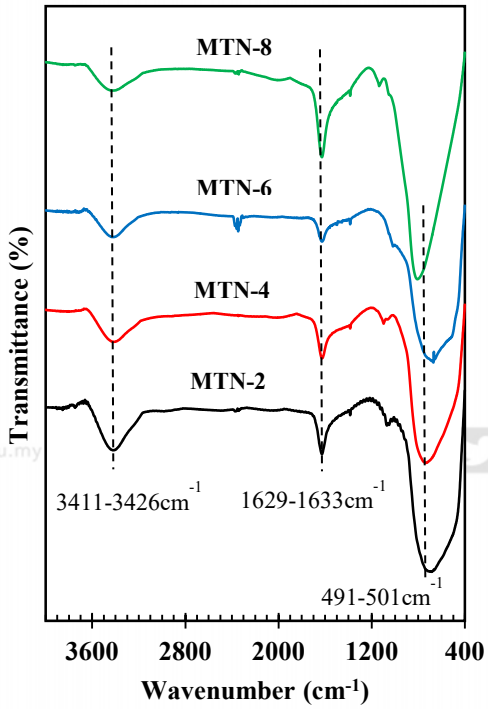


Figure 4.4. FTIR Spectra of MTN-2, MTN-4, MTN-6 and MTN-8

It can be observed that the FTIR spectrum of all the MTN samples have nearly similar patterns. From the FTIR data, the broad absorption band around 3411-3426 cm^{-1} was exhibited by all the catalysts, which indicated the presence of hydroxyl (OH) group that chemisorbed on the surface of TiO_2 framework (Marfur et al., 2019). The presence of the OH groups in the MTN confirmed the significant of these samples as the

05-4506832 pustaka.upsi.edu.my Perpustakaan Tuanku Bainun Kampus Sultan Abdul Jalil Shah PustakaTBainun ptbupsi

05-4506832 pustaka.upsi.edu.my Perpustakaan Tuanku Bainun Kampus Sultan Abdul Jalil Shah PustakaTBainun ptbupsi

photocatalytic reaction will be improved due to the formation of hydroxyl radicals ($^{\bullet}OH$) that was needed for the degradation of DBT (Ali et al., 2017). The absorption band around 1629-1633 cm^{-1} was also appeared for all catalysts, which was correlated to the H-O-H bending vibration of the surface-adsorbed water (Jiang et al., 2018). It can be observed that, the hydroxyl bands became less significant with the increasing aging time, which explained the large portion of adsorbed water from TiO_2 has been removed by the continuous condensation reaction (Anisah, Kanezashi, Nagasawa, & Tsuru, 2019).

Besides that, the bands around 491-501 cm^{-1} which was assigned to Ti-O-Ti stretching vibration were also seen for all the catalysts (Huang et al., 2015). Based on the spectra, it can be observed that the intense wide band at 491 cm^{-1} which attributed to the Ti-O-Ti vibration was slightly shifted to a higher frequency at 501 cm^{-1} when the MTN aging time was increased, indicating the different strength of Ti-O bonds. It was due to the major structural changes that occurred in the precursor sol as a function of aging. During the aging, the reaction of hydrolysis-condensation will take place which lead to the breaking of the bonds initially formed in the precursor and resulted in the formation of Ti-O-Ti bonds. However, with further aging, it caused the fragmentation of Ti-O-Ti network into Ti-O system, which was due to the greater bond strength of the Ti-O network (Verma, Kar, & Agnihotry, 2007).

05-4506832 pustaka.upsi.edu.my Perpustakaan Tuanku Bainun Kampus Sultan Abdul Jalil Shah PustakaTBainun ptbupsi

05-4506832 pustaka.upsi.edu.my Perpustakaan Tuanku Bainun Kampus Sultan Abdul Jalil Shah PustakaTBainun ptbupsi

4.1.4 Surface area/pore structure

The N_2 adsorption-desorption isotherms were conducted to indicate the surface area and pore structure of the prepared photocatalysts. The N_2 adsorption-desorption isotherms and pore size distributions of the MTN-2, MTN-4, MTN-6 and MTN-8 were shown in Figure 4.5 (a) and (b) respectively.

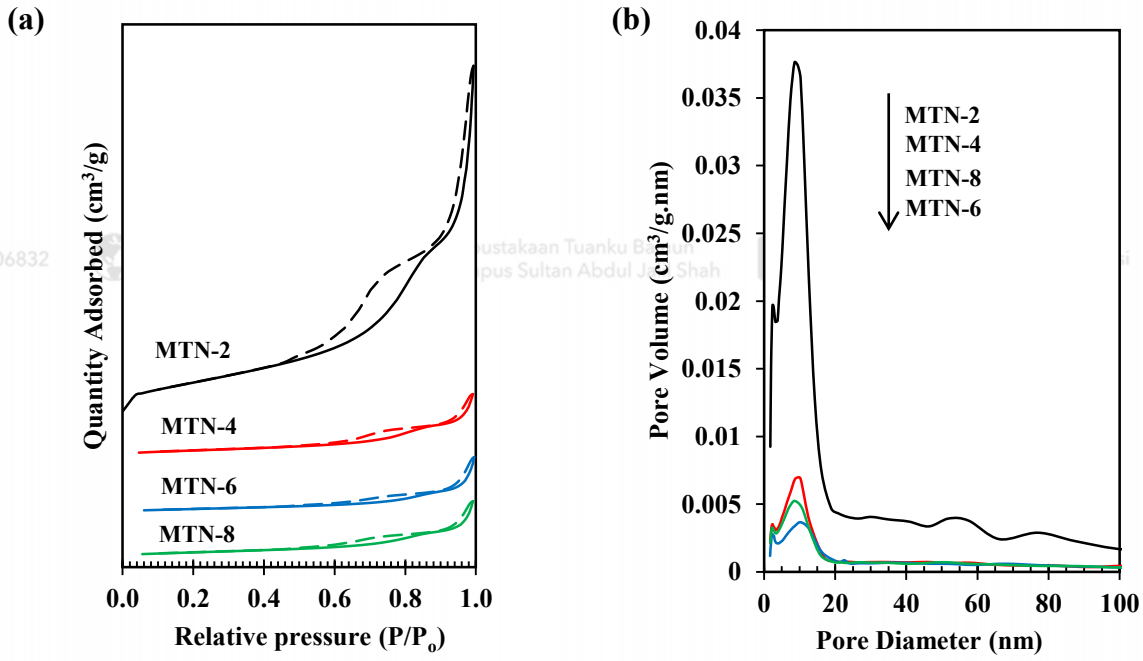


Figure 4.5. (a) N_2 Adsorption-Desorption Linear Isotherms and (b) Pore Size Distribution of MTN-2, MTN-4, MTN-6 and MTN-8

It was observed that MTN-2 exhibited a Type IV isotherm with a H3 hysteresis loop, which indicated the presence of mesoporous materials with slit-shaped pores that were non-uniform in size or shape in the synthesized photocatalysts (Marfur et al., 2019).

05-4506832 pustaka.upsi.edu.my Perpustakaan Tuanku Bainun Kampus Sultan Abdul Jalil Shah PustakaTBainun ptbupsi

05-4506832 pustaka.upsi.edu.my Perpustakaan Tuanku Bainun Kampus Sultan Abdul Jalil Shah PustakaTBainun ptbupsi

When the aging time were increased to 4, 6 and 8 days, the typical IV isotherm with H3 hysteresis loop was still maintained which showed that the samples still exhibited the close-packed agglomeration structure, but has differences in surface area. The surface area was significantly decreased upon the aging time due to the grain growth. The hysteresis loop at P/P_o = 0.46-0.99 was corresponded to nitrogen condensation that occurred within the nanoparticles voids, which was obtained from the textural porosity between particles (Jaafar et al., 2015). All the pore structural informations of each of the photocatalysts were represented in Table 4.1.

Table 4.1

Pore Structural Informations of MTN-2, MTN-4, MTN-6 and MTN-8 Photocatalysts

Photocatalyst	**Surface area (m^2/g)**	**Pore volume (cm^3/g)**	**Pore size (nm)**
MTN-2	232.53	0.0374	9.50
MTN-4	42.63	0.0069	10.2
MTN-6	28.69	0.0030	13.0
MTN-8	36.87	0.0047	10.7

According to BET results, the highest surface area was formed by MTN-2 (232.53 m^2/g), followed by MTN-4 (42.63 m^2/g), MTN-8 (36.87 m^2/g) and MTN-6 (28.69 m^2/g). According to Zhang et al. (2020), high surface area can generate abundant of active sites

05-4506832 pustaka.upsi.edu.my Perpustakaan Tuanku Bainun Kampus Sultan Abdul Jalil Shah PustakaTBainun ptbupsi

05-4506832 pustaka.upsi.edu.my Perpustakaan Tuanku Bainun Kampus Sultan Abdul Jalil Shah PustakaTBainun ptbupsi

for adsorption and reaction of reactants, thus, enhancing the photocatalytic activity. This statement was in accordance to the DBT degradation results, as MTN-2 obtained the highest degradation rate compared to other samples. Figure 4.5(b) shows the pore size distribution for all photocatalysts. It can be observed that at the pore size range from 5-20 nm, MTN-2 obtained the highest number of pores, followed by MTN-4, MTN-8 and MTN-6. The results indicated that the rudimentary pore formation favourably occurred in MTN-2. It also showed that the surface area and pore structure of the photocatalyst play a vital role to maintain the mesoporosity of the nanoparticles (Marfur et al., 2019).

4.1.5 Structural phases

05-4506832 pustaka.upsi.edu.my Perpustakaan Tuanku Bainun Kampus Sultan Abdul Jalil Shah PustakaTBainun ptbupsi

Raman characterization were carried out to analyze the structural phases and involved vibrational modes of the catalysts. Figure 4.6 shows the Raman spectra of MTN prepared under various days. The Raman bands at 144 cm^{-1} (E_g), 197 cm^{-1} (E_g), 399 cm^{-1} (B_{1g}), 515 cm^{-1} (A_{1g} + B_{1g}) and 639 cm^{-1} (E_g) which were corresponded to the six Raman active modes in the TiO_2 anatase phase were identified for all the photocatalysts. The Raman mode E_g was assigned to the symmetric stretching vibration of O-Ti-O in TiO_2 while A_{1g} and B_{1g} modes was corresponded to the antisymmetric and symmetric bending vibration of O-Ti-O in TiO_2, respectively (Halim et al., 2020). The presence of only TiO_2 anatase phase in the samples showed that the Raman spectral observations were consistent with the XRD results.

05-4506832 pustaka.upsi.edu.my Perpustakaan Tuanku Bainun Kampus Sultan Abdul Jalil Shah PustakaTBainun ptbupsi

05-4506832 pustaka.upsi.edu.my Perpustakaan Tuanku Bainun Kampus Sultan Abdul Jalil Shah PustakaTBainun ptbupsi

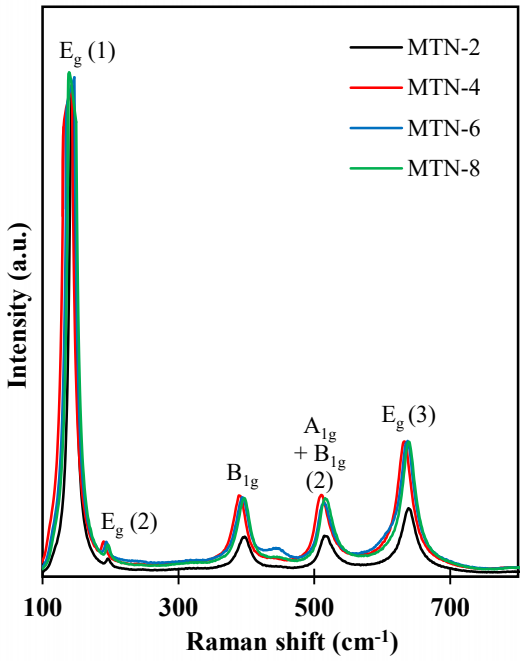


Figure 4.6. Raman Spectra of MTN-2, MTN-4, MTN-6 and MTN-8

05-4506832 pustaka.upsi.edu.my Perpustakaan Tuanku Bainun Kampus Sultan Abdul Jalil Shah PustakaTBainun ptbupsi

By comparing the Raman spectra, it can be seen that the peaks became narrow and shifted to lower wavenumber as well as the intensity was relatively increased upon the increasing of MTN aging time. The changes occurred in the Raman bands proved that the particle size of photocatalysts had been increased (Xue et al., 2012). In this case, the increased in particle size could be due to the amount of storage time that has influenced the viscosity of the produced sol to be increased and enhanced the anatase crystallite growth (Zieba et al., 2021). The results were in accordance to the XRD as the crystallite sizes of MTN-4, MTN-6 and MTN-8 were larger than MTN-2.

05-4506832 pustaka.upsi.edu.my Perpustakaan Tuanku Bainun Kampus Sultan Abdul Jalil Shah PustakaTBainun ptbupsi

05-4506832 pustaka.upsi.edu.my Perpustakaan Tuanku Bainun Kampus Sultan Abdul Jalil Shah PustakaTBainun ptbupsi

4.1.6 DBT degradation

The photocatalytic activity of MTN samples were investigated on the photodegradation of DBT under UV light irradiation, and the results were shown in Figure 4.7.

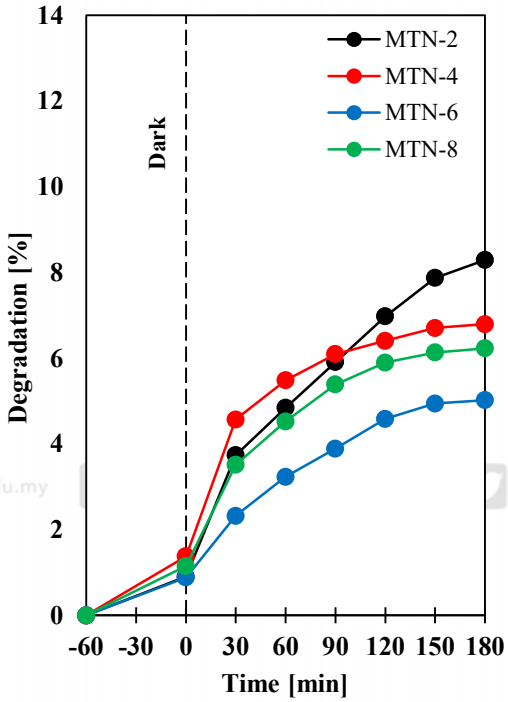


Figure 4.7. % Degradation of DBT for MTN-2, MTN-4, MTN-6 and MTN-8

All the catalysts were stirred in the dark for 60 min to achieve adsorption-desorption equilibrium before being exposed under light irradiation. However, there was no significant changing observed after 60 min of dark test which indicated that all samples have low ability in DBT physical adsorption in dark conditions (Abedini et al., 2021). From the results as illustrated in Figure 4.7, MTN-2 exhibited the highest degradation of DBT with 8.3%, followed by MTN-4, MTN-8 and MTN-6, with 6.8%,

05-4506832 pustaka.upsi.edu.my Perpustakaan Tuanku Bainun Kampus Sultan Abdul Jalil Shah PustakaTBainun ptbupsi

05-4506832 pustaka.upsi.edu.my Perpustakaan Tuanku Bainun Kampus Sultan Abdul Jalil Shah PustakaTBainun ptbupsi

6.2% and and 5.0% within 180 min of irradiation time, respectively. The photocatalytic performance could be influenced by the particle sizes and surface area obtained for each catalyst, in which according to the XRD and BET results, MTN-2 has the lowest particle size and highest surface area. Retamoso et al. (2019) and Reddy, Rajendar, Shekar, and Park (2018) reported that small particles sizes can help to improve the photocatalytic activity as it promoted large surface area that lead to the enhancement of active sites on the nanoparticles surface, which in turn will increase the removal of organic pollutants. The result obtained was in agreement with the reported study from Reddy et al. (2018), in which the degradation efficiency increased from 15% to 30% when the particle size decreases from 615 nm to 190 nm. The results for photodegradation of DBT using MTN at different aging time were summarized in Table 4.2.

05-4506832 pustaka.upsi.edu.my Perpustakaan Tuanku Bainun Kampus Sultan Abdul Jalil Shah PustakaTBainun ptbupsi

Table 4.2

Photodegradation of DBT using MTN-2, MTN-4, MTN-6 and MTN-8 Photocatalysts

Photocatalyst	**DBT degradation (%)**
MTN-2	8.3
MTN-4	6.8
MTN-6	5.0
MTN-8	6.2

Reaction conditions: model oil = 50 mL, Time = 180 min, Catalyst dosage = 5 g/L, DBT concentration = 40 mg/L, UV.

05-4506832 pustaka.upsi.edu.my Perpustakaan Tuanku Bainun Kampus Sultan Abdul Jalil Shah PustakaTBainun ptbupsi

05-4506832 pustaka.upsi.edu.my Perpustakaan Tuanku Bainun Kampus Sultan Abdul Jalil Shah PustakaTBainun ptbupsi

However, there was no significant changing observed by varying the bare MTN aging time, in which the photocatalytic performance of each photocatalyst was not showed any significant different. Therefore, in the next section, the effect of Fe addition towards all the bare MTN photocatalysts was studied to improve the photocatalytic properties of MTN and identify the best MTN which suitable to incorporate with Fe.

4.2 Effect of Fe addition into various MTN

In this section, the effect of Fe addition into MTN with various aging time (x = 2, 4, 6 and 8 days) were investigated. The addition of 5wt% Fe into MTN-x samples (5Fe/MTN-x) was performed to enhance the photocatalytic performance of photocatalysts. The 5wt% of Fe addition was chosen in this study because it was known to perform highest photocatalytic performance in degradation of organic pollutants from many studies. This statement can be supported by the study from Xu, Zhang, and Zhang (2020), in which 5wt% of Fe_2O_3 and 5wt% TiO_2 has been loaded into fluid catalytic cracking catalyst for degradation of MB. The catalyst then was denoted as Fe-Ti/SF composite. From this study, it showed that Fe-Ti/SF composite has exhibited the highest photocatalytic activity (94.2%) compared to other catalyst that used 10wt% Fe_2O_3 and 10wt% TiO_2 as a loading which only degraded 22.3% and 54.0% of MB, respectively. Besides that, another study from Abbas et al. (2016) has also doped 5wt% of Fe_2O_3 into TiO_2 which was noted as TiFe5 for degradation of MB. From the results, it can be observed that the catalyst has

05-4506832 pustaka.upsi.edu.my Perpustakaan Tuanku Bainun Kampus Sultan Abdul Jalil Shah PustakaTBainun ptbupsi

05-4506832 pustaka.upsi.edu.my Perpustakaan Tuanku Bainun Kampus Sultan Abdul Jalil Shah PustakaTBainun ptbupsi

performed maximum MB degradation compared to other catalyst that incorporated 2, 8, 15, 25 and 35wt% of Fe_2O_3 into TiO_2 photocatalyst.

4.2.1 Crystallinity

Figure 4.8 shows the XRD patterns of various 5Fe/MTN-x samples synthesized via wet-impregnation method.

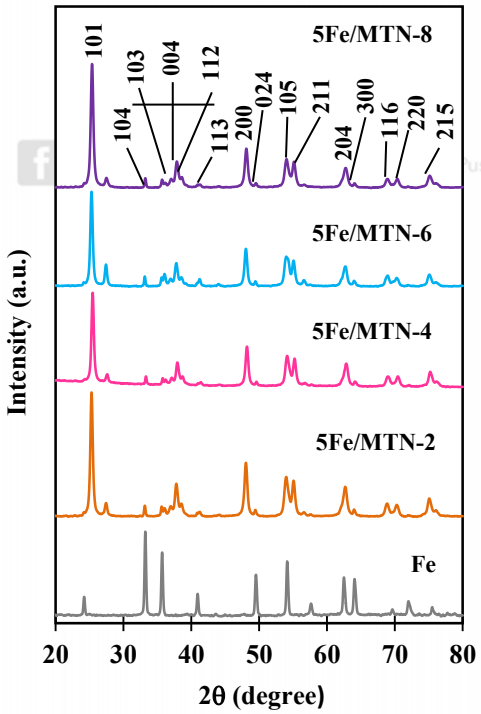


Figure 4.8. XRD Patterns of 5Fe/MTN-2, 5Fe/MTN-4, 5Fe/MTN-6, 5Fe/MTN-8 and Fe

05-4506832 pustaka.upsi.edu.my Perpustakaan Tuanku Bainun Kampus Sultan Abdul Jalil Shah PustakaTBainun ptbupsi

05-4506832 pustaka.upsi.edu.my Perpustakaan Tuanku Bainun Kampus Sultan Abdul Jalil Shah PustakaTBainun ptbupsi

A series of characteristic peaks were observed for 5Fe/MTN-x at 25.34^{o} (101), 36.93^{o} (103), 37.79^{o} (004), 38.54^{o} (112), 47.98^{o} (200), 53.88^{o} (105), 55.00^{o} (211), 62.64^{o} (204), 68.74^{o} (116), 70.20^{o} (220) and 75.00^{o} (215) which corresponding to the typical peaks of TiO_2 anatase phase (JCPDS card No. 00-064-0863). The XRD analysis also showed the presence of Fe as the diffraction peaks matched with hematite were appeared at 33.12^{o}, 40.80^{o}, 49.38^{o} and 63.94^{o} corresponding to (104), (113), (024) and (300) planes, respectively (JCPDS card No. 01-071-5088). The peaks for 5Fe/MTN-2, 5Fe/MTN-4, 5Fe/MTN-6 and 5Fe/MTN-8 appeared in similar pattern, but slight decrease in intensity was observed for 5Fe/MTN-4 and 5Fe/MTN-6. This illustrated that different aging time during the preparation of MTN might affect the particle size of TiO_2 but did not significantly change the structure of the catalyst (Jaafar et al., 2017).

05-4506832 pustaka.upsi.edu.my Perpustakaan Tuanku Bainun Kampus Sultan Abdul Jalil Shah PustakaTBainun ptbupsi

The calculated particle size of 5Fe/MTN-2, 5Fe/MTN-4, 5Fe/MTN-6 and 5Fe/MTN-8 were found to be 25.31, 25.09, 23.92 and 22.18 nm, respectively. It can be observed that the particle sizes of 5Fe/MTN-x samples were larger than the samples of bare MTN-x. These results could be due to the agglomeration of particles that occurred because of the presence of impurity that caused the formation of defects and dislocations in the crystal lattice (Khan & Berk, 2014). The addition of Fe into MTN with higher aging time showed a decrement in the particle size. The decrement in particle size exhibited by 5Fe/MTN-x samples could be attributed to the addition of Fe that acted as defects in crystal structure and hindering the crystalline growth and crystal size of MTN (Pradubkorn, Maensiri, Swatsitang, & Laokul, 2020). However, the variation of crystallite size could be related to a disorder in the location of Fe inside the lattice due to

05-4506832 pustaka.upsi.edu.my Perpustakaan Tuanku Bainun Kampus Sultan Abdul Jalil Shah PustakaTBainun ptbupsi

05-4506832 pustaka.upsi.edu.my Perpustakaan Tuanku Bainun Kampus Sultan Abdul Jalil Shah PustakaTBainun ptbupsi

the different particle size of MTN (Ahadi, Moalej, & Sheibani, 2019). From the obtained XRD results, it confirmed the successful formation of 5Fe/MTN-x photocatalysts.

4.2.2 Surface morphology with Elemental Analysis

The FESEM images of 5Fe/MTN-2, 5Fe/MTN-4, 5Fe/MTN-6 and 5Fe/MTN-8 were shown in Figure 4.9.

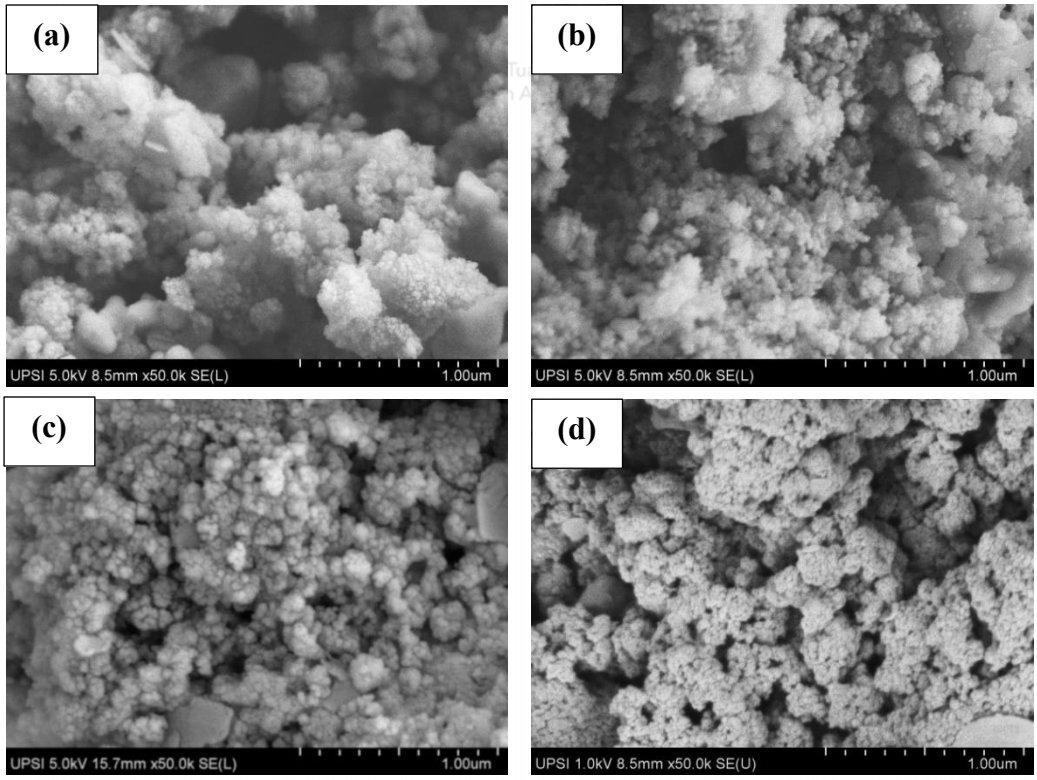


Figure 4.9. FESEM Images of the Samples (a) 5Fe/MTN-2, (b) 5Fe/MTN-4, (c) 5Fe/MTN-6 and (d) 5Fe/MTN-8

05-4506832 pustaka.upsi.edu.my Perpustakaan Tuanku Bainun Kampus Sultan Abdul Jalil Shah PustakaTBainun ptbupsi

05-4506832 pustaka.upsi.edu.my Perpustakaan Tuanku Bainun Kampus Sultan Abdul Jalil Shah PustakaTBainun ptbupsi

From the images, it can be seen that all the samples formed nanosized primary particles with slight agglomeration (Ali et al., 2017), which were completely different from bare MTN samples. The EDX analysis was performed and represented in Figure 4.10. From the dot-mapping images of 5Fe/MTN-6 samples, it confirmed the uniform distribution of Ti, O and Fe atoms in the photocatalyst, which were also observed in other 5Fe/MTN-x samples. The result was in accordance to the XRD, which showed that Fe was successfully loaded into MTN-x samples.

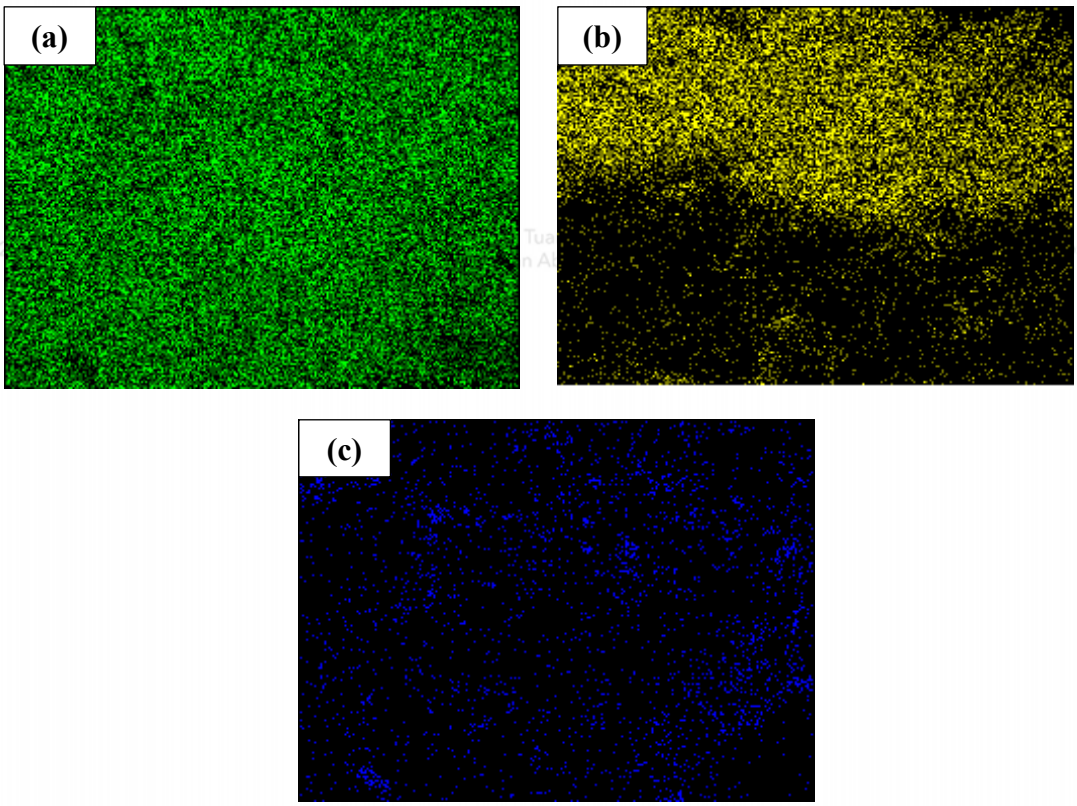


Figure 4.10. EDX Dot-Mapping Images of 5Fe/MTN-6 consist of (a) Ti, (b) O and (c) Fe

05-4506832 pustaka.upsi.edu.my Perpustakaan Tuanku Bainun Kampus Sultan Abdul Jalil Shah PustakaTBainun ptbupsi

05-4506832 pustaka.upsi.edu.my Perpustakaan Tuanku Bainun Kampus Sultan Abdul Jalil Shah PustakaTBainun ptbupsi

4.2.3 Measured band gap

UV-DRS was performed to investigate the optical absorption characteristics and the band gap energy of the prepared samples. The absorption spectra of the photocatalysts were measured between the wavelength ranges from 300 to 800 nm. Figure 4.11 showed the UV-DRS spectra of 5Fe/MTN-2, 5Fe/MTN-4, 5Fe/MTN-6 and 5Fe/MTN-8 samples.

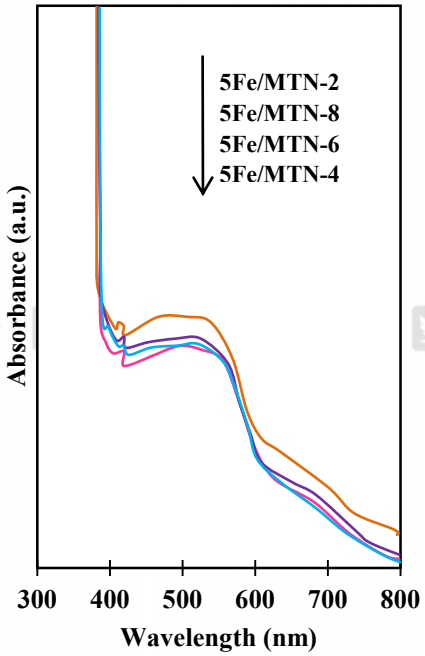


Figure 4.11. UV-DRS Spectra of (a) 5Fe/MTN-2, (b) 5Fe/MTN-4, (c) 5Fe/MTN-6 and (d) 5Fe/MTN-8

From the results, it can be observed that the absorption edge of 5Fe/MTN-x samples were shifted towards the visible region. The red shift of the absorption edge to the higher wavelengths was due to the incorporation of Fe into MTN that exhibited sp-d exchange interactions between band electrons and localized d electrons of metal ions

05-4506832 pustaka.upsi.edu.my Perpustakaan Tuanku Bainun Kampus Sultan Abdul Jalil Shah PustakaTBainun ptbupsi

05-4506832 pustaka.upsi.edu.my Perpustakaan Tuanku Bainun Kampus Sultan Abdul Jalil Shah PustakaTBainun ptbupsi

(Akshay et al., 2018). The decreased in intensity of the visible light absorbance was also seen at the visible light range of 600-800 nm, with the introduction of Fe into MTN with higher aging time. This proved that the addition of Fe into MTN could extend the optical absorption towards the visible light region (Zhang et al., 2017). Also, all the 5Fe/MTN-x samples showed a broad peak in the visible region. The white colour of MTN samples turned into dark pink after incorporating of Fe powder into the photocatalysts. On the other hand, the additional absorption peak around 550 nm was observed in all samples which corresponded to the presence of Fe_2O_3 (Sadanandam et al., 2018). The optical band gap for all the photocatalysts were calculated using the Tauc equation and Kubelka-Munk function, Eq. 4.1:

05-4506832 pustaka.upsi.edu.my Perpustakaan Tuanku Bainun Kampus Sultan Abdul Jalil Shah PustakaTBainun ptbupsi

$$(F(R)h\nu)^{0.5}=A(h\nu-E) \quad (4.1)$$

where hν is the photon energy, A is constant, E is the band gap energy and F(R) is proportional to the absorption constant of the material. The $(F(R)h\nu)^{0.5}$ versus the hν curve for all the photocatalysts were shown in Figure 4.12. The calculated band gap of the samples were 3.24, 3.24, 3.24 and 3.23 eV for 5Fe/MTN-2, 5Fe/MTN-4, 5Fe/MTN-6 and 5Fe/MTN-8, respectively. It can be observed that the band gap were closely to each other. The obtained band gap for all the catalysts illustrated that the catalysts will perform better under UV light irradiation instead of visible light. The incorporation of Fe into MTN in this study seems to not affected the band gap of photocatalysts, and thus can be

05-4506832 pustaka.upsi.edu.my Perpustakaan Tuanku Bainun Kampus Sultan Abdul Jalil Shah PustakaTBainun ptbupsi

05-4506832 pustaka.upsi.edu.my Perpustakaan Tuanku Bainun Kampus Sultan Abdul Jalil Shah PustakaTBainun ptbupsi

concluded that the band gap was not the main factor that influence the efficiency of photocatalysts' photocatalytic activity.

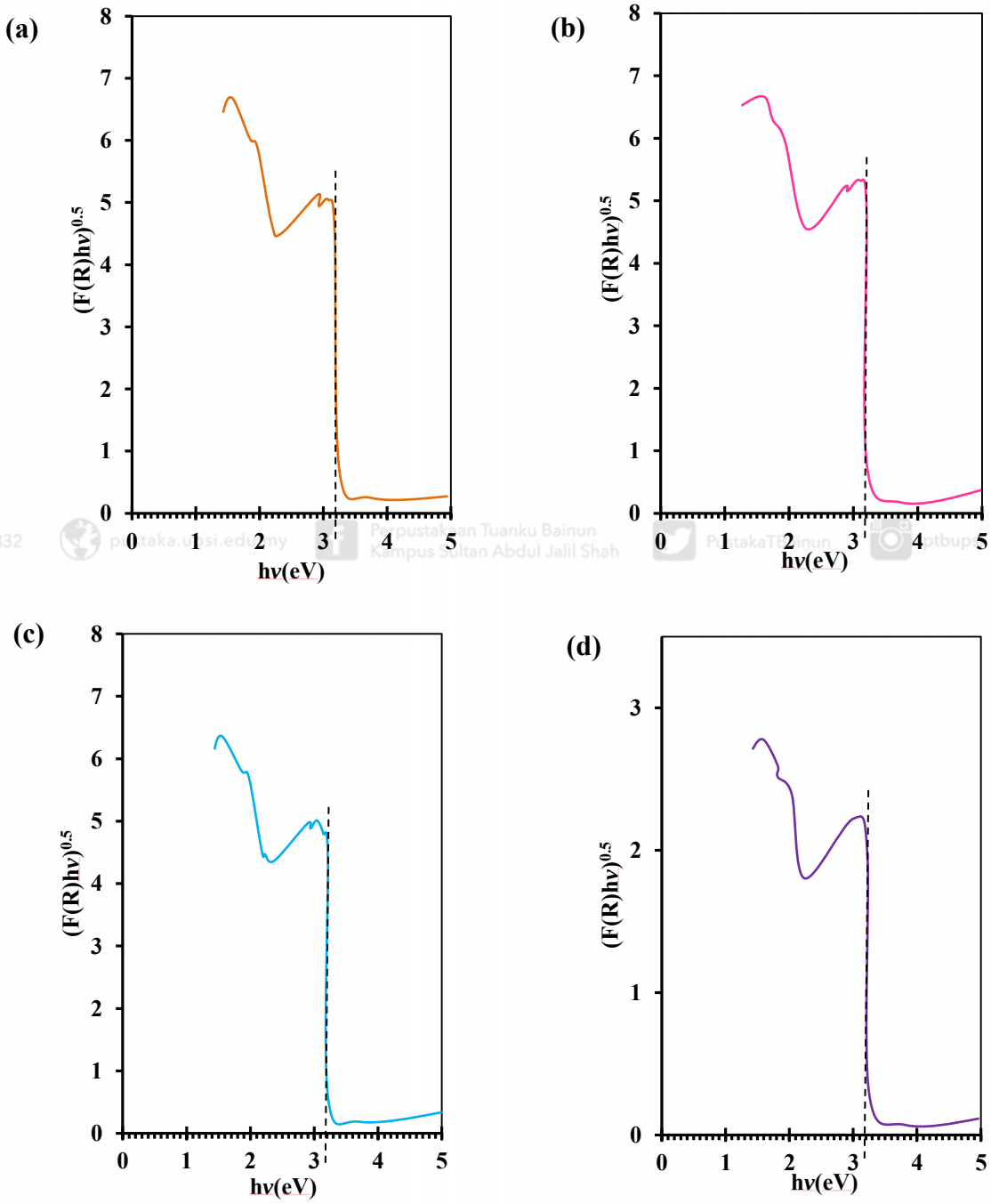


Figure 4.12. The Band Gap of Prepared (a) 5Fe/MTN-2, (b) 5Fe/MTN-4, (c) 5Fe/MTN-6 and (d) 5Fe/MTN-8 Photocatalysts

05-4506832 pustaka.upsi.edu.my Perpustakaan Tuanku Bainun Kampus Sultan Abdul Jalil Shah PustakaTBainun ptbupsi

05-4506832 pustaka.upsi.edu.my Perpustakaan Tuanku Bainun Kampus Sultan Abdul Jalil Shah PustakaTBainun ptbupsi

4.2.4 Functional group

The FTIR analysis between the region of 4000 and 400 cm^{-1} was then performed to confirm the functional groups presented in the prepared catalysts and the spectra were shown in Figure 4.13.

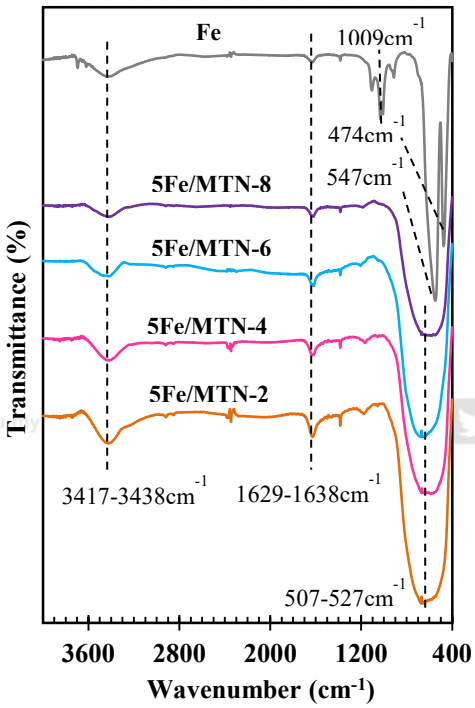


Figure 4.13. FTIR Spectra of 5Fe/MTN-2, 5Fe/MTN-4, 5Fe/MTN-6, 5Fe/MTN-8 and Fe

From the spectra, it can be observed that 5Fe/MTN-2, 5Fe/MTN-4, 5Fe/MTN-6 and 5Fe/MTN-8 exhibited nearly similar patterns of graph. All catalysts showed the broad band around 3417-3438 cm^{-1}, which were attributed to the stretching mode of the OH group that chemisorbed on the surface of MTN framework (Jaafar et al., 2017). The peak around 1629-1638 cm^{-1}, which corresponded to H-O-H bending vibration of

05-4506832 pustaka.upsi.edu.my Perpustakaan Tuanku Bainun Kampus Sultan Abdul Jalil Shah PustakaTBainun ptbupsi

05-4506832 pustaka.upsi.edu.my Perpustakaan Tuanku Bainun Kampus Sultan Abdul Jalil Shah PustakaTBainun ptbupsi

adsorbed water were also presented in all samples (Sood et al., 2015). The hydroxyl bands which referring to O-H and H-O-H vibrations became less significant as Fe was added into MTN with higher aging time. This showed that the large portion of adsorbed water from TiO_2 has been successfully removed by the continuous condensation reaction during the preparation of MTN (Anisah et al., 2019). Besides that, it probably caused by the perturbation in the MTN framework due to the addition of Fe species (Jaafar et al., 2017).

Then, the absorption band around 507-527 cm^{-1} which were assigned to the Ti-O-Ti stretching vibrations also became less significant as Fe was added into MTN with higher aging time which indicating the different strength of Ti-O bonds (Isari, Payan, Fattahi, Jorfi, & Kakavandi, 2018). It was due to the major structural changes that occurred in the precursor sol as a function of aging. During the aging, the reaction of hydrolysis-condensation will take place which lead to the breaking of the bonds initially formed in the precursor and resulted in the formation of Ti-O-Ti bonds. However, with further aging, it caused the fragmentation of Ti-O-Ti network into Ti-O system, which was due to the greater bond strength of the Ti-O network (Verma et al., 2007). The peaks observed at 1009 cm^{-1}, 547 cm^{-1} and 474 cm^{-1} which corresponded to stretching vibrations of Fe-O bonds were not seen at other samples (Abhilash, Akshatha, & Srikantaswamy, 2019). This might because of the low content Fe and overlap with the peak corresponded to Ti-O-Ti.

05-4506832 pustaka.upsi.edu.my Perpustakaan Tuanku Bainun Kampus Sultan Abdul Jalil Shah PustakaTBainun ptbupsi

05-4506832 pustaka.upsi.edu.my Perpustakaan Tuanku Bainun Kampus Sultan Abdul Jalil Shah PustakaTBainun ptbupsi

4.2.5 Surface area/pore structure

The N_2 adsorption-desorption isotherms and pore size distributions of the 5Fe/MTN-2, 5Fe/MTN-4, 5Fe/MTN-6 and 5Fe/MTN-8 were shown in Figure 4.14(a) and (b) respectively.

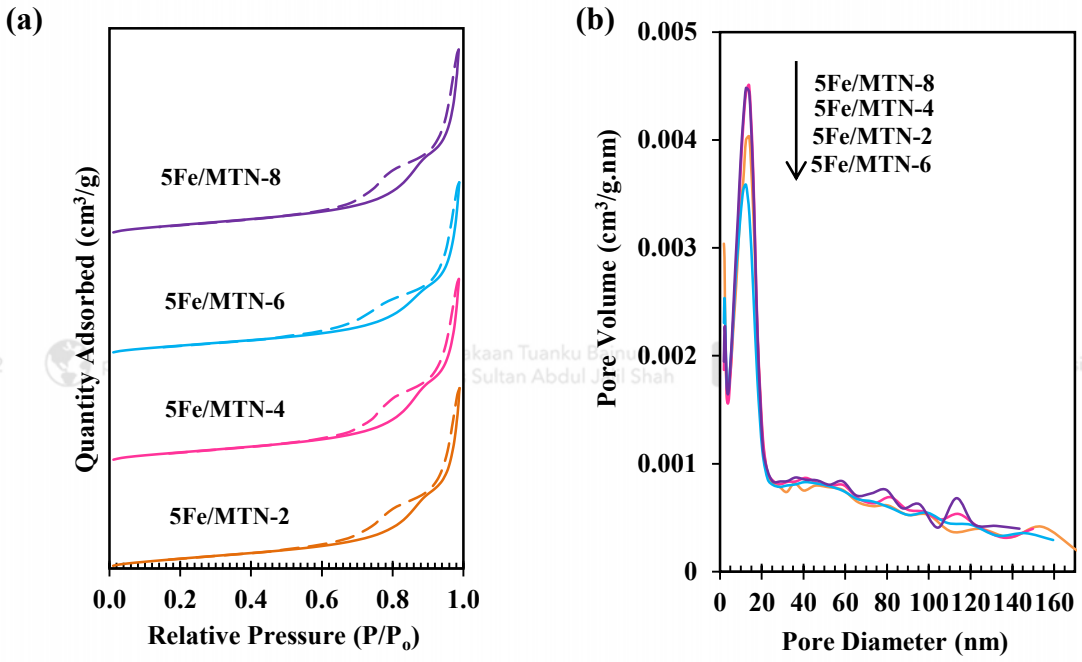


Figure 4.14. (a) N_2 Adsorption-Desorption Linear Isotherms and (b) Pore Size Distribution of 5Fe/MTN-2, 5Fe/MTN-4, 5Fe/MTN-6 and 5Fe/MTN-8

Although the adsorption trends of all the photocatalysts were seen to be nearly similar to each other, 5Fe/MTN-8 was found to exhibit the highest mesoporous volume. It was observed that all the photocatalysts exhibited a Type IV isotherm with a H3 hysteresis loop, which indicated the presence of mesoporous materials with slit-shaped

05-4506832 pustaka.upsi.edu.my Perpustakaan Tuanku Bainun Kampus Sultan Abdul Jalil Shah PustakaTBainun ptbupsi

05-4506832 pustaka.upsi.edu.my Perpustakaan Tuanku Bainun Kampus Sultan Abdul Jalil Shah PustakaTBainun ptbupsi

pores that were non-uniform in size and shape in the synthesized photocatalysts (Marfur et al., 2019). The hysteresis loop at P/P_o = 0.60-0.99 was corresponded to nitrogen condensation that occurred within the nanoparticles voids, which was obtained from the textural porosity between particles (Jaafar et al., 2015). All the pore structural informations of each of the photocatalysts were represented in Table 4.3.

Table 4.3

Pore Structural Informations of 5Fe/MTN-2, 5Fe/MTN-4, 5Fe/MTN-6 and 5Fe/MTN-8 Photocatalysts

Photocatalyst	**Surface area (m^2/g)**	**Pore volume (cm^3/g)**	**Pore size (nm)**
5Fe/MTN-2	28.65	0.0039	13.8
5Fe/MTN-4	29.87	0.0044	14.0
5Fe/MTN-6	27.56	0.0033	12.5
5Fe/MTN-8	30.58	0.0044	14.0

05-4506832 pustaka.upsi.edu.my Perpustakaan Tuanku Bainun Kampus Sultan Abdul Jalil Shah PustakaTBainun ptbupsi

According to BET results, the highest surface area was formed by 5Fe/MTN-8 (30.58 m^2/g), followed by 5Fe/MTN-4 (29.87 m^2/g), 5Fe/MTN-2 (28.65 m^2/g) and 5Fe/MTN-6 (27.56 m^2/g). The surface area obtained for all photocatalysts were closer to each other which in accordance to the photocatalytic performance of 5Fe/MTN-x photocatalysts that not showed any significant different as high surface area can generate abundant of active sites for adsorption and reaction of reactants, thus, enhancing the photocatalytic activity (Zhang et al., 2020).

05-4506832 pustaka.upsi.edu.my Perpustakaan Tuanku Bainun Kampus Sultan Abdul Jalil Shah PustakaTBainun ptbupsi

05-4506832 pustaka.upsi.edu.my Perpustakaan Tuanku Bainun Kampus Sultan Abdul Jalil Shah PustakaTBainun ptbupsi

Figure 4.14(b) shows the pore size distribution for all photocatalysts. It was observed that 5Fe/MTN-8 possess the highest number of narrow pore size at the range of 5-20 nm, followed by 5Fe/MTN-4, 5Fe/MTN-2 and 5Fe/MTN-6. According to previous study reported by Mao (2019), the lower pore volume indicates that the dopant was significantly loaded into the support which in turn will beneficial to enhance the photocatalytic activity. This statement was in agreement with the results of photodegradation of DBT as 5Fe/MTN-6 obtained the highest degradation rate compared to the other samples.

4.2.6 Structural phases

The characterization for structural properties of all the catalysts were investigated by Raman spectroscopy and the spectra were shown in Figure 4.15. The Raman spectroscopy of 5Fe/MTN-2, 5Fe/MTN-4, 5Fe/MTN-6 and 5Fe/MTN-8 revealed the five prominent peaks at 144 cm^{-1} (E_g), 197 cm^{-1} (E_g), 397 cm^{-1} (B_{1g}), 516 cm^{-1} ($A_{1g} + B_{1g}$) and 639 cm^{-1} (E_g), which corresponding to the six Raman active modes of anatase phase TiO_2. However, the peak attributed to Fe was not observed in the spectra of 5Fe/MTN-x samples which probably due to the low content of Fe species in the samples and below the detection limits of Raman instrument. The Raman analysis was consistent with the XRD results as the presence of TiO_2 anatase phase was seen in the samples.

05-4506832 pustaka.upsi.edu.my Perpustakaan Tuanku Bainun Kampus Sultan Abdul Jalil Shah PustakaTBainun ptbupsi

05-4506832 pustaka.upsi.edu.my Perpustakaan Tuanku Bainun Kampus Sultan Abdul Jalil Shah PustakaTBainun ptbupsi

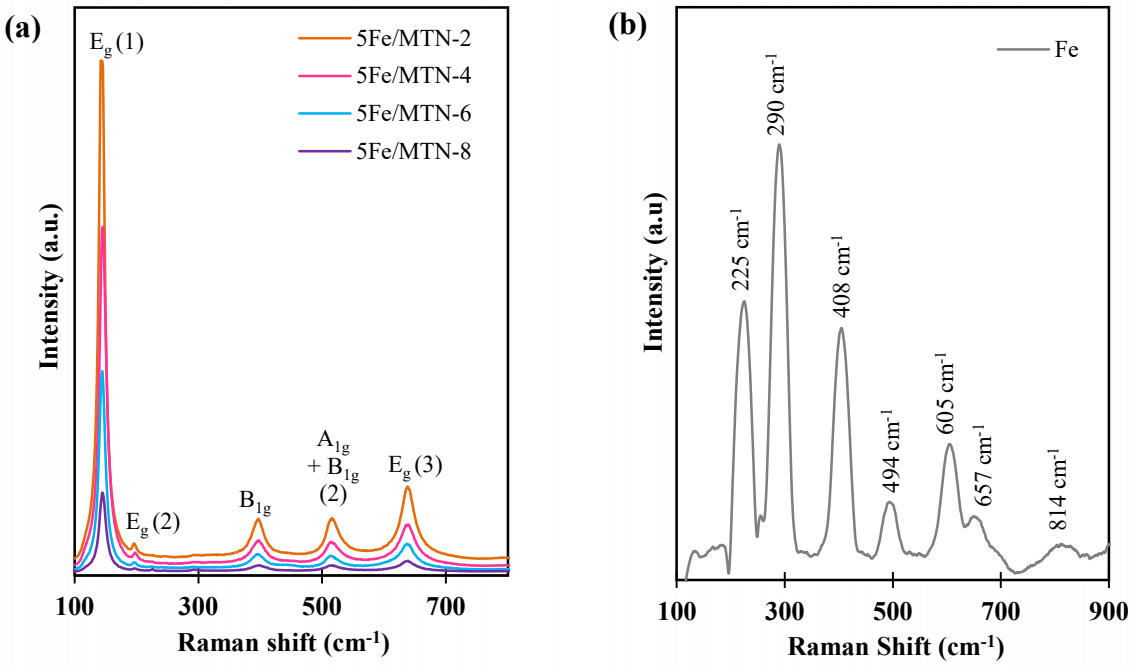


Figure 4.15. Raman Spectra of (a) 5Fe/MTN-2, 5Fe/MTN-4, 5Fe/MTN-6 and 5Fe/MTN-8 (b) Fe

By comparing the Raman spectra, it can be observed that the peaks broaden and shifted to longer wavenumber as well as the intensity of the catalysts tend to decrease as 5wt% of Fe was added into MTN with higher aging time. The changes occurred in the Raman bands proved that the particle sizes of the photocatalysts had been relatively decreased (Komaraiah et al., 2019). The obtained results could be affected by the presence of impurity and number of defects which resulted in different crystallite size (Castro & Duran, 2016). In this case, the addition of Fe^{3+} ions presented as the induced defects in the crystal lattice causing the disruption of the lattice periodicity and long range translational crystal symmetry to be occurred, which resulted in the decreased of

05-4506832 pustaka.upsi.edu.my Perpustakaan Tuanku Bainun Kampus Sultan Abdul Jalil Shah PustakaTBainun ptbupsi

05-4506832 pustaka.upsi.edu.my Perpustakaan Tuanku Bainun Kampus Sultan Abdul Jalil Shah PustakaTBainun ptbupsi

particle size (Komaraiah et al., 2019). The results were in accordance to the XRD as the particle size became smaller with the addition of Fe into MTN with higher aging time.

4.2.7 DBT degradation

The photocatalytic performance of all the 5Fe/MTN-x samples were evaluated through the photodegradation of DBT under UV light irradiation, and the results were shown in Figure 4.16.

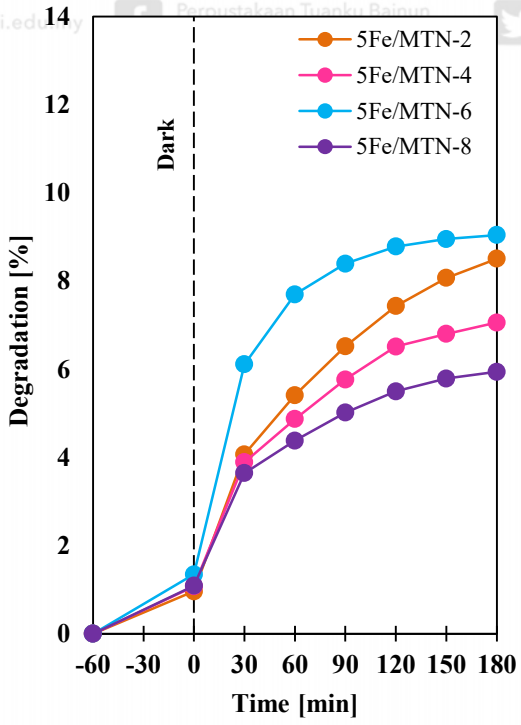


Figure 4.16. % Degradation of DBT for 5Fe/MTN-2, 5Fe/MTN-4, 5Fe/MTN-6 and 5Fe/MTN-8

05-4506832 pustaka.upsi.edu.my Perpustakaan Tuanku Bainun Kampus Sultan Abdul Jalil Shah PustakaTBainun ptbupsi

05-4506832 pustaka.upsi.edu.my Perpustakaan Tuanku Bainun Kampus Sultan Abdul Jalil Shah PustakaTBainun ptbupsi

All the catalysts were stirred in the dark for 60 min to achieve adsorption-desorption equilibrium before being exposed under light irradiation. However, there was no significant changing observed after 60 min of dark test which indicated that all samples have low ability in DBT physical adsorption in dark conditions (Abedini et al., 2021). From the results as shown in Figure 4.16, it can be observed that 5Fe/MTN-6 exhibited the highest photocatalytic activity in which 9.0% of DBT has been successfully degraded within 180 min. The results for photodegradation of DBT using 5Fe/MTN-x samples were summarized in Table 4.4.

Table 4.4

Photodegradation of DBT using 5Fe/MTN-2, 5Fe/MTN-4, 5Fe/MTN-6 and 5Fe/MTN-8 Photocatalysts

05-4506832 pustaka.upsi.edu.my Perpustakaan Tuanku Bainun Kampus Sultan Abdul Jalil Shah PustakaTBainun ptbupsi

Photocatalyst	**DBT degradation (%)**
5Fe/MTN-2	8.5
5Fe/MTN-4	7.1
5Fe/MTN-6	9.0
5Fe/MTN-8	5.9

Reaction conditions: model oil = 50 mL, Time = 180 min, Catalyst dosage = 5 g/L, DBT concentration = 40 mg/L, UV.

The efficiency of the photocatalysts in DBT degradation were found to be in the order of 5Fe/MTN-2 > 5Fe/MTN-4 > 5Fe/MTN-8 in which 8.5%, 7.1% and 5.9% of DBT has been degraded, respectively. The photocatalytic performance obtained by all the

05-4506832 pustaka.upsi.edu.my Perpustakaan Tuanku Bainun Kampus Sultan Abdul Jalil Shah PustakaTBainun ptbupsi

05-4506832 pustaka.upsi.edu.my Perpustakaan Tuanku Bainun Kampus Sultan Abdul Jalil Shah PustakaTBainun ptbupsi

samples do not show any significant different. The results could be influenced to their band gaps and surface area that were closely to each other in which probably play a vital role to enhance the efficiency of photocatalytic activity (Marfur et al., 2019). However, the DBT degaradation was in agreement with the pore distribution result as 5Fe/MTN-6 has the lowest pore volume, which indicated the successful incorporation of Fe into MTN-6 and in turn, exhibited the efficient photocatalytic activity. Since 5Fe/MTN-6 showed the highest photocatalytic activity than the other samples, it was chosen to further study on another factors that might affect the photodegradation of DBT.

4.3 Effect of dopant addition

05-4506832 pustaka.upsi.edu.my Perpustakaan Tuanku Bainun Kampus Sultan Abdul Jalil Shah PustakaTBainun ptbupsi

In this section, the 5Fe/MTN-6 photocatalyst was further investigated with incorporation of 5wt% gC_3N_4 as dopant and the photocatalyst was denoted as 5FeMTN-6/5gC_3N_4. The addition of gC_3N_4 into 5Fe/MTN-6 has significantly improved its photocatalytic performance. The enhancement of photocatalytic activity could be correlated to the gC_3N_4 that has narrow band gap and coupled with other semiconductors that has wide band gap, which in turn will improve the separation of photogenerated electron-hole pairs and extending the light absorption towards longer wavelength (Wu, Chen, Liu, Yang, & Yang, 2019). According to Lu et al. (2021), gC_3N_4 offered advantages in photocatalytic degradation of pollutants since it has 2D morphology similar to graphene, non-toxic and

05-4506832 pustaka.upsi.edu.my Perpustakaan Tuanku Bainun Kampus Sultan Abdul Jalil Shah PustakaTBainun ptbupsi

05-4506832 pustaka.upsi.edu.my Perpustakaan Tuanku Bainun Kampus Sultan Abdul Jalil Shah PustakaTBainun ptbupsi

attractive electronic structure, which consist of strong covalent bonds between the carbon and nitrogen atoms.

4.3.1 Crystallinity

Figure 4.17 shows the XRD patterns of MTN-6, 5Fe/MTN-6, 5FeMTN-6/5gC_3N_4, Fe and gC_3N_4.

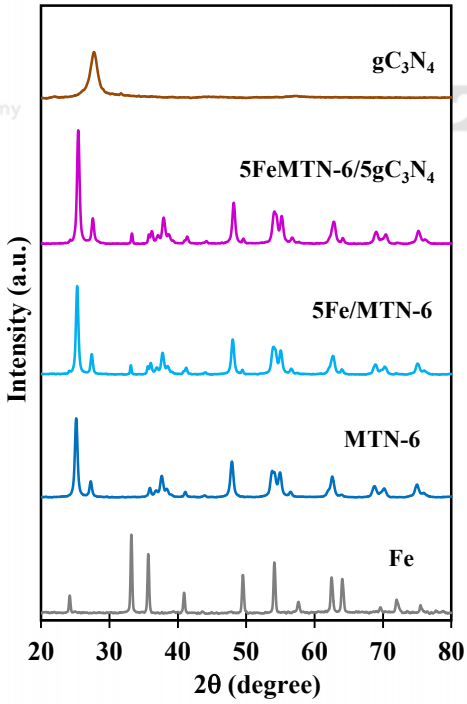


Figure 4.17. XRD Patterns of Fe, MTN-6, 5Fe/MTN-6, 5FeMTN-6/5gC_3N_4 and gC_3N_4

05-4506832 pustaka.upsi.edu.my Perpustakaan Tuanku Bainun Kampus Sultan Abdul Jalil Shah PustakaTBainun ptbupsi

05-4506832 pustaka.upsi.edu.my Perpustakaan Tuanku Bainun Kampus Sultan Abdul Jalil Shah PustakaTBainun ptbupsi

From the results, it can be observed that MTN-6, 5Fe/MTN-6 and 5FeMTN-6/5gC_3N_4 showed the dominant peaks of anatase phase TiO_2 that were detected at 25.41°, 37.05°, 37.88°, 38.63°, 48.15°, 54.04°, 55.17°, 62.88, 69.08°, 70.44° and 75.13° which were designated by their corresponding indexes (101), (103), (004), (112), (200), (105), (211), (204), (116), (220) and (215), respectively (JCPDS card No. 00-064-0863) (Anjugam Vandarkuzhali et al., 2018). The prominent peaks at 2θ values of Fe can be detected in the samples of 5Fe/MTN-6 and 5FeMTN-6/5gC_3N_4 which showed the peaks corresponded to the crystal structure of hematite were appeared at 33.12° (104), 40.80° (113), 49.38° (024) and 63.94° (300) (JCPDS card No. 00-033-0664). Meanwhile, the peak corresponded to gC_3N_4 can be found in the sample of 5FeMTN-6/5gC_3N_4 at 27.55° with an index of (002) (JCPDS card No. 00-066-0813) (Zhang et al., 2018).

05-4506832 pustaka.upsi.edu.my Perpustakaan Tuanku Bainun Kampus Sultan Abdul Jalil Shah PustakaTBainun ptbupsi

The calculated particle size of MTN-6, 5Fe/MTN-6 and 5FeMTN-6/5gC_3N_4 based on the major peak at $2\theta = 25.41°$ were 21.77 nm, 23.92 nm and 23.04 nm, respectively. It clearly showed that 5Fe/MTN-6 and 5FeMTN-6/5gC_3N_4 exhibited the larger particle sizes compared to MTN-6. These results could be due to the agglomeration of particles that occurred because of the presence of impurity that caused the formation of defects and dislocations in the crystal lattice (Khan & Berk, 2014). The peak intensity at $2\theta = 25.41°$ also showed an increment for the 5Fe/MTN-6 and 5FeMTN-6/5gC_3N_4 photocatalysts, which indicated the increased of crystallite size has been occurred (Zaid et al., 2016). From the discussion above, it confirmed the successful preparation of all the photocatalysts.

05-4506832 pustaka.upsi.edu.my Perpustakaan Tuanku Bainun Kampus Sultan Abdul Jalil Shah PustakaTBainun ptbupsi

05-4506832 pustaka.upsi.edu.my Perpustakaan Tuanku Bainun Kampus Sultan Abdul Jalil Shah PustakaTBainun ptbupsi

4.3.2 Surface morphology with Elemental Analysis

The surface morphology of Fe, gC_3N_4, MTN-6, 5Fe/MTN-6 and 5FeMTN-6/5gC_3N_4 were analyzed using FESEM technique and the results were shown in Figure 4.18.

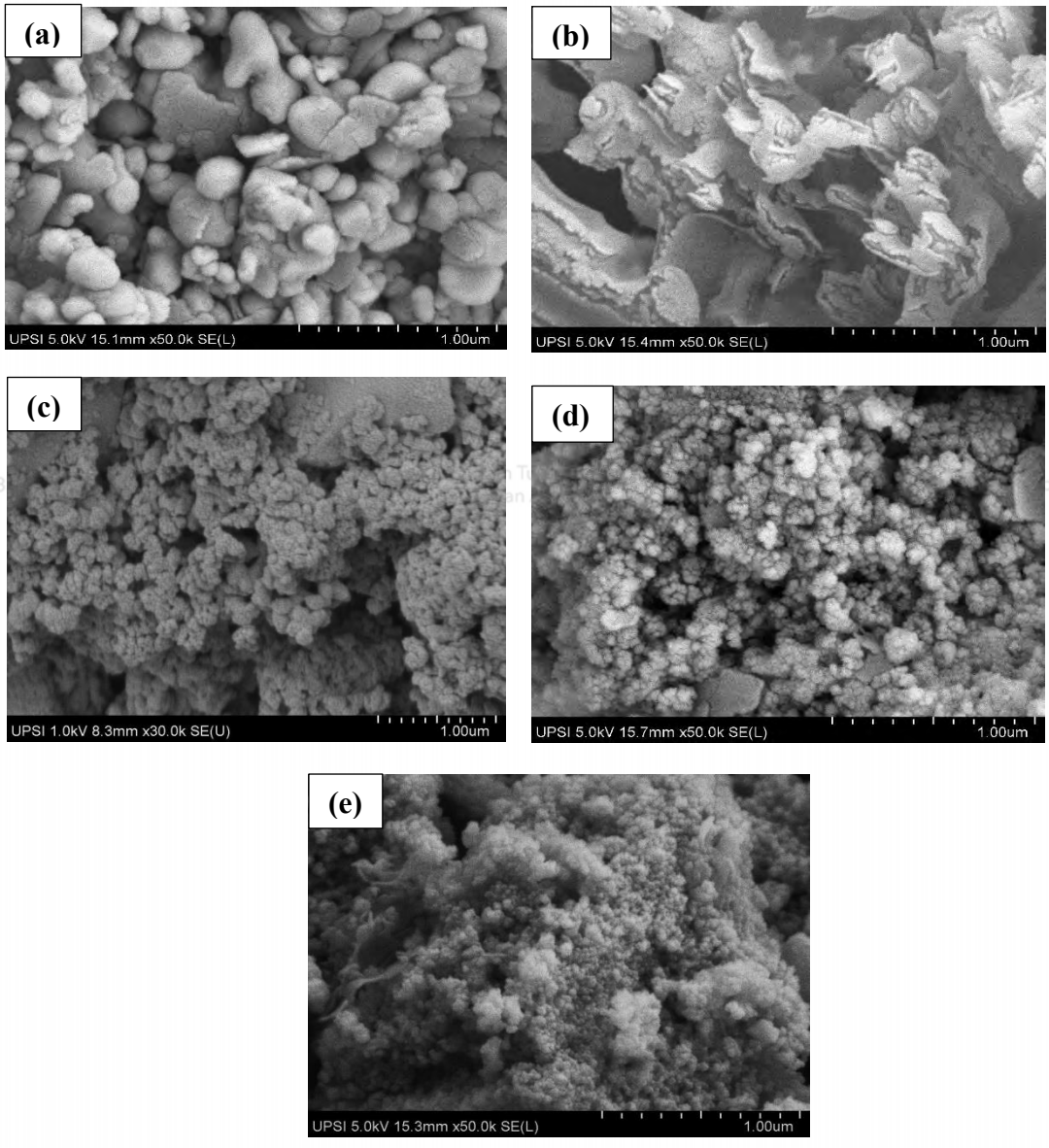


Figure 4.18. FESEM Images of the Samples (a) Fe, (b) gC_3N_4, (c) MTN-6, (d) 5Fe/MTN-6 and (e) 5FeMTN-6/5gC_3N_4

05-4506832 pustaka.upsi.edu.my Perpustakaan Tuanku Bainun Kampus Sultan Abdul Jalil Shah PustakaTBainun ptbupsi

05-4506832 pustaka.upsi.edu.my Perpustakaan Tuanku Bainun Kampus Sultan Abdul Jalil Shah PustakaTBainun ptbupsi

Figure 4.18(a) shows the FESEM images of pure Fe, which exhibited large irregular shape that agglomerated with each other. Then, FESEM images of pristine gC_3N_4 (Figure 4.18(b)) was observed to appear as a tremella with some crinkles (Chen, Man, Chen, & Zhang, 2016). Figure 4.18(c) shows the FESEM images of MTN-6. As can be seen, it formed spherical nanoparticles that interconnect with each other to form disordered mesoporous network structure (Mani et al.,2021). The FESEM image of 5Fe/MTN-6 was shown Figure 4.18(d) and the sample possess of nanosized primary particles with slight agglomeration (Ali et al., 2017). The complete formation of 5FeMTN-6/5gC_3N_4 was shown in Figure 4.18(e). As can be observed from the images, the rough spherical surface was formed which indicated the physical contact between two semiconductors had been successfully occurred and proved the probable formation of heterojunction or Z-scheme composites (Zhu et al., 2018). The chemical composition of the 5FeMTN-6/5gC_3N_4 photocatalyst was determined using EDX technique and shown in Figure 4.19. The corresponding EDX dot-mapping results showed the uniform distribution of Ti, O, Fe, C and N elements in the 5FeMTN-6/5gC_3N_4 sample. The elemental results were in accordance to the XRD and FESEM analysis which showed the successful incorporation of gC_3N_4 into the 5Fe/MTN-6 as a dopant.

05-4506832 pustaka.upsi.edu.my Perpustakaan Tuanku Bainun Kampus Sultan Abdul Jalil Shah PustakaTBainun ptbupsi

05-4506832 pustaka.upsi.edu.my Perpustakaan Tuanku Bainun Kampus Sultan Abdul Jalil Shah PustakaTBainun ptbupsi

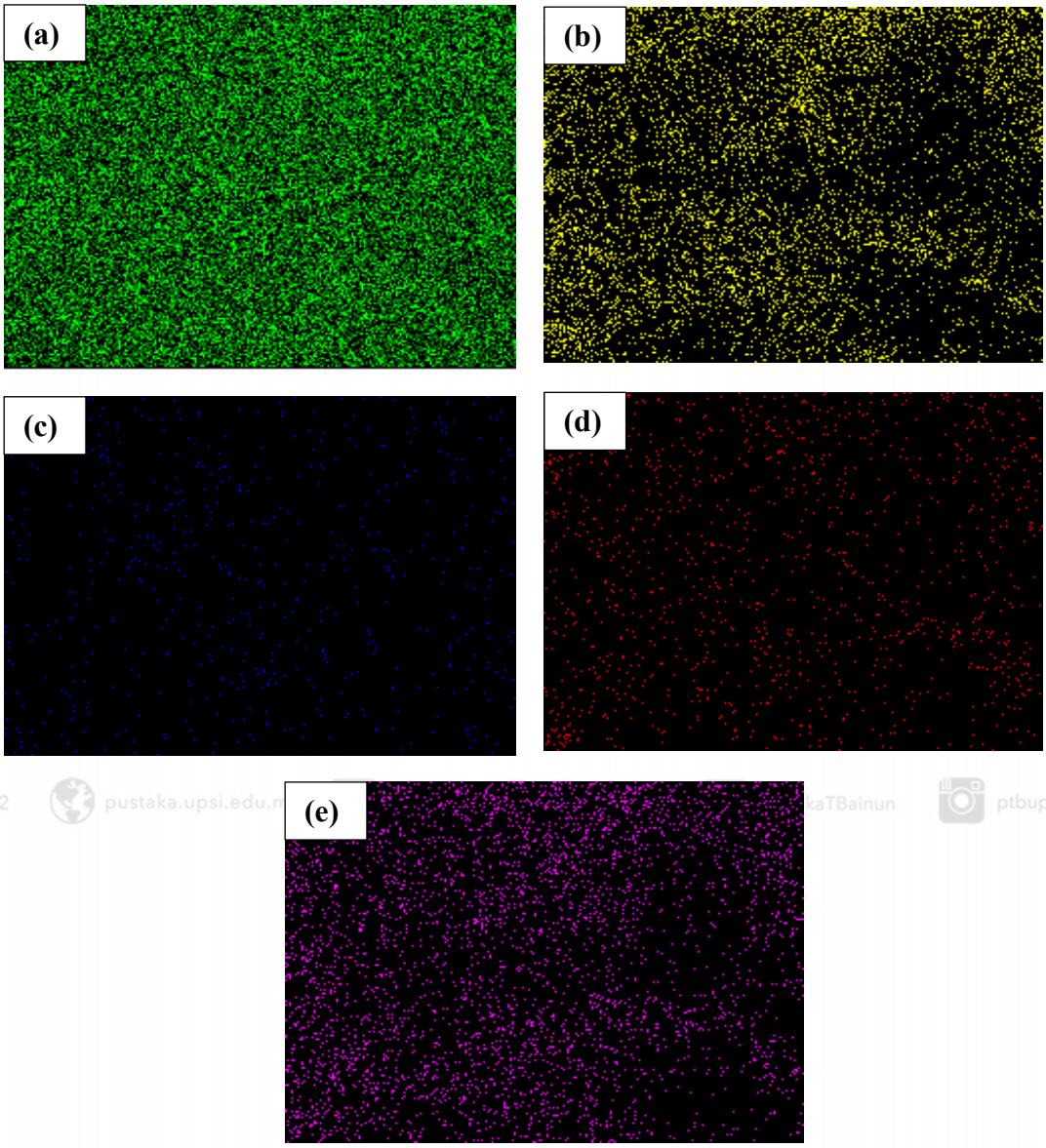


Figure 4.19. EDX Dot-Mapping Images of 5FeMTN-6/5gC_3N_4 consist of (a) Ti, (b) O, (c) Fe, (d) C and (e) N

05-4506832 pustaka.upsi.edu.my Perpustakaan Tuanku Bainun Kampus Sultan Abdul Jalil Shah PustakaTBainun ptbupsi

05-4506832 pustaka.upsi.edu.my Perpustakaan Tuanku Bainun Kampus Sultan Abdul Jalil Shah PustakaTBainun ptbupsi

4.3.3 Measured band gap

Figure 4.20 showed the UV-DRS results of MTN-6, 5Fe/MTN-6 and 5FeMTN-6/5gC_3N_4 samples.

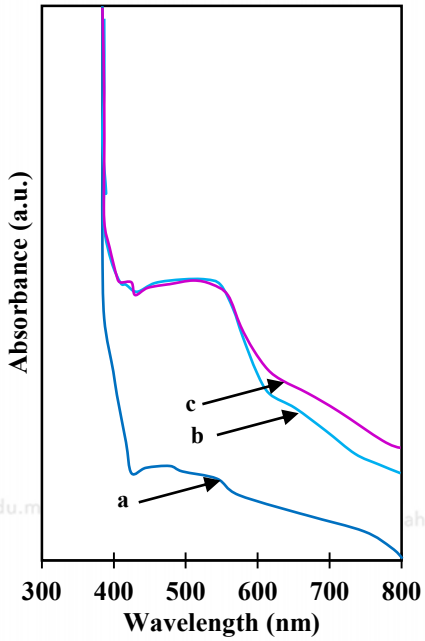


Figure 4.20. UV-DRS Spectra of (a) MTN-6, (b) 5Fe/MTN-6 and (c) 5FeMTN-6/5gC_3N_4

As can be seen in Figure 4.20, a red-shift of absorption edge towards the visible region has occurred for 5Fe/MTN-6 and 5FeMTN-6/5gC_3N_4 samples. The results was corroborated with the study by Akshay et al. (2018) in which the incorporation of Fe content into bare MTN-6 caused the significant shift towards longer wavelength to be occurred due to the sp-d exchange interactions between band electrons and localized d electrons of metal ions. The additional absorption peak around 550 nm was also appeared in these two samples which attributed to the presence Fe_2O_3 (Sadanandam et al., 2018). A

05-4506832 pustaka.upsi.edu.my Perpustakaan Tuanku Bainun Kampus Sultan Abdul Jalil Shah PustakaTBainun ptbupsi

05-4506832 pustaka.upsi.edu.my Perpustakaan Tuanku Bainun Kampus Sultan Abdul Jalil Shah PustakaTBainun ptbupsi

significant shifted to a longer wavelength in the visible region was also observed in 5FeMTN-6/5gC_3N_4 sample, in which could be due to the synergistic relationship between MTN-6 and gC_3N_4 in the composite sample (Wu et al., 2019). The increased in absorption intensity at the visible light range of 600-800 nm was also seen due to the presence of Fe and gC_3N_4 into MTN-6. Also, all the doped samples showed a broad peak in the visible region. The extending of light absorption towards longer wavelength promoted the generation of electron-hole pairs, resulting to improve the photocatalytic activity of the photocatalysts (Rodriguez et al., 2019). This statement was in agreement with the DBT degradation results as 5FeMTN-6/5gC_3N_4 obtained the highest degradation rate of DBT compared to MTN-6 and 5Fe/MTN-6. All the photocatalysts obtained the same band gap value which were 3.24 eV and was shown in Figure 4.21. The results of the band gap showed that all the catalyst will properly work under irradition of UV light instead of visible light. The incorporation of 5wt% Fe and 5wt% gC_3N_4 into bare MTN-6 have not affected the band gap of photocatalysts, which can be concluded that the band gap was not the main factor that influence the photocatalytic efficiency.

05-4506832 pustaka.upsi.edu.my Perpustakaan Tuanku Bainun Kampus Sultan Abdul Jalil Shah PustakaTBainun ptbupsi

05-4506832 pustaka.upsi.edu.my Perpustakaan Tuanku Bainun Kampus Sultan Abdul Jalil Shah PustakaTBainun ptbupsi

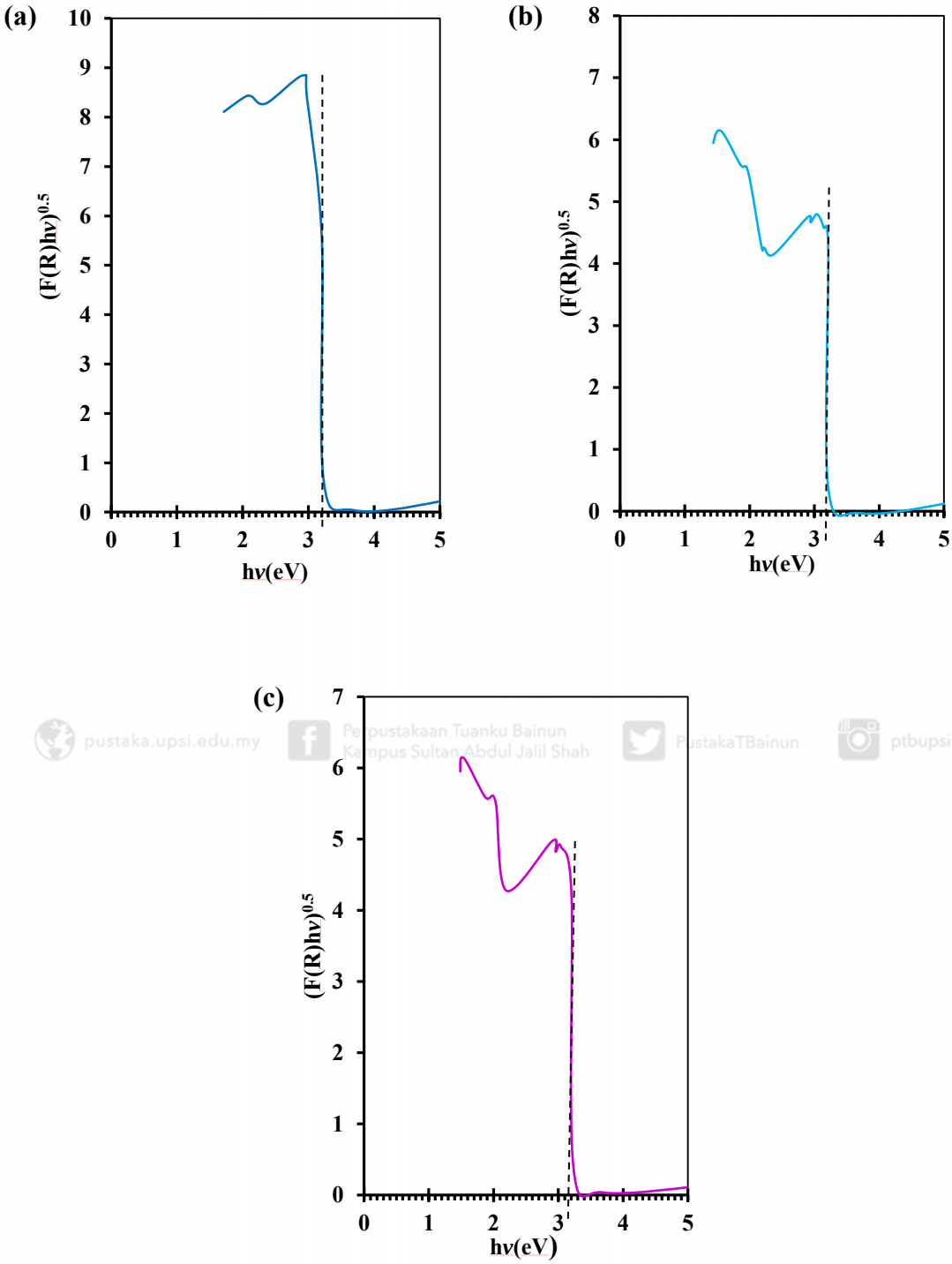


Figure 4.21. The Band Gap of Prepared (a) MTN-6, (b) 5Fe/MTN-6 and (c) 5FeMTN-6/5gC_3N_4 Photocatalysts

05-4506832 pustaka.upsi.edu.my Perpustakaan Tuanku Bainun Kampus Sultan Abdul Jalil Shah PustakaTBainun ptbupsi

05-4506832 pustaka.upsi.edu.my Perpustakaan Tuanku Bainun Kampus Sultan Abdul Jalil Shah PustakaTBainun ptbupsi

4.3.4 Functional group

The FTIR spectra of Fe, MTN-6, 5Fe/MTN-6, 5FeMTN-6/5gC_3N_4 and gC_3N_4 photocatalysts were shown in Figure 4.22.

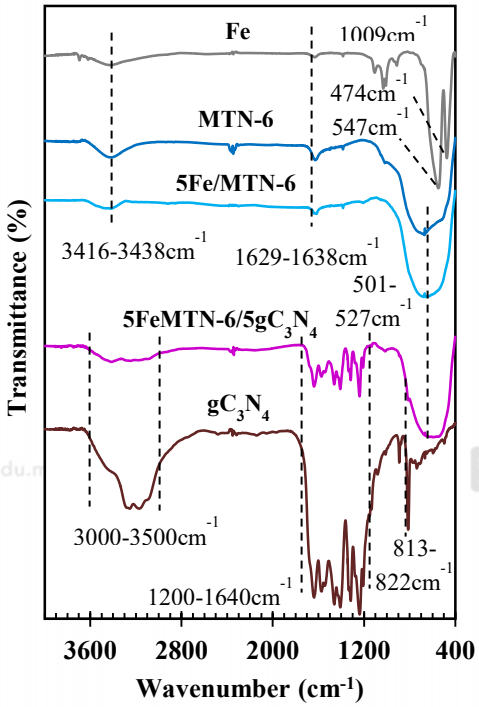


Figure 4.22. FTIR Spectra of Fe, MTN-6, 5Fe/MTN-6, 5FeMTN-6/5gC_3N_4 and gC_3N_4

The broad absorption band appeared in the range of 3416-3438 cm^{-1} were seen in the samples of Fe, MTN-6 and 5Fe/MTN-6. The peaks were attributed to the stretching mode of the O-H groups that chemisorbed on the surface of MTN framework (Jaafar et al., 2017). Then, the peak appeared around 1629-1638 cm^{-1}, which corresponded to H-O-H bending vibration of adsorbed water were also presented in these three samples. The peaks in the range of 501-527 cm^{-1} corresponding to Ti-O-Ti stretching vibrations were

05-4506832 pustaka.upsi.edu.my Perpustakaan Tuanku Bainun Kampus Sultan Abdul Jalil Shah PustakaTBainun ptbupsi

05-4506832 pustaka.upsi.edu.my Perpustakaan Tuanku Bainun Kampus Sultan Abdul Jalil Shah PustakaTBainun ptbupsi

observed in the MTN-6, 5Fe/MTN-6 and 5FeMTN-6/5gC_3N_4 samples (Isari et al., 2018). However, the absorption peaks at 1009 cm^{-1}, 547 cm^{-1} and 474 cm^{-1} corresponding to Fe-O stretching vibrations were not detected in 5Fe/MTN-6 and 5FeMTN-6/5gC_3N_4. This might be due to the low content of Fe and overlap with the peak of Ti-O-Ti. As expected, all the main absorption peaks of gC_3N_4 at 813 cm^{-1}, 1200-1640 cm^{-1} and 3000-3500 cm^{-1} were also detected in the spectra of 5FeMTN-6/5gC_3N_4. The peak at approximately 813 cm^{-1} was attributed to the stretching vibration characteristic absorption of s-triazine rings (Prakash, Kumar, Latha, Kumar, & Karuthapandian, 2019). Then, the peaks appeared in the range of 1200-1640 cm^{-1} were corresponded to the typical C-N stretching vibration of heterocycles, in which the absorption band at 1640 cm^{-1} was assigned to the stretching mode of C=N that formed at sp^2 hybridized network in the gC_3N_4 while the characteristic peaks at 1239, 1316, 1407, 1469, and 1572 can be attributed to the aromatic stretching vibration of C-N (Huu et al., 2021; Prakash et al., 2019). Additionally, the broad absorption bands between 3000-3500 cm^{-1} were attributed to the N-H and O-H stretching, formed from terminal amino groups and adsorbed H_2O, respectively (Huu et al., 2021; Liu, Lu, & Wu, 2018).

From the spectra, it can be observed that the absorption bands seems to decrease with the addition of Fe and gC_3N_4 into bare MTN-6 which indicated the possible perturbation has occurred and caused the shifting in the MTN framework (Marfur et al., 2019). However, the absorption band of Ti-O-Ti stretching vibration showed a slight shifting with the addition of Fe and gC_3N_4 as can be observed in 5Fe/MTN-6 and 5FeMTN-6/5gC_3N_4 samples. It was due to the strong interfacial interaction between the

05-4506832 pustaka.upsi.edu.my Perpustakaan Tuanku Bainun Kampus Sultan Abdul Jalil Shah PustakaTBainun ptbupsi

05-4506832 pustaka.upsi.edu.my Perpustakaan Tuanku Bainun Kampus Sultan Abdul Jalil Shah PustakaTBainun ptbupsi

active species and MTN that would facilitate the electron transfer, which in turn will enhance the photocatalytic efficiency (Huang et al., 2015).

4.3.5 Surface area/pore structure

The N_2 adsorption-desorption isotherms and pore size distributions of the MTN-6, 5Fe/MTN-6, 5FeMTN-6/5gC_3N_4 were shown in Figure 4.23(a) and (b) respectively.

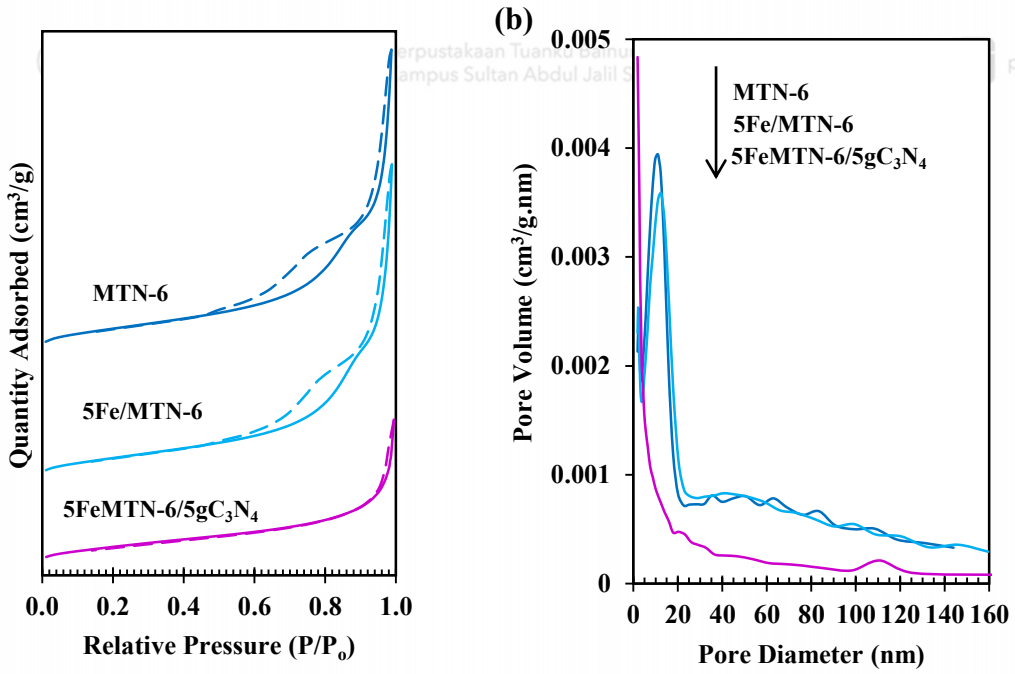


Figure 4.23. (a) N_2 Adsorption-Desorption Linear Isotherms and (b) Pore Size Distribution of MTN-6, 5Fe/MTN-6 and 5FeMTN-6/5gC_3N_4

05-4506832 pustaka.upsi.edu.my Perpustakaan Tuanku Bainun Kampus Sultan Abdul Jalil Shah PustakaTBainun ptbupsi

05-4506832 pustaka.upsi.edu.my Perpustakaan Tuanku Bainun Kampus Sultan Abdul Jalil Shah PustakaTBainun ptbupsi

It was observed that all of the photocatalysts exhibited a Type IV isotherm, which indicated the presence of mesoporous materials with slit-shaped pores that were non-uniform in size and shape in the synthesized photocatalysts (Marfur et al., 2019). According to BET results, the highest surface area was formed by MTN-6 (28.69 m^2/g), followed by 5Fe/MTN-6 (27.56 m^2/g) and 5FeMTN-6/5gC_3N_4 (21.09 m^2/g). The hysteresis loop at P/P_o = 0.50-0.99 obtained by MTN-6 and 5Fe/MTN-6 were corresponded to nitrogen condensation that occurred within the nanoparticles voids, which was obtained from the textural porosity between particles (Jaafar et al., 2015). However, when 5wt% of gC_3N_4 was incorporated into 5Fe/MTN-6, the nitogen uptake were dramatically decreased due to the presence of gC_3N_4 that may cause the internal pore structures of 5Fe/MTN-6 to be blocked and also results in the decrement of BET surface area of the photocatalyst (Liu et al., 2018). All the pore structural informations of each of the photocatalysts were shown in Table 4.5.

Table 4.5

Pore Structural Informations of MTN-6, 5Fe/MTN-6 and 5FeMTN-6/5gC_3N_4 Photocatalysts

Photocatalyst	**Surface area (m^2/g)**	**Pore volume (cm^3/g)**	**Pore size (nm)**
MTN-6	28.69	0.0039	11.0
5Fe/MTN-6	27.56	0.0033	12.5
5FeMTN-6/5gC_3N_4	21.09	0.0005	14.0

05-4506832 pustaka.upsi.edu.my Perpustakaan Tuanku Bainun Kampus Sultan Abdul Jalil Shah PustakaTBainun ptbupsi

05-4506832 pustaka.upsi.edu.my Perpustakaan Tuanku Bainun Kampus Sultan Abdul Jalil Shah PustakaTBainun ptbupsi

Figure 4.23(b) shows the pore size distribution for all the synthesized photocatalysts. It was seen that both MTN-6 and 5Fe/MTN-6 possess the narrow pore sizes at the range of 5-20 nm. The average pore size and pore volume of 5FeMTN-6/5gC_3N_4 was significantly decreased, indicating the addition of gC_3N_4 into 5Fe/MTN-6 has partially closed the mesopores. According to previous study reported by Mao (2019), the lower pore volume indicates that the dopant was significantly loaded into the support which in turn will beneficial to enhance the photocatalytic activity. This statement was in agreement with the results of photodegradation of DBT as 5FeMTN-6/5gC_3N_4 obtained the highest degradation rate compared to MTN-6 and 5Fe/MTN-6.

05-4506832 pustaka.upsi.edu.my Perpustakaan Tuanku Bainun Kampus Sultan Abdul Jalil Shah PustakaTBainun ptbupsi

4.3.6 Photochemical properties

Photoluminescence (PL) spectra was used to investigate the electron-hole separation, immigration and recombination rate of the synthesized materials. The measured PL spectra of gC_3N_4, MTN-6, 5FeMTN-6/5gC_3N_4 and 5Fe/MTN-6 were illustrated in Figure 4.24. It can be observed that, the highest intensity of emission peak appeared at 480 nm. The peaks in the range of 450-500 nm were corresponding to surface OV and Ti^{3+} while peaks at around 530 nm were attributed to the OV buried in the bulk materials (Li et al., 2020). From the results, it can be observed that the decrement of PL intensity has been occurred for 5Fe/MTN-6 and 5FeMTN-6/5gC_3N_4 samples. The reduced of PL intensity for 5Fe/MTN-6 could be due to its lower recombination rate of electron-hole pairs

05-4506832 pustaka.upsi.edu.my Perpustakaan Tuanku Bainun Kampus Sultan Abdul Jalil Shah PustakaTBainun ptbupsi

05-4506832 pustaka.upsi.edu.my Perpustakaan Tuanku Bainun Kampus Sultan Abdul Jalil Shah PustakaTBainun ptbupsi

compared to MTN-6 upon incorporation of Fe (Zeng, Zhang, Liu, Zhang, & Guo, 2019). On the other hand, the bare gC_3N_4 showed a sharp emission peak at 480 nm which described the strong electron-hole recombination rate. However, the emission peak at 480 nm was dramatically reduced as gC_3N_4 was combined with 5Fe/MTN-6 which attributed to the suppressing of charge recombination in 5FeMTN-6/5gC_3N_4 had occurred.

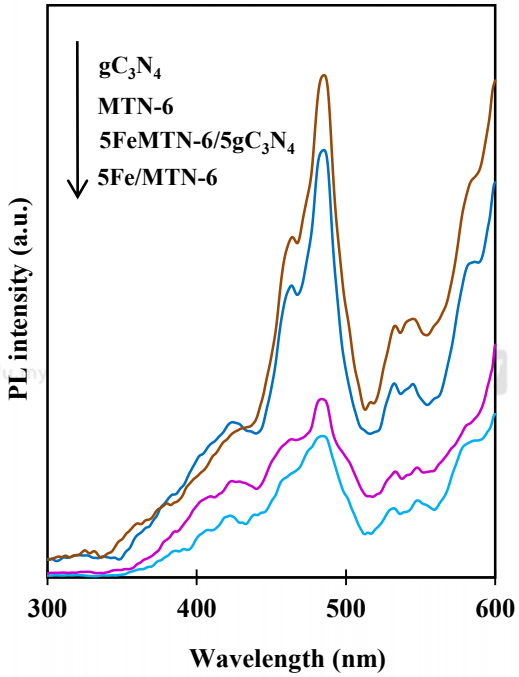


Figure 4.24. PL Spectra of gC_3N_4, MTN-6, 5FeMTN-6/5gC_3N_4 and 5Fe/MTN-6

The results could be influenced by strong synergistic effect between gC_3N_4 and 5Fe/MTN-6 that enhanced the slower recombination process of photogenerated electron hole pairs (Balu et al., 2019). According to Eshaghi and Moradi (2018), the lower recombination rate of photogenerated charges will significantly increased the photocatalytic activity of photocatalysts.

05-4506832 pustaka.upsi.edu.my Perpustakaan Tuanku Bainun Kampus Sultan Abdul Jalil Shah PustakaTBainun ptbupsi

05-4506832 pustaka.upsi.edu.my Perpustakaan Tuanku Bainun Kampus Sultan Abdul Jalil Shah PustakaTBainun ptbupsi

4.3.7 Structural phases

Figure 4.25(a) shows the Raman spectra of the as-synthesized MTN-6, 5Fe/MTN-6 and 5FeMTN-6/5gC_3N_4 samples.

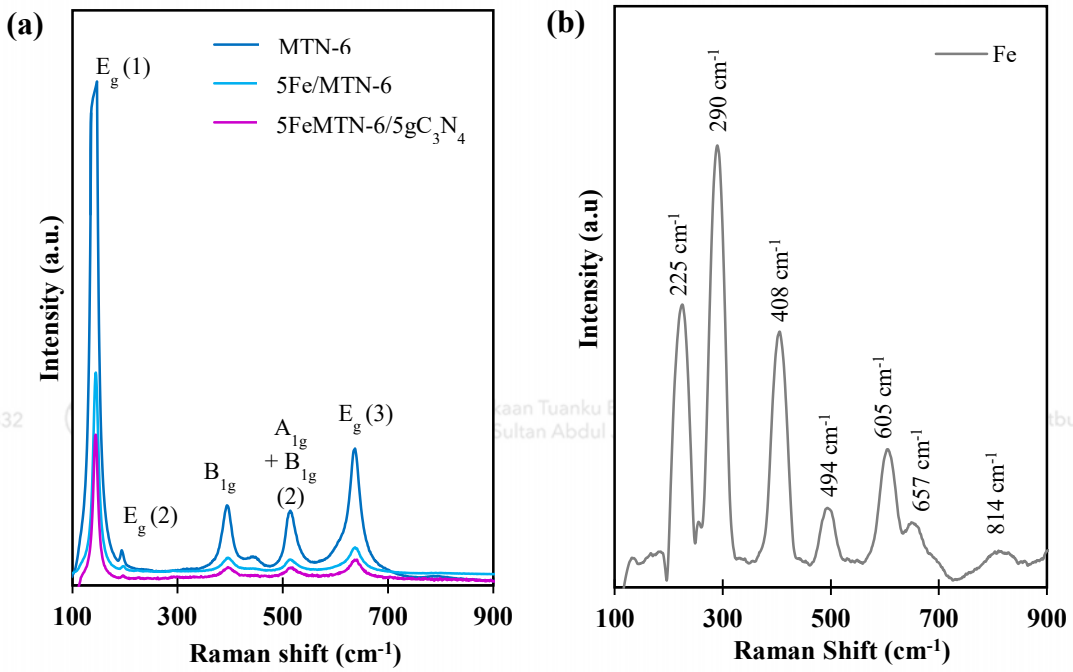


Figure 4.25. Raman Spectra of (a) MTN-6, 5Fe/MTN-6 and 5FeMTN-6/5gC_3N_4 (b) Fe

It can be observed that the Raman signals at 144 cm^{-1} (E_g), 197 cm^{-1} (E_g), 399 cm^{-1} (B_{1g}), 515 cm^{-1} (A_{1g} + B_{1g}) and 639 cm^{-1} (E_g) which were corresponded to the six Raman active modes in the TiO_2 anatase phase were presented in all the photocatalysts. However, the peaks corresponded to Fe and gC_3N_4 were not observed in the spectra of 5Fe/MTN-6 and 5FeMTN-6/5gC_3N_4 which could be due to their low content in the

05-4506832 pustaka.upsi.edu.my Perpustakaan Tuanku Bainun Kampus Sultan Abdul Jalil Shah PustakaTBainun ptbupsi

05-4506832 pustaka.upsi.edu.my Perpustakaan Tuanku Bainun Kampus Sultan Abdul Jalil Shah PustakaTBainun ptbupsi

samples and below the detection limits of Raman instrument. On the other hand, the absence of Fe and gC_3N_4 related signals showed that the uniform distribution in MTN-6 and 5Fe/MTN-6 samples had occurred, respectively (Lin & Zhao, 2019). The Raman analysis was consistent with the XRD results as the presence of TiO_2 anatase phase was seen in the samples. By comparing the Raman spectra, it can be observed that the peaks broaden and shifted to longer wavenumber as well as the intensity of the catalysts tend to decrease with the incorporation of Fe and gC_3N_4 into the photocatalyst. The obtained results could be affected by the presence of impurity and number of defects in which the addition of Fe and gC_3N_4 causing the disorder in the lattice to be increased and ruined the ideal symmetry of the crystal which resulted in broadening and shifting of the Raman bands (Akshay et al., 2018; Castro & Duran, 2016).

05-4506832 pustaka.upsi.edu.my Perpustakaan Tuanku Bainun Kampus Sultan Abdul Jalil Shah PustakaTBainun ptbupsi

4.3.8 DBT degradation

Photocatalytic activity of MTN-6, gC_3N_4, 5Fe/MTN-6 and 5FeMTN-6/5gC_3N_4 for the degradation of DBT under UV light irradiation were shown in Figure 4.26. All the catalysts were stirred in the dark for 60 min in order to achieve adsorption-desorption equilibrium before being exposed under light irradiation. However, there was no significant changing observed after 60 min of dark test which indicated that all samples have low ability in DBT physical adsorption in dark conditions (Abedini et al., 2021). Figure 4.26(a) shows the UV-Vis absorption spectra of DBT at different time intervals

05-4506832 pustaka.upsi.edu.my Perpustakaan Tuanku Bainun Kampus Sultan Abdul Jalil Shah PustakaTBainun ptbupsi

05-4506832 pustaka.upsi.edu.my Perpustakaan Tuanku Bainun Kampus Sultan Abdul Jalil Shah PustakaTBainun ptbupsi

using 5FeMTN-6/5gC_3N_4 photocatalyst under UV light irradiation. It was seen that the the absorbance at λ_{max} = 325 nm progressively decreases as the irradiation time increases. The result indicates that the pollutant was successfully degraded by the photocatalyst with time.

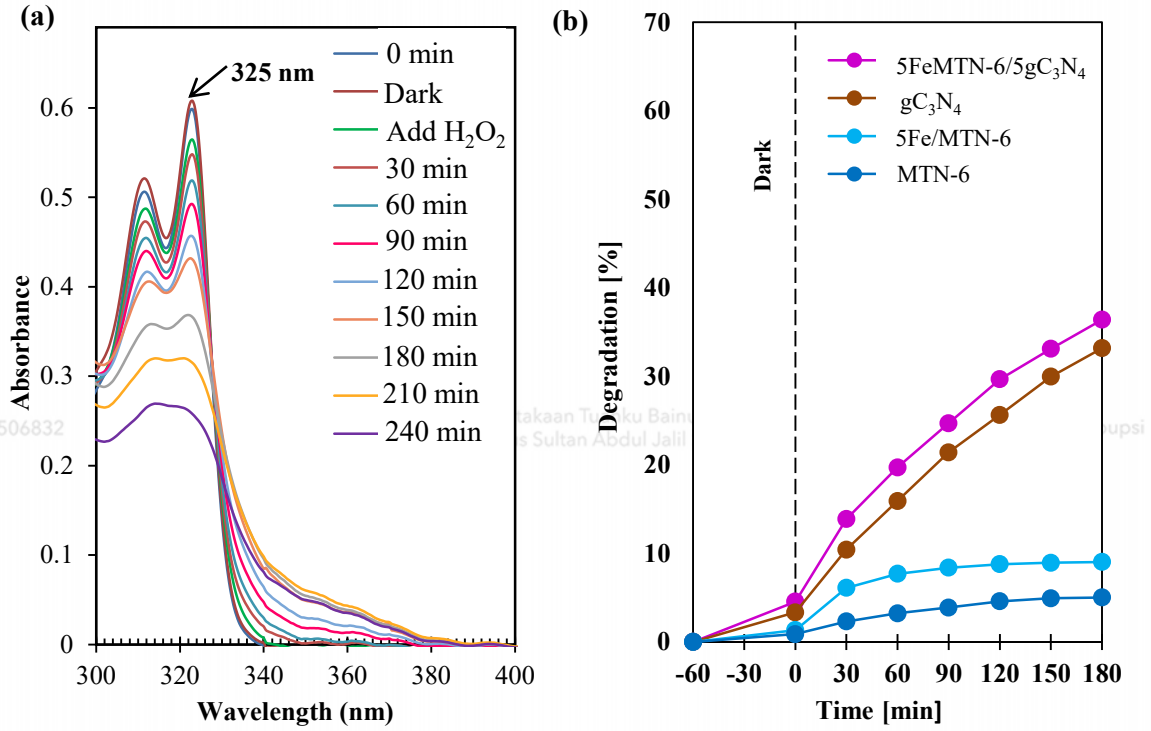


Figure 4.26. (a) UV-Vis Absorption Spectra of Photodegradation of DBT Solution (40 mg/L) in the Presence of 5FeMTN-6/5gC_3N_4 Photocatalyst (b) % Degradation of DBT for MTN-6, 5Fe/MTN-6, gC_3N_4 and 5FeMTN-6/5gC_3N_4

The results for photodegradation of DBT using MTN-6, 5Fe/MTN-6, gC_3N_4 and 5FeMTN-6/5gC_3N_4 samples were summarized in Table 4.6.

05-4506832 pustaka.upsi.edu.my Perpustakaan Tuanku Bainun Kampus Sultan Abdul Jalil Shah PustakaTBainun ptbupsi

05-4506832 pustaka.upsi.edu.my Perpustakaan Tuanku Bainun Kampus Sultan Abdul Jalil Shah PustakaTBainun ptbupsi

Table 4.6

Photodegradation of DBT using MTN-6, 5Fe/MTN-6, gC_3N_4 and 5FeMTN-6/5gC_3N_4 Photocatalysts

Photocatalyst	DBT degradation (%)
MTN-6	5.0
5Fe/MTN-6	9.0
gC_3N_4	33.1
5FeMTN-6/5gC_3N_4	38.2

Reaction conditions: model oil = 50 mL, Time = 180 min, Catalyst dosage = 5 g/L, DBT concentration = 40 mg/L, UV.

Then, from the results as shown in Figure 4.26(b), it was observed that 5FeMTN-6/5gC_3N_4 presented the highest photodegradation (38.2%) followed by gC_3N_4 (33.1%), 5Fe/MTN-6 (9.0%) and MTN-6 (5.0%). Therefore, 5FeMTN-6/5gC_3N_4 was chosen as the best catalyst for photodegradation of DBT as it exhibited better photocatalytic performance than gC_3N_4, MTN-6 and 5Fe/MTN-6. This result was due to the formation of heterojunction between gC_3N_4 and 5Fe/MTN-6, which inhibited the recombination of electron-hole pairs and resulted in a sufficient increased of sulfur removal.

The proposed mechanism of heterojunction-type photocatalytic system of TiO_2 incorporated with Fe and gC_3N_4 for photodegradation of DBT was shown in Figure 4.27.

05-4506832 pustaka.upsi.edu.my Perpustakaan Tuanku Bainun Kampus Sultan Abdul Jalil Shah PustakaTBainun ptbupsi

05-4506832 pustaka.upsi.edu.my Perpustakaan Tuanku Bainun Kampus Sultan Abdul Jalil Shah PustakaTBainun ptbupsi

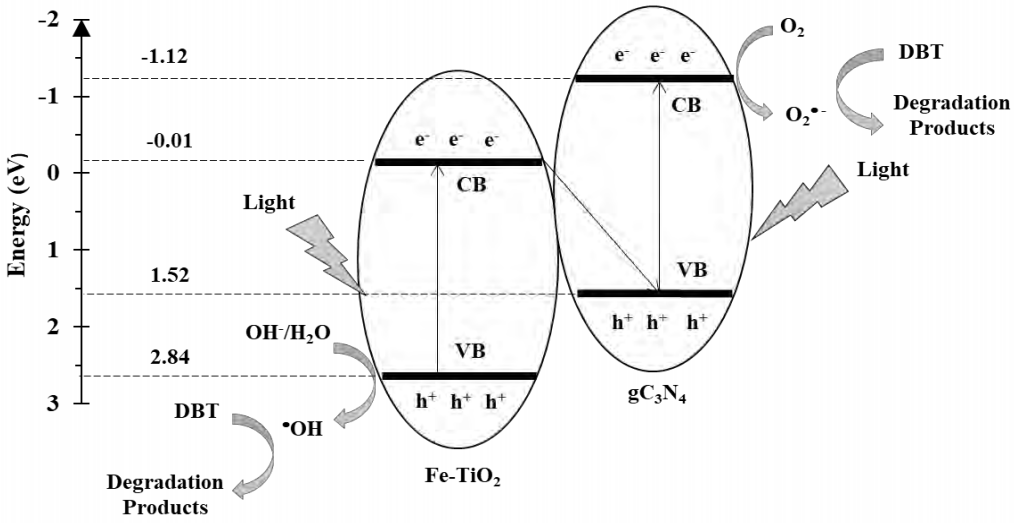


Figure 4.27. Proposed Mechanism of Heterojunction-Type Photocatalytic System of TiO_2 Incorporated with Fe and gC_3N_4 for Photodegradation of DBT. Adapted from Zhu et al., 2018

From the figure, it can be seen that the Z-scheme mechanism was used to interpret the improvement of photoactivity of TiO_2 with incorporation of Fe and gC_3N_4. It can be observed that Fe-TiO_2 exhibited lower CB and VB positions compared to gC_3N_4, in which forced the photogenerated electrons (e^-) in the CB of Fe-TiO_2 to be transported to the VB of gC_3N_4 and recombined with its photogenerated holes (h^+). The leaving photogenerated holes in the VB of Fe-TiO_2 then can directly react with H_2O to form hydroxyl radicals ($^{\bullet}OH$), in which responsible for the degradation of DBT. At the same time, the remaining photogenerated electrons in the CB of gC_3N_4 will react with adsorbed O_2 to produce superoxide radicals ($O_2^{\bullet-}$), which also help in DBT degradation. To be concluded, the Z-scheme mechanism applied to the Fe-TiO_2/gC_3N_4 composite can enhanced the efficient photodegradation of DBT due to its ability that can perform high separation and transfer of the photogenerated charge carriers (Zhu et al., 2018).

05-4506832 pustaka.upsi.edu.my Perpustakaan Tuanku Bainun Kampus Sultan Abdul Jalil Shah PustakaTBainun ptbupsi

05-4506832 pustaka.upsi.edu.my Perpustakaan Tuanku Bainun Kampus Sultan Abdul Jalil Shah PustakaTBainun ptbupsi

Similar effect has been reported in previously researched works. Lu et al. (2021) observed that the degradation rate of DBT using CeF_3/gC_3N_4 was significantly increased compared to pure gC_3N_4 and CeF_3 which indicated the synergistic effect of CeF_3 and gC_3N_4 as a nanocomposite has enhanced the photocatalytic performance. The result was consistent with the obtained PL and UV-DRS analyses as 5FeMTN-6/5gC_3N_4 exhibited lower recombination rate of photogenerated charges and the absorption edge was shifted towards visible light region which could enhance the photocatalytic efficiency.

4.4 Optimization parameters

05-4506832 pustaka.upsi.edu.my Perpustakaan Tuanku Bainun Kampus Sultan Abdul Jalil Shah PustakaTBainun ptbupsi

As shown in Figure 4.26(b), the degradation of DBT were 5.0%, 9.0% and 33.1% within 180 min in the presence of MTN-6, 5FeMTN-6 and gC_3N_4 photocatalysts. However, photoremoval rate of DBT reached 38.2% over 5FeMTN-6/5gC_3N_4 at the same reaction conditions. Therefore, it was favourable to use 5FeMTN-6/5gC_3N_4 as the best catalyst to identify the optimum conditions of photodegradation of DBT and thus, improving its photocatalytic activity. In addition, the reaction condition was prolonging to 240 min and the increment of DBT degradation rate was successfully obtained.

05-4506832 pustaka.upsi.edu.my Perpustakaan Tuanku Bainun Kampus Sultan Abdul Jalil Shah PustakaTBainun ptbupsi

05-4506832 pustaka.upsi.edu.my Perpustakaan Tuanku Bainun Kampus Sultan Abdul Jalil Shah PustakaTBainun ptbupsi

4.4.1 Effect of addition of Hydrogen peroxide (H_2O_2)

The photocatalytic activity of 5FeMTN-6/5gC_3N_4 was heavily influenced by the addition of 30% H_2O_2 solution. As can be seen in Figure 4.28, the photocatalytic activity of the catalyst was observed to be the highest when 0.01 mL of H_2O_2 was added into DBT solution with 55.2% degradation followed by 0.09, 0.03 and 0.06 mL with 49.2%, 47.0% and 46.8% of sulfur removal, respectively.

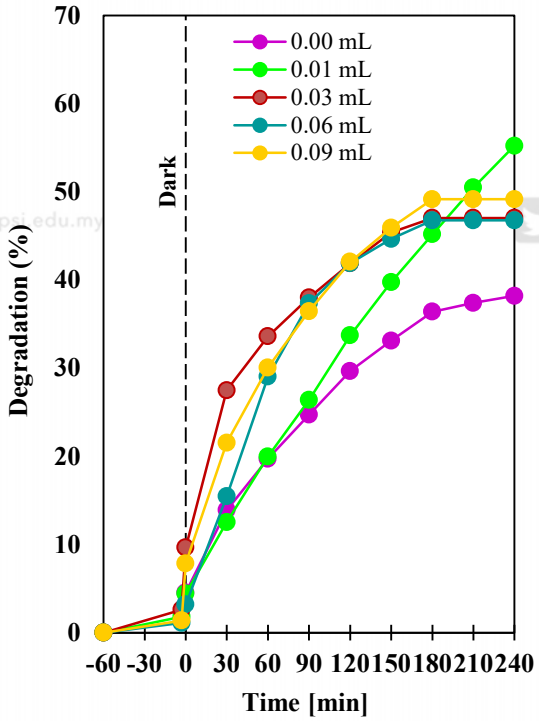


Figure 4.28. % Degradation of DBT using 5FeMTN-6/5gC_3N_4 with addition of 0.00, 0.01, 0.03, 0.06 and 0.09 mL of H_2O_2

05-4506832 pustaka.upsi.edu.my Perpustakaan Tuanku Bainun Kampus Sultan Abdul Jalil Shah PustakaTBainun ptbupsi

05-4506832 pustaka.upsi.edu.my Perpustakaan Tuanku Bainun Kampus Sultan Abdul Jalil Shah PustakaTBainun ptbupsi

From the results, it showed that the photodegradation of DBT increased as H_2O_2 was added as an oxidizing agent. This was due to the involvement of dual process which were photo-Fenton and photocatalysis in one system. The photo-Fenton process involved the combination of Fenton reagent ($Fe^{2+/}H_2O_2$) and light energy while photocatalysis was generated through the surface-active of MTN layer and also with the incorporation of gC_3N_4 (Puri et al., 2021; Chen, Liu, & Tong, 2018). The photo-Fenton reaction occurred when the electron from the conduction band was trapped by ferric ions and tend to produce more hydroxyl radicals ($^{\bullet}OH$) and regenerating the Fe^{2+} by photoreduction from Fe^{3+}, which can be expressed using the equations below, Eq. (4.2) and Eq. (4.3) (Kaur, Verma, Thakur, & Basu, 2021; Banic et al., 2011).

$$Fe^{2+} + H_2O_2 \rightarrow Fe(OH)^{2+} + {}^{\bullet}OH \quad (4.2)$$

$$Fe(OH)^{2+} + h\nu \rightarrow Fe^{2+} + {}^{\bullet}OH \quad (4.3)$$

Both processes (photocatalysis and photo-Fenton process) tend to utilize H_2O_2 simultaneously and enhance the photodegradation rate by continuous production of $^{\bullet}OH$. The addition of H_2O_2 in the system also reduced the recombination of electron-hole pairs with the utilization of excited electron by H_2O_2 to generate $^{\bullet}OH$ as showed in Eq. (4.4) (Kaur et al.,2021).

$$H_2O_2 + {}^{\bullet}O_2 \rightarrow {}^{\bullet}OH + OH^- + O_2 \quad (4.4)$$

05-4506832 pustaka.upsi.edu.my Perpustakaan Tuanku Bainun Kampus Sultan Abdul Jalil Shah PustakaTBainun ptbupsi

05-4506832 pustaka.upsi.edu.my Perpustakaan Tuanku Bainun Kampus Sultan Abdul Jalil Shah PustakaTBainun ptbupsi

However, the excessive use of H_2O_2 will poison the 5FeMTN-6/5gC_3N_4 catalyst surface, and thus hinder the degradation of DBT (Pham et al., 2018). This is because the extra amount of H_2O_2 will trap the hydroxyl radicals ($^{\bullet}OH$) and convert them to active species of hydroperoxyl radicals ($HO^{\bullet}_2$) that has weaker oxidizing properties as shown in Eq. (4.5), which in turn caused the degradation rate of DBT to be restrained (Hosseini et al., 2018).

$$H_2O_2 + {}^{\bullet}OH \rightarrow H_2O + HO^{\bullet}_2 \quad (4.5)$$

It can be observed that when 0.03 and 0.06 mL of H_2O_2 were added into DBT solution within a reaction time of 240 min, the removal of DBT can reach 47.0% and 46.8%, respectively, in which did not show any significant different. By further increasing the volume of H_2O_2 solution to 0.09 mL, the photodegradation of DBT was increased to 49.2%. However, 55.2% of DBT removal was achieved when the amount of H_2O_2 solution was reduced to 0.01 mL. The effect of addition of H_2O_2 for photodegradation of DBT using 5FeMTN-6/5gC_3N_4 were summarized in Table 4.7.

05-4506832 pustaka.upsi.edu.my Perpustakaan Tuanku Bainun Kampus Sultan Abdul Jalil Shah PustakaTBainun ptbupsi

05-4506832 pustaka.upsi.edu.my Perpustakaan Tuanku Bainun Kampus Sultan Abdul Jalil Shah PustakaTBainun ptbupsi

Table 4.7

Effect of Addition of H_2O_2 for Photodegradation of DBT

Volume of H_2O_2 (mL)	**DBT degradation (%)**
0.00	38.2
0.01	55.2
0.03	47.0
0.06	46.8
0.09	49.2

Reaction conditions: model oil = 50 mL, Time = 240 min, Catalyst dosage = 5 g/L, DBT concentration = 40 mg/L, UV.

The results showed that, as the amount of H_2O_2 solution was reduced, the photodegradation of DBT was dramatically increased. Therefore, 0.01 mL was chosen as the optimal amount of H_2O_2 for the degradation of DBT. On the other hand, photocatalytic performace of 5FeMTN-6/5gC_3N_4 with the absence of H_2O_2 as the oxidant only performed 38.2% of DBT degradation. Similar study has been reported in the previously published papers. Mandizadeh et al. (2017) observed that the addition of 30% of H_2O_2 solution into model oil has significantly increased the degradation rate of DBT, which showed the synergistic effect of $BaFe_2O_4$, H_2O_2 and acetonitrile was approved for the enhancement of DBT removal.

05-4506832 pustaka.upsi.edu.my Perpustakaan Tuanku Bainun Kampus Sultan Abdul Jalil Shah PustakaTBainun ptbupsi

05-4506832 pustaka.upsi.edu.my Perpustakaan Tuanku Bainun Kampus Sultan Abdul Jalil Shah PustakaTBainun ptbupsi

4.4.2 Effect of catalyst dosage

The effect of catalyst dosage was also used as a parameter to identify the optimal amount of catalyst for improving the degradation rate of DBT. The selected dosages were 1, 3, 5, 7 and 9 g/L and the results were shown in Figure 4.29.

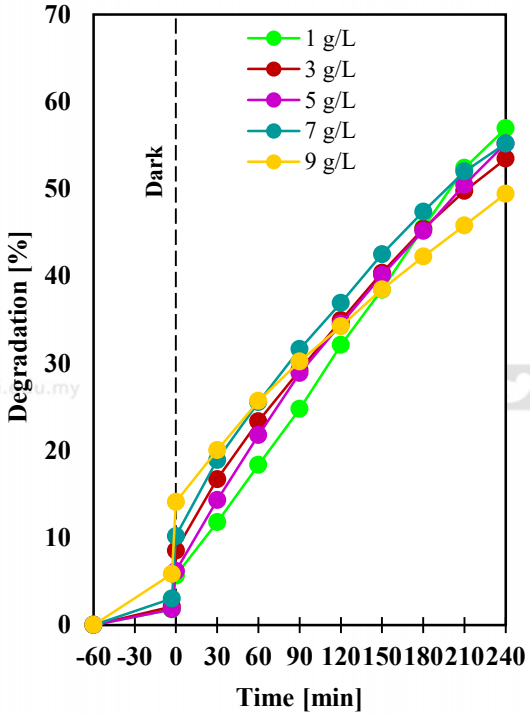


Figure 4.29. % Degradation of DBT using 5FeMTN-6/5gC_3N_4 with addition of 1, 3, 5, 7 and 9 g/L of Catalyst Dosage

As can be seen in Figure 4.29, 1 g/L exhibited the highest degradation of DBT (57.0%), followed by 5 (55.2%), 7 (55.2%), 3 (53.5%) and 9 g/L (49.5%). The effect of catalyst dosages for photodegradation of DBT using 5FeMTN-6/5gC_3N_4 were summarized in Table 4.8.

05-4506832 pustaka.upsi.edu.my Perpustakaan Tuanku Bainun Kampus Sultan Abdul Jalil Shah PustakaTBainun ptbupsi

05-4506832 pustaka.upsi.edu.my Perpustakaan Tuanku Bainun Kampus Sultan Abdul Jalil Shah PustakaTBainun ptbupsi

Table 4.8

Effect of Catalyst Dosage for Photodegradation of DBT

Catalyst dosage (g/L)	DBT degradation (%)
1	57.0
3	53.5
5	55.2
7	55.2
9	49.5

Reaction conditions: model oil = 50 mL, Time = 240 min, H_2O_2 = 0.01 mL, DBT concentration = 40 mg/L, UV.

The optimum amount of catalyst dosage was 1 g/L and as the amount of catalyst was increased, the DBT degradation was slowly reduced. This is because as the catalyst dosage was beyond the optimum amount, the aggregation of photocatalyst particles tend to occur and reduced the surface area of the photocatalyst which resulted to lower degradation efficiency. Moreover, the aggregated particles caused the scattering of the incident photon to be higher and thus, decreased the number of generated electron-hole pairs (Hosseini et al., 2018). It also caused the turbidity of the suspension in the solution, which in turn will complicate the penetration of light towards the photocatalyst's surface (Marfur et al.,2019).

05-4506832 pustaka.upsi.edu.my Perpustakaan Tuanku Bainun Kampus Sultan Abdul Jalil Shah PustakaTBainun ptbupsi

05-4506832 pustaka.upsi.edu.my Perpustakaan Tuanku Bainun Kampus Sultan Abdul Jalil Shah PustakaTBainun ptbupsi

4.4.3 Effect of DBT initial concentration

In addition, the photocatalytic performance of the photocatalyst was also investigated by varying the initial concentrations of DBT solution in the range of 20 to 60 mg/L. Figure 4.30 showed the photocatalytic performance of 5FeMTN-6/5gC_3N_4 when various initial concentrations of DBT were used.

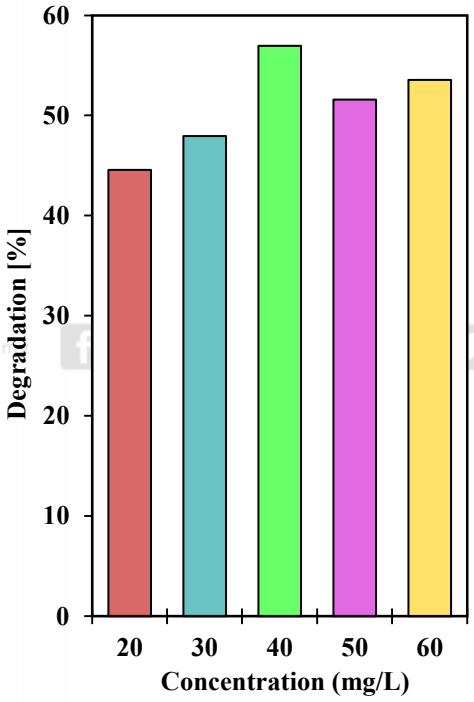


Figure 4.30. % Degradation of DBT using 5FeMTN-6/5gC_3N_4 with 20, 30, 40, 50 and 60 mg/L Concentration of DBT Solution

The effect of DBT initial concentrations for photodegradation of DBT using 5FeMTN-6/5gC_3N_4 were summarized in Table 4.9.

05-4506832 pustaka.upsi.edu.my Perpustakaan Tuanku Bainun Kampus Sultan Abdul Jalil Shah PustakaTBainun ptbupsi

05-4506832 pustaka.upsi.edu.my Perpustakaan Tuanku Bainun Kampus Sultan Abdul Jalil Shah PustakaTBainun ptbupsi

Table 4.9

Effect of DBT Initial Concentration for Photodegradation of DBT

DBT initial concentration (mg/L)	DBT degradation (%)
20	44.6
30	47.9
40	57.0
50	51.6
60	53.6

Reaction conditions: model oil = 50 mL, Time = 240 min, H_2O_2 = 0.01 mL, Catalyst dosage = 1 g/L, UV.

The degradation of DBT was the highest at 40 mg/L with 57.0% of degradation rate. From the results, it can be observed that the degradation rate tend to increase as the DBT initial concentration was increased from 20 to 40 mg/L. It could be due to the high interaction between sulfur components with active species and also catalyst surface (Abedini et al., 2021). However, further increasing the DBT initial concentration beyond 40 mg/L caused the decrement to occur in photodegradation activity. It can be justified that by increasing the pollutant concentration beyond the optimum amount will complicate the light penetration towards the catalyst's surface which in turn reduced the formation of hydroxyl ions and thus, give impacts in the degradation activity (Marfur et al.,2019).

05-4506832 pustaka.upsi.edu.my Perpustakaan Tuanku Bainun Kampus Sultan Abdul Jalil Shah PustakaTBainun ptbupsi

05-4506832 pustaka.upsi.edu.my Perpustakaan Tuanku Bainun Kampus Sultan Abdul Jalil Shah PustakaTBainun ptbupsi

The excess of DBT solution at optimum condition was collected to identify the degradation product formed after the photocatalytic reaction of DBT in acetonitrile. The sample taken was separated by high-speed centrifuge and then the upper layer model oil was collected to be analyzed by GC-MS. As shown in Figure 4.31, the DBT has been oxidized to DBT sulfone ($DBTO_2$) which was identified based on the mass spectra (Lu et al., 2020; Ma et al., 2019).

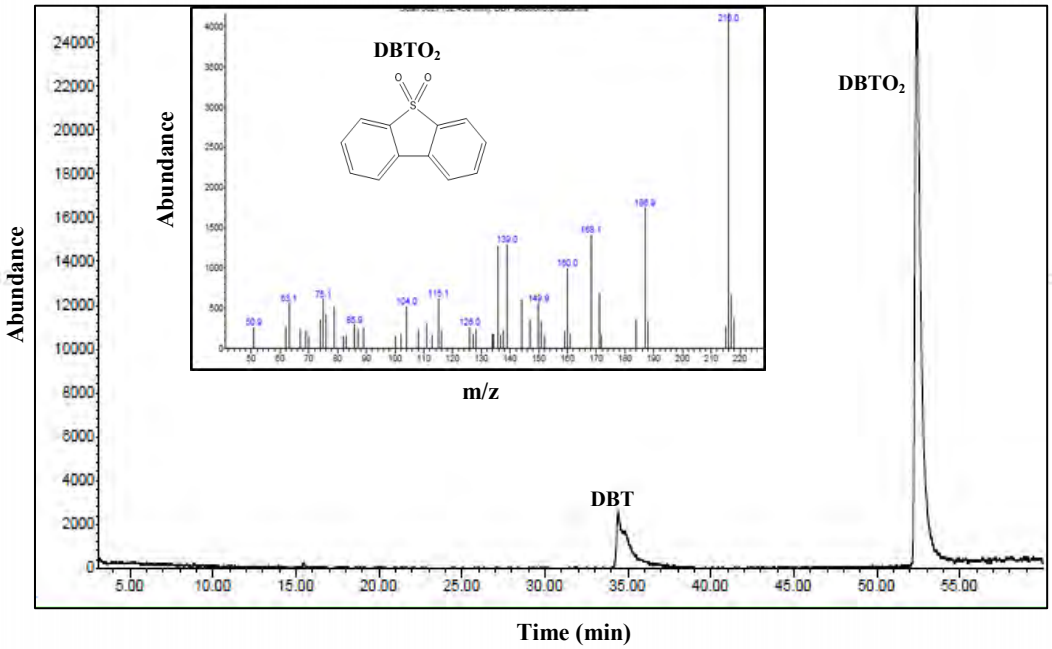


Figure 4.31. The MS Product of $DBTO_2$

The similarities of the product formed compared to GC-MS NIST library was about 87%. However, the characteristic peak of DBT was still exist in the model oil phase, which indicated that DBT has not been completely degraded since the highest

05-4506832 pustaka.upsi.edu.my Perpustakaan Tuanku Bainun Kampus Sultan Abdul Jalil Shah PustakaTBainun ptbupsi

05-4506832 pustaka.upsi.edu.my Perpustakaan Tuanku Bainun Kampus Sultan Abdul Jalil Shah PustakaTBainun ptbupsi

DBT degradation obtained was 57.0%. The optimum conditions obtained for photodegradation of DBT using 5FeMTN-6/5gC_3N_4 were summarized in Table 4.10.

Table 4.10

Optimum Conditions for Photodegradation of DBT using 5FeMTN-6/5gC_3N_4 under UV Light

Optimization parameters	**Optimum amount**
Catalyst dosage (g/L)	1
Volume of H_2O_2 (mL)	0.01
DBT initial concentration (mg/L)	40
Reaction time (min)	240 min
Total DBT degradation (%)	57.0

05-4506832 pustaka.upsi.edu.my Perpustakaan Tuanku Bainun Kampus Sultan Abdul Jalil Shah PustakaTBainun ptbupsi

05-4506832 pustaka.upsi.edu.my Perpustakaan Tuanku Bainun Kampus Sultan Abdul Jalil Shah PustakaTBainun ptbupsi

CHAPTER 5

CONCLUSION AND RECOMMENDATIONS

05-4506832 pustaka.upsi.edu.my Perpustakaan Tuanku Bainun Kampus Sultan Abdul Jalil Shah PustakaTBainun ptbupsi

In this research, MTN with various aging time (x = 2, 4, 6 and 8 days) were synthesized using sol-gel method and then modified with the incorporation of 5wt% Fe and 5wt% gC_3N_4 using wet-impregnation. From the XRD results, it can be observed that the MTN aging time has influenced the particle sizes of the photocatalyst. However, there was no significant changing observed by varying the MTN aging time, in which the photocatalytic performance of each photocatalyst was not showed any significant different. Then, 5wt% of Fe was added into MTN-x via wet impregnation method in order to improve its photocatalytic performance. The addition of 5wt% Fe into MTN-6 (5Fe/MTN-6) has obtained the highest photocatalytic performance in which 9.0% of DBT

05-4506832 pustaka.upsi.edu.my Perpustakaan Tuanku Bainun Kampus Sultan Abdul Jalil Shah PustakaTBainun ptbupsi

05-4506832 pustaka.upsi.edu.my Perpustakaan Tuanku Bainun Kampus Sultan Abdul Jalil Shah PustakaTBainun ptbupsi

has been degraded within 180 min compared to 5Fe/MTN-2, 5Fe/MTN-4 and 5Fe/MTN-8 which only degrade 8.5%, 7.1% and 5.9% of DBT under the same condition, respectively. Since 5Fe/MTN-6 obtained the highest degradation rate, it was chosen to be modified with 5wt% of gC_3N_4 (5FeMTN-6/5gC_3N_4), since the photoactivity results of 5Fe/MTN-x samples also not showed any significant different with each other. The gC_3N_4 was incorporated into 5Fe/MTN-6 as a dopant due to its ability that can improve the photocatalytic performance by enhancing the separation of photogenerated electron-hole pairs. The DBT degradation was significantly increased as 5FeMTN-6/5gC_3N_4 was used as a photocatalyst in which 38.2% of DBT has been removed within 180 min. The significant result could be due to the incorporation of Fe and gC_3N_4 that formed heterojunction known as Z-scheme mechanism that promote the generation and inhibit the recombination of electron-hole pairs. The PL and UV-DRS results also confirmed that this photocatalyst exhibited lower recombination rate of photogenerated charges and the optical absorption was extended towards visible light region which could be the reason of enhanced photocatalytic performance.

The optimization study of 5FeMTN-6/5gC_3N_4 was carried out to obtain the optimum condition of its photoactivity. In addition, the reaction condition was prolonging to 240 min and the increment of DBT degradation rate was successfully obtained. The optimum conditions for 5FeMTN-6/5gC_3N_4 were 1 g/L of catalyst in a 40 mg/L of DBT solution with addition of 0.01 mL of H_2O_2 solution. To be concluded, highest degradation rate was obtained by using these conditions in which 57.0% of DBT was successfully degraded.

05-4506832 pustaka.upsi.edu.my Perpustakaan Tuanku Bainun Kampus Sultan Abdul Jalil Shah PustakaTBainun ptbupsi

05-4506832 pustaka.upsi.edu.my Perpustakaan Tuanku Bainun Kampus Sultan Abdul Jalil Shah PustakaTBainun ptbupsi

Some recommendations were suggested in order to improve the efficiency and reusability of these photocatalyst for profitable use. First of all, the photocatalyst with visible light absorption ability was still not perfectly developed and more improvements were needed especially in the part of cost, technical hurdles and safety. Therefore, the design of effective photoreactor with full utilization of solar energy should be focused in future works, in which can help to reduce the electricity costs by replacing the electrical lamp being used for sources of light. Besides that, further exploration on the reaction parameters should be included in order to increase the degradation rate of DBT. Last but not least, the use of commercial Fe as a metal doping can also be replaced by extraction of slags which was described as hazardous waste. Without realizing, this solid waste can be taken as a potential secondary source as it contains large amount of Fe and recycling these slags for beneficial used can also help in reducing the environmental pollution as it caused risk to environment when discarded in landfills.

05-4506832 pustaka.upsi.edu.my Perpustakaan Tuanku Bainun Kampus Sultan Abdul Jalil Shah PustakaTBainun ptbupsi

05-4506832 pustaka.upsi.edu.my Perpustakaan Tuanku Bainun Kampus Sultan Abdul Jalil Shah PustakaTBainun ptbupsi

REFERENCES

Aazam, E. S. (2014). Visible light photocatalytic degradation of thiophene using Ag–TiO_2/multi-walled carbon nanotubes nanocomposite. *Ceramics International*, *40*(5), 6705-6711.

Abbas, N., Shao, G. N., Haider, M. S., Imran, S. M., Park, S. S. & Kim, H. T. (2016). Sol–gel synthesis of TiO_2-Fe_2O_3 systems: Effects of Fe_2O_3 content and their photocatalytic properties. *Journal of Industrial and Engineering Chemistry*, *39*, 112-120.

Abdelaal, M. Y. & Mohamed, R. M. (2014). Environmental remediation from thiophene solution by photocatalytic oxidation using a Pd/ZrO_2–chitosan nanocomposite. *Ceramics International*, *40*(6), 7693-7699.

Abdennouri, M., Baalala, M., Galadi, A., El Makhfouk, M., Bensitel, M., Nohair, K., et al. (2016). Photocatalytic degradation of pesticides by titanium dioxide and titanium pillared purified clays. *Arabian Journal of Chemistry*, *9*, 313–318.

Abdul Mutalib, M., Rahman, M. A., Othman, M. H. D., Ismail, A. F. & Jaafar, J. (2017). Scanning electron microscopy (SEM) and energy-dispersive X-ray (EDX) spectroscopy. *Membrane characterization*, *20*, 161-179.

Abedini, F., Allahyari, S. & Rahemi, N. (2021). Oxidative desulfurization of dibenzothiophene and simultaneous adsorption of products on BiOBr-C_3N_4/MCM-41 visible-light-driven core–shell nano photocatalyst. *Applied Surface Science*, *569*, 1-13.

Abhilash, M. R., Akshatha, G. & Srikantaswamy, S. (2019). Photocatalytic dye degradation and biological activities of the Fe_2O_3/Cu_2O nanocomposite. *RSC advances*, *9*(15), 8557-8568.

Abro, R., Abdeltawab, A. A., Al-Deyab, S. S., Yu, G., Qazi, A. B., Gao, S., et al. (2014). A review of extractive desulfurization of fuel oils using ionic liquids. *RSC Advances*, *4*(67), 35302-35317.

Ahadi, S., Moalej, N. S. & Sheibani, S. (2019). Characteristics and photocatalytic behavior of Fe and Cu doped TiO_2 prepared by combined sol-gel and mechanical alloying. *Solid State Sciences*, *96*, 1-10.

05-4506832 pustaka.upsi.edu.my Perpustakaan Tuanku Bainun Kampus Sultan Abdul Jalil Shah PustakaTBainun ptbupsi

05-4506832 pustaka.upsi.edu.my Perpustakaan Tuanku Bainun Kampus Sultan Abdul Jalil Shah PustakaTBainun ptbupsi

Akshay, V. R., Arun, B., Mandal, G., Mutta, G. R., Chanda, A. & Vasundhara, M. (2018). Observation of optical band-gap narrowing and enhanced magnetic moment in co-doped sol–gel-derived anatase TiO_2 nanocrystals. *The Journal of Physical Chemistry C*, *122*(46), 26592-26604.

Ali, T., Tripathi, P., Azam, A., Raza, W., Ahmed, A. S., Ahmed, A., et al. (2017). Photocatalytic performance of Fe-doped TiO_2 nanoparticles under visible-light irradiation. *Materials Research Express*, *4*(1), 1-13.

Ali, T., Ahmed, A., Alam, U., Uddin, I., Tripathi, P. & Muneer, M. (2018). Enhanced photocatalytic and antibacterial activities of Ag-doped TiO_2 nanoparticles under visible light . *Materials Chemistry and Physics*, *212*, 325-335.

Almashjary, K. H., Khalid, M., Dharaskar, S., Jagadish, P., Walvekar, R. & Gupta, T. C. S. M. (2018). Optimisation of extractive desulfurization using Choline Chloride-based deep eutectic solvents. *Fuel*, *234,* 1388-1400.

Altin, I., Sokmen, M. & Biyiklioglu, Z. (2016). Sol gel synthesis of cobalt doped TiO_2 and its dye sensitization for efficient pollutant removal. *Materials Science in Semiconductor Processing*, *45*, 36-44.

Ammar, S. H., Kareem, Y. S. & Ali, A. D. (2018). Photocatalytic oxidative desulfurization of liquid petroleum fuels using magnetic CuO-Fe_3O_4 nanocomposites. *Journal of Environmental Chemical Engineering*, *6*(6), 6780-6786.

Anandalakshmi, K., Venugobal, J. & Ramasamy, V. (2016). Characterization of silver nanoparticles by green synthesis method using Pedalium murex leaf extract and their antibacterial activity. *Applied Nanoscience*, *6*(3), 399–408.

Anandan, S., Sivasankar, T. & Lana-Villarreal, T. (2014). Synthesis of TiO_2/WO_3 nanoparticles via sonochemical approach for the photocatalytic degradation of methylene blue under visible light illumination. *Ultrasonics Sonochemistry*, *21*(6), 1964-1968.

Anisah, S., Kanezashi, M., Nagasawa, H. & Tsuru, T. (2019). TiO_2-ZrO_2 membranes of controlled pore sizes with different Ti/Zr ratios for nanofiltration. *Journal of Sol-Gel Science and Technology*, *92*(1), 12-24.

05-4506832 pustaka.upsi.edu.my Perpustakaan Tuanku Bainun Kampus Sultan Abdul Jalil Shah PustakaTBainun ptbupsi

05-4506832 pustaka.upsi.edu.my Perpustakaan Tuanku Bainun Kampus Sultan Abdul Jalil Shah PustakaTBainun ptbupsi

Anjugam Vandarkuzhali, S. A., Pugazhenthiran, N., Mangalaraja, R. V., Sathishkumar, P., Viswanathan, B. & Anandan, S. (2018). Ultrasmall plasmonic nanoparticles decorated hierarchical mesoporous TiO_2 as an efficient photocatalyst for photocatalytic degradation of textile dyes. *ACS Omega*, *3*(8), 9834−9845.

Anku, W., Oppong, S. O. B., Shukla, S. K. & Govender, P. P. (2016). Comparative photocatalytic degradation of monoazo and diazo dyes under simulated visible light using Fe^{3+}/C/S doped-TiO_2 nanoparticles. *Acta Chimica Slovenica*, *63*(2), 380–391.

Aoki, T. (2012). Photoluminescence spectroscopy. *Characterization of Materials*, 1-12.

Arabkhani, P. & Abedini-Khorrami, S. (2019). Synthesis of $SrAl_2O_4$ nanoparticles by reverse micelle method: An investigation of the effect of aging time, hydrophilic chain length and calcination temperature. *Nano-Structures & Nano-Objects*, *17*, 84–91.

Arfanis, M. K., Adamou, P., Moustakas, N. G., Triantis, T. M., Kontos, A. G. & Falaras, P. (2017). Photocatalytic degradation of salicylic acid and caffeine emerging contaminants using titania nanotubes. *Chemical Engineering Journal*, *310*, 525-536.

Arfanis, M. K., Athanasekou, C. P., Sakellis, E., Boukos, N., Ioannidis, N., Likodimos, V., et al. (2019). Photocatalytic properties of copper–modified core-shell titania nanocomposites. *Journal of Photochemistry and Photobiology A: Chemistry*, *370*, 145-155.

Azami, M. S., Ismail, K., Ishak, M. A. M., Zuliahani, A., Hamzah, S. R. & Nawawi, W. I. (2020). Formation of an amorphous carbon nitride/titania composite for photocatalytic degradation of RR4 dye. *Journal of Water Process Engineering*, *35*, 1-8.

Bagheri, S., Hir, Z. A. M., Yousefi, A. T. & Hamid, S. B. A. (2015). Progress on mesoporous titanium dioxide: Synthesis, modification and applications. *Microporous and Mesoporous Materials*, *218*, 206-222.

Balu, S., Velmurugan, S., Palanisamy, S., Chen, S. W., Velusamy, V., Yang, T. C., et al. (2 19). Synthesis of -Fe_2O_3 decorated g-C_3N_4/ZnO ternary Z-scheme photocatalyst for degradation of tartrazine dye in aqueous media. *Journal of the Taiwan Institute of Chemical Engineers*, *99*, 258-267.

05-4506832 pustaka.upsi.edu.my Perpustakaan Tuanku Bainun Kampus Sultan Abdul Jalil Shah PustakaTBainun ptbupsi

05-4506832 pustaka.upsi.edu.my Perpustakaan Tuanku Bainun Kampus Sultan Abdul Jalil Shah PustakaTBainun ptbupsi

Banic, N., Abramovic, B., Krstic, J., Sojic, D., Loncarevic, D., Cherkezova-Zheleva, Z., et al. (2011). Photodegradation of thiacloprid using Fe/TiO_2 as a heterogeneous photo-Fenton catalyst. *Applied Catalysis B: Environmental*, *107*(3-4), 363-371.

Bardestani, R., Patience, G. S. & Kaliaguine, S. (2019). Experimental methods in chemical engineering: specific surface area and pore size distribution measurements—BET, BJH, and DFT. *The Canadian Journal of Chemical Engineering*, *97*(11), 2781-2791.

Barkhade, T. & Banerjee, I. (2018). Photocatalytic degradation of Rhodamine B dye using Fe doped TiO_2 nanocomposites. *AIP Conference Proceedings*, *1961*, 1-7.

Betiha, M. A., Rabie, A. M., Ahmed, H. S., Abdelrahman, A. A. & El-Shahat, M. F. (2018). Oxidative desulfurization using graphene and its composites for fuel containing thiophene and its derivatives: An update review. *Egyptian Journal of Petroleum*, 715-730.

Bhutto, A. W., Abro, R., Gao, S., Abbas, T., Chen, X. & Yu, G. (2016). Oxidative desulfurization of fuel oils using ionic liquids: A review. *Journal of the Taiwan Institute of Chemical Engineers*, *62*, 84-97.

Biru, M., Qaderi, J., Mamat, C. R. & Jalil, A. A. (2021). Preparation and characterization of copper, iron, and nickel doped titanium dioxide photocatalysts for decolorization of methylene blue. *Sains Malaysiana*, *50*(1), 135-149.

Blanco-Vega, M. P., Guzman-Mar, J. L., Villanueva-Rodriguez, M., Maya-Trevino, L., Garza-Tovar, L. L., Hernandez-Ramirez, A., et al. (2017). Photocatalytic elimination of bisphenol A under visible light using Ni-doped TiO_2 synthesized by microwave assisted sol-gel method. *Materials Science in Semiconductor Processing*, *71*, 275-282.

Blitz, J. P. (1998). Diffuse reflectance spectroscopy. *Modern Techniques in Applied Molecular Spectroscopy*, *14*, 185-219.

Bumbrah, G. S. & Sharma, R. M. (2016). Raman spectroscopy–Basic principle, instrumentation and selected applications for the characterization of drugs of abuse. *Egyptian Journal of Forensic Sciences*, *6*(3), 209-215.

05-4506832 pustaka.upsi.edu.my Perpustakaan Tuanku Bainun Kampus Sultan Abdul Jalil Shah PustakaTBainun ptbupsi

05-4506832 pustaka.upsi.edu.my Perpustakaan Tuanku Bainun Kampus Sultan Abdul Jalil Shah PustakaTBainun ptbupsi

Byranvand, M. M., Nemati Kharat, A., Fatholahi, L. & Beiranvand, M. Z. (2013). A Review on Synthesis of Nano-TiO_2 via Different Methods. *Journal of Nanostructures*, *3*(1), 1-9.

Camarillo, R., Rizaldos, D., Jimenez, C., Martinez, F. & Rincon, J. (2019). Enhancing the photocatalytic reduction of CO_2 with undoped and Cu-doped TiO_2 nanofibers synthesized in supercritical medium. *The Journal of Supercritical Fluids*, *147*, 70-80.

Castro, Y. & Duran, A. (2016). Ca doping of mesoporous TiO_2 films for enhanced photocatalytic efficiency under solar irradiation . *Journal of Sol-Gel Science and Technology*, *78*(3), 482-491.

Castro, Y., Arconada, N. & Duran, A. (2015). Synthesis and photocatalytic characterisation of mesoporous TiO_2 films doped with Ca, W and N. *Boletín de la Sociedad Española de Cerámica y Vidrio*, *54*(1), 11-20.

Chanu, L. A., Singh, W. J., Singh, K. J. & Devi, K. N. (2019). Effect of operational parameters on the photocatalytic degradation of Methylene blue dye solution using manganese doped ZnO nanoparticles. *Results in Physics*, *12*, 1230–1237.

Chen, Y., Chen, D., Chen, J., Lu, Q., Zhang, M., Liu, B., et al. (2015). Facile synthesis of Bi nanoparticle modified TiO_2 with enhanced visible light photocatalytic activity. *Journal of Alloys and Compounds*, *651*, 114-120.

Chen, W., Liu, M., Wang, Y., Gao, L., Dang, H. & Mao, L. (2019). Non-noble metal Co as active sites on TiO_2 nanorod for promoting photocatalytic H_2 production. *Materials Research Bulletin*, *116*, 16-21.

Chen, Q. L., Liu, Y. L. & Tong, L. G. (2018). Enhanced visible light photocatalytic activity of g-C_3N_4 assisted by hydrogen peroxide. *Materials Research Express*, *5*(4), 1-19.

Chen, K., Liu, N., Zhang, M. & Wang, D. (2017). Oxidative desulfurization of dibenzothiophene over monoclinic VO_2 phase-transition catalysts. *Applied Catalysis B: Environmental*, *212*, 32-40.

05-4506832 pustaka.upsi.edu.my Perpustakaan Tuanku Bainun Kampus Sultan Abdul Jalil Shah PustakaTBainun ptbupsi

05-4506832 pustaka.upsi.edu.my Perpustakaan Tuanku Bainun Kampus Sultan Abdul Jalil Shah PustakaTBainun ptbupsi

Chen, L., Man, Y., Chen, Z. & Zhang, Y. (2016). Ag/g-C_3N_4 layered composites with enhanced visible light photocatalytic performance. *Materials Research Express*, *3*(11), 1-11.

Chen, Y., Shen, C., Wang, J., Xiao, G. & Luo, G. (2018). Green synthesis of Ag–TiO_2 supported on porous glass with enhanced photocatalytic performance for oxidative desulfurization and removal of dyes under visible light. *ACS Sustainable Chemistry & Engineering*, *6*(10), 13276-13286.

Chowdhury, I. H. & Naskar, M. K. (2018). Sol-gel synthesis of mesoporous hollow titania microspheres for photodegradation of 4-chlorophenol. *Indian Journal Of Chemistry Section A-Inorganic Bio-Inorganic Physical Theoretical & Analytical Chemistry*, *57*(7), 910-914.

Chowdhury, I. H., Ghosh, S. & Naskar, M. K. (2016). Aqueous-based synthesis of mesoporous TiO_2 and Ag–TiO_2 nanopowders for efficient photodegradation of methylene blue. *Ceramics International*, *42*(2), 2488-2496.

Cialla-May, D., Schmitt, M. & Popp, J. (2019). Theoretical principles of Raman spectroscopy. *Physical Sciences Reviews*, *4*(6), 1-9.

Ciriminna, R., Albanese, L., Meneguzzo, F. & Pagliaro, M. (2016). Hydrogen peroxide: a key chemical for today's sustainable development. *ChemSusChem*, *9*(24), 3374-3381.

Dehghan, R. & Anbia, M. (2017). Zeolites for adsorptive desulfurization from fuels: A review. *Fuel Processing Technology*, *167*, 99-116.

Demirbas, A., Alidrisi, H. & Balubaid, M. A. (2015). API gravity, sulfur content, and desulfurization of crude oil. *Petroleum Science and Technology*, *33*(1), 93-101.

Ding, W., Zhu, W., Xiong, J., Yang, L., Wei, A., Zhang, M., et al. (2015). Novel heterogeneous iron-based redox ionic liquid supported on SBA-15 for deep oxidative desulfurization of fuels. *Chemical Engineering Journal*, *266*, 213-221.

05-4506832 pustaka.upsi.edu.my Perpustakaan Tuanku Bainun Kampus Sultan Abdul Jalil Shah PustakaTBainun ptbupsi

05-4506832 pustaka.upsi.edu.my Perpustakaan Tuanku Bainun Kampus Sultan Abdul Jalil Shah PustakaTBainun ptbupsi

Dorraj, M., Goh, B. T., Sairi, N. A., Woi, P. M. & Basirun, W. J. (2018). Improved visible-light photocatalytic activity of TiO_2 co-doped with Copper and Iodine. *Applied Surface Science*, *439*, 999-1009.

El-Yazeed, W. A. & Ahmed, A. I. (2019). Photocatalytic activity of mesoporous WO_3/TiO_2 nanocomposites for the photodegradation of methylene blue. *Inorganic Chemistry Communications*, *105*, 102-111.

Epp, J. (2016). X-ray diffraction (XRD) techniques for materials characterization. *Materials characterization using nondestructive evaluation (NDE) methods*, 81-124.

Eshaghi, A. & Moradi, H. (2018). Optical and photocatalytic properties of the Fe-doped TiO_2 nanoparticles loaded on the activated carbon. *Advanced Powder Technology*, *29*(8), 1879-1885.

Fajriati, I., Mudasir, M. & Wahyuni, E. T. (2017). The effect of pH and aging time on the synthesis of TiO_2–Chitosan nanocomposites as photocatalyst by sol-gel method at room temperature. *Molekul*, *12*(2), 117-125.

Fang, W., Xing, M. & Zhang, J. (2017). Modifications on reduced titanium dioxide photocatalysts: A review. *Journal of Photochemistry and Photobiology C: Photochemistry Reviews*, *32*, 21-39.

Fernandes, A., Gagol, M., Makos, P., Khan, J. A. & Boczkaj, G. (2019). Integrated photocatalytic advanced oxidation system ($TiO_2/UV/O_3/H_2O_2$) for degradation of volatile organic compounds. *Separation and Purification Technology*, *224*, 1-14.

Gahlot, S., Dappozze, F., Mishra, S. & Guillard, C. (2021). High surface area g-C_3N_4 and g-C_3N_4-TiO_2 photocatalytic activity under UV and visible light: Impact of individual component. *Journal of Environmental Chemical Engineering*, *9*(4), 1-9.

Geng, Y., Zhang, P., Li, N. & Sun, Z. (2015). Synthesis of Co doped $BiVO_4$ with enhanced visible-light photocatalytic activities. *Journal of Alloys and Compounds*, *651*, 744-748.

05-4506832 pustaka.upsi.edu.my Perpustakaan Tuanku Bainun Kampus Sultan Abdul Jalil Shah PustakaTBainun ptbupsi

05-4506832 pustaka.upsi.edu.my Perpustakaan Tuanku Bainun Kampus Sultan Abdul Jalil Shah PustakaTBainun ptbupsi

Govindaraj, R., Pandian, M. S., Ramasamy, P. & Mukhopadhyay, S. (2014). Sol–gel synthesized mesoporous anatase titanium dioxide nanoparticles for dye sensitized solar cell (DSSC) applications. *Int. J. ChemTech Res*, *38*(2), 5220-5225.

Halim, W., Coste, S., Zeroual, S., Kassiba, A. & Ouaskit, S. (2020). Latex copolymer-assisted synthesis of metal-doped TiO_2 mesoporous structures for photocatalytic applications under solar simulator. *Journal of Materials Science: Materials in Electronics*, *31*(5), 4161-4169.

Han, F., Kambala, V. S. R., Dharmarajan, R., Liu, Y. & Naidu, R. (2018). Photocatalytic degradation of azo dye acid orange 7 using different light sources over Fe^{3+}-doped TiO_2 nanocatalysts. *Environmental Technology & Innovation*, *12*, 27-42.

Hassena, H. (2016). Photocatalytic degradation of methylene blue by using Al_2O_3/Fe_2O_3 nano composite under visible light. *Modern Chemistry & Applications*, *4*(5), 1-5.

Hitam, C. N. C., Jalil, A. A., Triwahyono, S., Rahman, A. F. A., Hassan, N. S., Khusnun, N. F., et al. (2018). Effect of carbon-interaction on structure-photoactivity of Cu doped amorphous TiO_2 catalysts for visible-light-oriented oxidative desulphurization of dibenzothiophene. *Fuel*, *216*, 407-417.

Hitam, C. N. C., Jalil, A. A. & Triwahyono, S. (2018). Synthesis of zinc oxide supported on titanium dioxide for photocatalytic oxidative desulfurization of dibenzothiophene. *Journal of Energy and Safety Technology*, *1*(1), 1-6.

Hitam, C. N. C., Jalil, A. A. & Abdulrasheed, A. A. (2019). A review on recent progression of photocatalytic desulphurization study over decorated photocatalysts. *Journal of Industrial and Engineering Chemistry*, *74*, 172-186.

Holder, C. F. & Schaak, R. E. (2019). Tutorial on powder X-ray diffraction for characterizing nanoscale materials. *Acs Nano*, *13*(7), 7359-7365.

Hossain, M. N., Park, H. C. & Choi, H. S. (2019). A comprehensive review on catalytic oxidative desulfurization of liquid fuel oil. *Catalysts*, *9*(3), 229.

05-4506832 pustaka.upsi.edu.my Perpustakaan Tuanku Bainun Kampus Sultan Abdul Jalil Shah PustakaTBainun ptbupsi

05-4506832 pustaka.upsi.edu.my Perpustakaan Tuanku Bainun Kampus Sultan Abdul Jalil Shah PustakaTBainun ptbupsi

Hosseini, A. & Faghihian, H. (2019). Application of FSM-16 impregnated by TiO_2 as an efficient photocatalyst for elimination of benzothiophene and dibenzothiophene, adsorptive removal of degradation products by MCM-41. *Journal of Industrial and Engineering Chemistry*, *76*, 122-132.

Hosseini, A., Faghihian, H. & Sanati, A. M. (2018). Elimination of dibenzothiophene from transportation fuel by combined photocatalytic and adsorptive method. *Materials Science in Semiconductor Processing*, *87*, 110-118.

Huang, Z., Sun, Q., Lv, K., Zhang, Z., Li, M. & Li, B. (2015). Effect of contact interface between TiO_2 and g-C_3N_4 on the photoreactivity of g-C_3N_4/TiO_2 photocatalyst: (0 0 1) vs (1 0 1) facets of TiO_2. *Applied Catalysis B: Environmental*, *164*, 420-427.

Humayun, M., Raziq, F., Khan, A. & Luo, W. (2018). Modification strategies of TiO_2 for potential applications in photocatalysis: a critical review. *Green Chemistry Letters and Reviews*, *11*(2), 86-102.

Huu, H. T., Thi, M. D. N., Nguyen, V. P., Thi, L. N., Phan, T. T. T., Hoang, Q. D., et al. (2021). One-pot synthesis of S-scheme MoS_2/g-C_3N_4 heterojunction as effective visible light photocatalyst. *Scientific Reports*, *11*(1), 1-12.

Isari, A. A., Payan, A., Fattahi, M., Jorfi, S. & Kakavandi, B. (2018). Photocatalytic degradation of Rhodamine B and Real Textile Wastewater using Fe-Doped TiO_2 anchored on Reduced Graphene Oxide (Fe-TiO_2/rGO): Characterization and feasibility, mechanism and pathway studies. *Applied Surface Science*, *462*, 549-564.

Jaafar, N. F., Jalil, A. A. & Triwahyono, S. (2017). Visible-light photoactivity of plasmonic silver supported on Mesoporous TiO_2 Nanoparticles (Ag-MTN) for enhanced degradation of 2-chlorophenol: Limitation of Ag-Ti interaction. *Applied Surface Science*, *392*, 1068-1077.

Jaafar, N. F., Jalil, A. A., Triwahyono, S. & Shamsuddin, N. (2015). New insights into self-modification of mesoporous titania nanoparticles for enhanced photoactivity: effect of microwave power density on formation of oxygen vacancies and Ti^{3+} defects. *RSC Advances*, *5*(110), 90991–91000.

05-4506832 pustaka.upsi.edu.my Perpustakaan Tuanku Bainun Kampus Sultan Abdul Jalil Shah PustakaTBainun ptbupsi

05-4506832 pustaka.upsi.edu.my Perpustakaan Tuanku Bainun Kampus Sultan Abdul Jalil Shah PustakaTBainun ptbupsi

Jiang, H., Liu, J., Li, M., Tian, L., Ding, G., hen, P., et al. (2 18). Facile synthesis of - decorated Fe, N co-doped TiO_2 with enhanced visible-light photocatalytic activity by a novel co-precursor method. *Chinese Journal of Catalysis*, *39*(4), 747-759.

Kalantari, K., Kalbasi, M., Sohrabi, M. & Royaee, S. J. (2016). Synthesis and characterization of N-doped TiO_2 nanoparticles and their application in photocatalytic oxidation of dibenzothiophene under visible light. *Ceramics International*, *42*(13), 14834-14842.

Kalantari, K., Kalbasi, M., Sohrabi, M. & Royaee, S. J. (2017). Enhancing the photocatalytic oxidation of dibenzothiophene using visible light responsive Fe and N co-doped TiO_2 nanoparticles. *Ceramics International*, *43*(1), 973-981.

Kamal, S., Balu, S., Palanisamy, S., Uma, K., Velusamy, V. & Yang, T. C. (2019). Synthesis of boron doped $C_3N_4/NiFe_2O_4$ nanocomposite: An enhanced visible light photocatalyst for the degradation of methylene blue. *Results in Physics*, *12*, 1238-1244.

05-4506832 pustaka.upsi.edu.my Perpustakaan Tuanku Bainun Kampus Sultan Abdul Jalil Shah PustakaTBainun ptbupsi

Kamble, R., Mahajan, S., Puri, V., Shinde, H. & Garadkar, K. (2018). Visible light-driven high photocatalytic activity of Cu-doped TiO_2 nanoparticles synthesized by hydrothermal method . *Material Science Research India*, *15*(3), 197-208.

Kang, M., Wang, X., Zhang, J., Lu, Y., Chen, X., Yang, L., et al. (2019). Boosting the photocatalytic oxidative desulfurization of dibenzothiophene by decoration of MWO_4 (M=Cu, Zn, Ni) on WO_3. *Journal of Environmental Chemical Engineering*, *7*(1), 1-36.

Karasek, F. W. & Clement, R. E. (2012). *Basic gas chromatography-mass spectrometry: principles and techniques.* Canada: Elsevier.

Kaur, N., Verma, A., Thakur, I. & Basu, S. (2021). In-situ dual effect of Ag-Fe-TiO_2 composite for the photocatalytic degradation of Ciprofloxacin in aqueous solution. *Chemosphere*, *276*, 1-9.

05-4506832 pustaka.upsi.edu.my Perpustakaan Tuanku Bainun Kampus Sultan Abdul Jalil Shah PustakaTBainun ptbupsi

05-4506832 pustaka.upsi.edu.my Perpustakaan Tuanku Bainun Kampus Sultan Abdul Jalil Shah PustakaTBainun ptbupsi

Kesarla, M. K., Fuentez-Torres, M. O., Alcudia-Ramos, M. A., Ortiz-Chi, F., Espinosa-Gonzalez, C. G., Aleman, M., et al. (2018). Article Synthesis of g-C_3N_4/N-doped CeO_2 composite for photocatalytic degradation of an herbicide. *Journal of Materials Research and Technology*, *8*(2), 1-8.

Keynejad, K., Nikazar, M. & Dabir, B. (2017). Diesel desulfurization using a UV-photocatalytic process. *Petroleum Science and Technology*, *35*(9), 813-819.

Khaki, M. R. D., Shafeeyan, M. S., Raman, A. A. A. & Daud, W. M. A. W. (2017). Application of doped photocatalysts for organic pollutant degradation- A review. *Journal of Environmental Management*, *198*, 78-94.

Khalid, N. R., Majid, A., Tahir, M. B., Niaz, N. A. & Khalid, S. (2017). Carbonaceous-TiO_2 nanomaterials for photocatalytic degradation of pollutants: A review. *Ceramics International*, *43*(17), 14552-14571.

Khan, H. & Berk, D. (2014). Characterization and mechanistic study of Mo^{+6} and V^{+5} codoped TiO_2 as a photocatalyst. *Journal of Photochemistry and Photobiology A: Chemistry*, *294*, 96-109.

Khayyat, S. & Roselin, L. S. (2017). Photocatalytic degradation of Benzothiophene and Dibenzothiophene using Supported Gold Nanoparticle. *Journal of Saudi Chemical Society*, *21*(3), 349-357.

Komaraiah, D., Radha, E., Kalarikkal, N., Sivakumar, J., Reddy, M. R. & Sayanna, R. (2019). Structural, optical and photoluminescence studies of sol-gel synthesized pure and iron doped TiO_2 photocatalysts. *Ceramics International*, *45*(18), 25060-25068.

Kumar, A. & Pandey, G. (2018). Different methods used for the synthesis of TiO_2 based nanomaterials: A review. *American Journal of Nano Research and Applications*, *6*(1), 1-10.

Lakshmanareddy, N., Rao, V. N., Cheralathan, K. K., Subramaniam, E. P. & Shankar, M. V. (2019). Pt/TiO_2 nanotube photocatalyst – Effect of synthesis methods on valance state of Pt and its influence on hydrogen production and dye degradation. *Journal of Colloid and Interface Science*, *538*, 83-98.

05-4506832 pustaka.upsi.edu.my Perpustakaan Tuanku Bainun Kampus Sultan Abdul Jalil Shah PustakaTBainun ptbupsi

05-4506832 pustaka.upsi.edu.my Perpustakaan Tuanku Bainun Kampus Sultan Abdul Jalil Shah PustakaTBainun ptbupsi

Lavand, A. B., Bhatu, M. N. & Malghe, Y. S. (2019). Visible light photocatalytic degradation of malachite green using modified titania. *Journal of Materials Research and Technology*, *8*(1), 299-308.

Lei, J., Chen, Y., Shen, F., Wang, L., Liu, Y. & Zhang, J. (2015). Surface modification of TiO_2 with g-C_3N_4 for enhanced UV and visible photocatalytic activity. *Journal of Alloys and Compounds*, *631*, 328-334.

Leng, K., Sun, Y., Zhang, X., Yu, M. & Xu, W. (2016). Ti-modified hierarchical mordenite as highly active catalyst for oxidative desulfurization of dibenzothiophene. *Fuel*, *174*, 9-16.

Li, Y., Liu, C., Xu, P., Li, M., Zen, M. & Tang, S. (2014). Controlled fabrication of ordered mesoporous titania / carbon fiber composites with high photoactivity: synergistic relationship between surface adsorption and photocatalysis. *Chemical Engineering Journal*, *243*, 108-116.

Li, X., Zhang, Z., Yao, C., Lu, X., Zhao, X. & Ni, C. (2016). Attapulgite-CeO_2/MoS_2 ternary nanocomposite for photocatalytic oxidative desulfurization. *Applied Surface Science*, *364*, 589-596.

Li, D., Song, H., Meng, X., Shen, T., Sun, J., Han, W., et al. (2020). Effect of particle size on the structure and photocatalytic performance by alkali-treated TiO_2. *Nanomaterials*, *10*(3), 546-560.

Li, C., Sun, Z., Xue, Y., Yao, G. & Zheng, S. (2016). A facile synthesis of g-C_3N_4/TiO_2 hybrid photocatalysts by sol–gel method and its enhanced photodegradation towards methylene blue under visible light . *Advanced Powder Technology*, *27*(2), 330–337.

Li, J. J., Xiao, H., Tang, X. D. & Zhou, M. (2016). Green carboxylic acid-based deep eutectic solvents as solvents for the extractive desulfurization. *Energy Fuels*, *30*(7), 5411-5418.

Li, J., Yang, D. & Zhu, X. (2017). Effects of aging time and annealing temperature on structural and optical properties of sol-gel ZnO thin films. *Aip Advances*, *7*(6), 65-70.

05-4506832 pustaka.upsi.edu.my Perpustakaan Tuanku Bainun Kampus Sultan Abdul Jalil Shah PustakaTBainun ptbupsi

05-4506832 pustaka.upsi.edu.my Perpustakaan Tuanku Bainun Kampus Sultan Abdul Jalil Shah PustakaTBainun ptbupsi

Lin, H. & Zhao, L. (2019). Novel g-C_3N_4/TiO_2 nanorods with enhanced photocatalytic activity for water treatment and H_2 production. *Journal of Materials Science: Materials in Electronics*, *30*(19), 18191–18199.

Liu, D., Lu, C. & Wu, J. (2018). CuO/g-C_3N_4 nanocomposite for elemental mercury capture at low temperature. *Journal of Nanoparticle Research*, *20*(10), 1-11.

Lu, X., Li, X., Chen, F., Chen, Z., Qian, J. & Zhang, Q. (2020). Biotemplating synthesis of N-doped two-dimensional CeO_2-TiO_2 nanosheets with enhanced visible light photocatalytic desulfurization performance. *Journal of Alloys and Compounds*, *815*, 1-11.

Lu, X., Chen, F., Qian, J., Fu, M., Jiang, Q. & Zhang, Q. (2021). Facile fabrication of CeF_3/g-C_3N_4 heterojunction photocatalysts with upconversion properties for enhanced photocatalytic desulfurization performance. *Journal of Rare Earths*, *39*(10), 1204-1210.

Lu, H., Deng, C., Ren, W. & Yang, X. (2014). Oxidative desulfurization of model diesel using $[(C_4H_9)_4N]_6Mo_7O_{24}$ as a catalyst in ionic liquids. *Fuel Processing Technology*, *119*, 87-91.

Lutic, D., Petrovschi, D., Ignat, M., Cretescu, I. & Bulai, G. (2016). Mesoporous cerium-doped titania for the photocatalytic removal of persistent dyes. *Catalysis Today*, *306*, 300-309.

Ma, R., Guo, J., Wang, D., He, M., Xun, S., Gu, J., et al. (2019). Preparation of highly dispersed WO_3/few layer g-C_3N_4 and its enhancement of catalytic oxidative desulfurization activity. *Colloids and Surfaces A*, *572*, 250-258.

Ma, J., He, H. & Liu, F. (2015). Effect of Fe on the photocatalytic removal of NOx over visible light responsive Fe/TiO_2 catalysts. *Applied Catalysis B: Environmental*, *179*, 21-28.

05-4506832 pustaka.upsi.edu.my Perpustakaan Tuanku Bainun Kampus Sultan Abdul Jalil Shah PustakaTBainun ptbupsi

05-4506832 pustaka.upsi.edu.my Perpustakaan Tuanku Bainun Kampus Sultan Abdul Jalil Shah PustakaTBainun ptbupsi

Maeda, K., An, D., Kuriki, R., Lu, D. & Ishitani, O. (2018). Graphitic carbon nitride prepared from urea as a photocatalyst for visible-light carbon dioxide reduction with the aid of a mononuclear ruthenium (II) complex. *Beilstein Journal of Organic Chemistry*, *14*(1), 1806-1812.

Mandizadeh, S., Salavati-Niasari, M. & Sadri, M. (2017). Hydrothermal synthesis, characterization and magnetic properties of $BaFe_2O_4$ nanostructure as a photocatalytic oxidative desulfurization of dibenzothiophene. *Separation and Purification Technology*, *175*, 399-405.

Mani, S. S., Rajendran, S., Nalajala, N., Mathew, T. & Gopinath, C. S. (2021). Electronically integrated mesoporous Ag–TiO_2 nanocomposite thin films for efficient solar hydrogen production in direct sunlight. *Energy Technology*, *10*(1), 1-12.

Mao, N. (2019). Investigating the Heteronjunction between ZnO/Fe_2O_3 and g-C_3N_4 for an Enhanced Photocatalytic H_2 production under visible-light irradiation. *Scientific reports*, *9*(1), 1-9.
05-4506832 pustaka.upsi.edu.my Perpustakaan Tuanku Bainun Kampus Sultan Abdul Jalil Shah PustakaTBainun ptbupsi
Marami, M. B., Farahmandjou, M. & Khoshnevisan, B. (2018). Sol–gel synthesis of Fe-doped TiO_2 nanocrystals. *Journal of electronic Materials*, *47*(7), 3741-3748.

Marfur, N. A., Jaafar, N. F. & Habibullah, N. H. H. M. (2019). Electrogenerated iron supported on mesoporous titania nanoparticles for the photocatalytic degradation of 2-chlorophenol. *Comptes Rendus Chimie*, *22*(11-12), 813-821.

Meriem-Benziane, M., Bou-Said, B. & Boudouani, N. (2017). The effect of crude oil in the pipeline corrosion by the naphthenic acid and the sulfur: A numerical approach. *Journal of Petroleum Science and Engineering*, *158*, 672-679.

Miao, G., Huang, D., Ren, X., Li, X., Li, Z. & Xiao, J. (2016). Visible-light induced photocatalytic oxidative desulfurization using $BiVO_4/C_3N_4@SiO_2$ with air/cumene hydroperoxide under ambient conditions. *Applied Catalysis B: Environmental*, *192*, 72-79.
05-4506832 pustaka.upsi.edu.my Perpustakaan Tuanku Bainun Kampus Sultan Abdul Jalil Shah PustakaTBainun ptbupsi

05-4506832 pustaka.upsi.edu.my Perpustakaan Tuanku Bainun Kampus Sultan Abdul Jalil Shah PustakaTBainun ptbupsi

Mironyuk, I., Danyliuk, N., Tatarchuk, T., Mykytyn, I. & Kotsyubynsky, V. (2021). Photocatalytic degradation of Congo red dye using Fe-doped TiO_2 nanocatalysts. *Physics and Chemistry of Solid State*, *22*(4), 697-710.

Mohamed, M. A., Salleh, W. N. W., Jaafar, J., Rosmi, M. S., Hir, Z. A. M., Abd Mutalib, M., et al. (2017). Carbon as amorphous shell and interstitial dopant in mesoporous rutile TiO_2: Bio-template assisted sol-gel synthesis and photocatalytic activity. *Applied Surface Science*, *393,* 46-59.

Mohamed, M. A., Jaafar, J., Ismail, A. F., Othman, M. H. D. & Rahman, M. A. (2017). Fourier Transform Infrared (FTIR) Spectroscopy. *Membrane Characterization*, 3-29.

Mohseni-Salehi, M. S., Taheri-Nassaj, E. & Hosseini-Zori, M. (2018). Effect of dopant (Co, Ni) concentration and hydroxyapatite compositing on photocatalytic activity of titania towards dye degradation. *Journal of Photochemistry and Photobiology A: Chemistry*, *356*, 57-70.

Moradi, H., Eshaghi, A., Hosseini, S. R. & Ghani, K. (2016). Fabrication of Fe-doped TiO_2 nanoparticles and investigation of photocatalytic decolorization of reactive red 198 under visible light irradiation. *Ultrasonics Sonochemistry*, *32*, 314-319.

Mostafa, M. M., El saied, M. & Morshedy, A. S. (2019). Novel Calcium Carbonate-titania nanocomposites for enhanced sun light photo catalytic desulfurization process. *Journal of Environmental Management*, *250*, 1-9.

Nasirian, M., Lin, Y. P., Bustillo-Lecompte, C. F. & Mehrvar, M. (2018). Enhancement of photocatalytic activity of titanium dioxide using non-metal doping methods under visible light: a review. *International Journal of Environmental Science and Technology*, *15*(9), 2009-2032.

Nasr, M., Viter, R., Eid, C., Habchi, R., Miele, P. & Bechelany, M. (2017). Enhanced photocatalytic performance of novel electrospun BN/TiO_2 composite nanofibers. *New Journal of Chemistry*, *41*(1), 81-89.

Nasr, M., Eid, C., Habchi, R., Miele, P. & Bechelany, M. (2018). Recent Progress on Titanium Dioxide Nanomaterials for Photocatalytic Applications. *ChemSusChem*, *11*(18), 3023 – 3047.

05-4506832 pustaka.upsi.edu.my Perpustakaan Tuanku Bainun Kampus Sultan Abdul Jalil Shah PustakaTBainun ptbupsi

05-4506832 pustaka.upsi.edu.my Perpustakaan Tuanku Bainun Kampus Sultan Abdul Jalil Shah PustakaTBainun ptbupsi

Niessen, W. M. (2001). *Current practice of gas chromatography-mass spectrometry.* USA: CRC Press.

Niu, B., Wang, X., Wu, K., He, X. & Zhang, R. (2018). Mesoporous titanium dioxide: synthesis and applications in photocatalysis, energy and biology. *Materials*, *11*(10), 1-23.

Noor, N. A. M., Sidik, S. M., Rosmi, M. S., Hitam, C. N. C. & Jaafar, N. F. (2022). Advancement of TiO_2-based photocatalyst for photodegradation of organic pollutants in wastewater. *Central Asia & the Caucasus*, *23*(1), 2021-2049.

Ong, C. B., Ng, L. Y. & Mohammad, A. W. (2018). A review of ZnO nanoparticles as solar photocatalysts: Synthesis, mechanisms and applications. *Renewable and Sustainable Energy Reviews*, *81*, 536-551.

Ovodok, E., Maltanava, H., Poznyak, S., Ivanovskaya, M., Kudlash, A., Scharnagl, N., et al. (2017). Synthesis and characterization of efficient TiO_2 mesoporous photocatalysts. *Materials Today: Proceedings*, *4*(11), 11526-11533.
05-4506832 pustaka.upsi.edu.my Perpustakaan Tuanku Bainun Kampus Sultan Abdul Jalil Shah PustakaTBainun ptbupsi
Parangi, T. & Mishra, M. K. (2019). Titania nanoparticles as modified photocatalysts: A review on design and development. *Comments on Inorganic Chemistry*, *39*(2), 90-126.

Perkowitz, S. (2012). *Optical characterization of semiconductors: infrared, Raman, and photoluminescence spectroscopy.* USA: Elsevier.

Petronella, F., Truppi, A., Ingrosso, C., Placido, T., Striccoli, M., Curri, M. L., et al. (2017). Nanocomposite materials for photocatalytic degradation of pollutants. *Catalysis Today*, *281*, 85-100.

Petronella, F., Truppi, A., Dell'Edera, M., Agostiano, A., Curri, M. L. & Comparelli, R. (2019). Scalable synthesis of mesoporous TiO_2 for environmental photocatalytic applications. *Materials*, *12*(11), 1-21.
05-4506832 pustaka.upsi.edu.my Perpustakaan Tuanku Bainun Kampus Sultan Abdul Jalil Shah PustakaTBainun ptbupsi

05-4506832 pustaka.upsi.edu.my Perpustakaan Tuanku Bainun Kampus Sultan Abdul Jalil Shah PustakaTBainun ptbupsi

Pham, X. N., Nguyen, B. M., Thi, H. T. & Doan, H. V. (2018). Synthesis of Ag-AgBr/Al-MCM-41 nanocomposite and its application in photocatalytic oxidative desulfurization of dibenzothiophene. *Advanced Powder Technology*, *29*(8), 1827-1837.

Pham, X. N., Pham, T. D., Nguyen, B. M., Tran, H. T. & Pham, D. T. (2018). Synthesis of Al-MCM-41@Ag/TiO_2 nanocomposite and its photocatalytic activity for degradation of dibenzothiophene. *Journal of Chemistry*, *2018*, 1-10.

Piumetti, M., Freyria, F. S., Armandi, M., Geobaldo, F., Garrone, E. & Bonelli, B. (2014). Fe- and V-doped mesoporous titania prepared by direct synthesis: Characterization and role in the oxidation of AO7 by H_2O_2 in the dark. *Catalysis Today*, *227*, 71-79.

Pradubkorn, P., Maensiri, S., Swatsitang, E. & Laokul, P. (2020). Preparation and characterization of hollow TiO_2 nanospheres: The effect of Fe^{3+} doping on their microstructure and electronic structure. *Current Applied Physics*, *20*(1), 178-185.

05-4506832 pustaka.upsi.edu.my Perpustakaan Tuanku Bainun Kampus Sultan Abdul Jalil Shah PustakaTBainun ptbupsi

Prakash, K., Kumar, J. V., Latha, P., Kumar, P. S. & Karuthapandian, S. (2019). Fruitful fabrication of CDs on GO/g-C_3N_4 sheets layers: A carbon amalgamation for the remediation of carcinogenic pollutants. *Journal of Photochemistry and Photobiology A: Chemistry*, *370*, 94-104.

Puri, S., Thakur, I., Verma, A. & Barman, S. (2021). Degradation of pharmaceutical drug paracetamol via UV irradiation using Fe-TiO_2 composite photocatalyst: statistical analysis and parametric optimization. *Environmental science and pollution research*, *28*(34), 47327-47341.

Rahdar, A., Aliahmad, M. & Azizi, Y. (2015). NiO Nanoparticles: Synthesis and characterization. *Journal of Nanostructures*, *5*(2), 145-151.

Raziq, F., Li, C., Humayun, M., Qu, Y., Zada, A., Yu, H., et al. (2015). Synthesis of TiO_2/g-C_3N_4 nanocomposites as efficient photocatalysts dependent on the enhanced photogenerated charge separation. *Materials Research Bulletin*, *70*, 494–499.

05-4506832 pustaka.upsi.edu.my Perpustakaan Tuanku Bainun Kampus Sultan Abdul Jalil Shah PustakaTBainun ptbupsi

05-4506832 pustaka.upsi.edu.my Perpustakaan Tuanku Bainun Kampus Sultan Abdul Jalil Shah PustakaTBainun ptbupsi

Reddy, P. A. K., Reddy, P. V. L., Kwon, E., Kim, K. H., Akter, T. & Kalagara, S. (2016). Recent advances in photocatalytic treatment of pollutants in aqueous media. *Environment International*, *91*, 94-103.

Reddy, P. V. L., Kavitha, B., Reddy, P. A. K. & Kim, K. H. (2017). TiO_2-based photocatalytic disinfection of microbes in aqueous media: A review. *Environmental Research*, *154*, 296-303.

Reddy, B. P., Rajendar, V., Shekar, M. C. & Park, S. H. (2018). Particle size effects on the photocatalytic activity of $BiFeO_3$ particles. *Digest Journal of Nanomaterials and Biostructures*, *13*(1), 87 - 95.

Retamoso, C., Escalona, N., Gonzalez, M., Barrientos, L., Allende-Gonzalez, P., Stancovich, S., et al. (2019). Effect of particle size on the photocatalytic activity of modified rutile sand (TiO_2) for the discoloration of methylene blue in water. *Journal of Photochemistry and Photobiology A: Chemistry*, *378*, 136-141.

Ribao, P., Corredor, J., Rivero, M. J. & Ortiz, I. (2019). Role of reactive oxygen species on the activity of noble metal-doped TiO_2 photocatalysts. *Journal of Hazardous Materials*, *372*, 45-51.

Rodriguez, P. A. O., Pecchi, G. A., Casuscelli, S. G., Elias, V. R. & Eimer, G. A. (2019). A simple synthesis way to obtain iron-doped TiO_2 nanoparticles as photocatalytic surfaces. *Chemical Physics Letters*, *732*, 1-6.

Sadanandam, G., Zhang, L. & Scurrell, M. S. (2018). Enhanced photocatalytic hydrogen formation over Fe-loaded TiO_2 and g-C_3N_4 composites from mixed glycerol and water by solar irradiation. *Journal of Renewable and Sustainable Energy*, *10*(3), 30-42.

Saha, D., Desipio, M. M., Hoinkis, T. J., Smeltz, E. J., Thorpe, R., Hensley, D. K., et al. (2018). Influence of hydrogen peroxide in enhancing photocatalytic activity of carbon nitride under visible light: An insight into reaction intermediates. *Journal of Environmental Chemical Engineering*, *6*(4), 4927-4936.

Samet, L., March, K., Brun, N., Hosni, F., Stephan, O. & Chtourou, R. (2018). Effect of gamma radiation on the photocatalytic properties of Cu doped titania nanoparticles. *Materials Research Bulletin*, *107*, 1-7.

05-4506832 pustaka.upsi.edu.my Perpustakaan Tuanku Bainun Kampus Sultan Abdul Jalil Shah PustakaTBainun ptbupsi

05-4506832 pustaka.upsi.edu.my Perpustakaan Tuanku Bainun Kampus Sultan Abdul Jalil Shah PustakaTBainun ptbupsi

Saravanan, R., Khan, M. M., Gupta, V. K., Mosquera, E., Gracia, F., Narayanan, V., et al. (2015). ZnO/Ag/CdO nanocomposite for visible light-induced photocatalytic degradation of industrial textile effluents. *Journal of Colloid and Interface Science*, *452*, 126-133.

Saravanan, R., Gracia, F. & Stephen, A. (2017). Basic principles, mechanism, and challenges of photocatalysis. *Nanocomposites for Visible Light-induced Photocatalysis*, 19-40.

Sescu, A. M., Favier, L., Lutic, D., Soto-Donoso, N., Ciobanu, G. & Harja, M. (2021). TiO_2 doped with noble metals as an efficient solution for the photodegradation of hazardous organic water pollutants at ambient conditions. *Water*, *13*(1), 1-18.

Shafei, A. & Sheibani, S. (2019). Visible light photocatalytic activity of Cu doped TiO_2-CNT nanocomposite powder prepared by sol-gel method. *Materials Research Bulletin*, *110*, 198-206.

Shayegan, Z., Lee, C. S. & Haghighat, F. (2018). TiO_2 photocatalyst for removal of volatile organic compounds in gas phase-A review. *Chemical Engineering Journal*, *334*, 2408-2439.

Singh, D., Chopra, A., Mahendra, P. K., Kagdiyal, V. & Saxena, D. (2016). Sulfur compounds in the fuel range fractions from different crude oils. *Petroleum Science and Technology*, *34*(14), 1248-1254.

Sinha, P., Datar, A., Jeong, C., Deng, X., Chung, Y. G. & Lin, L. C. (2019). Surface area determination of porous materials using the Brunauer−Emmett−Teller (BET) method: Limitations and improvements. *The Journal of Physical Chemistry*, *123*(33), 20195-20209.

Skoog, D. A., Holler, F. J. & Crouch, S. R. (2016). *Principles of Instrumental Analysis.* USA: Cengage Learning.

Sood, S., Umar, A., Mehta, S. K. & Kansal, S. K. (2015). Highly effective Fe-doped TiO_2 nanoparticles photocatalysts for visible-light driven photocatalytic degradation of toxic organic compounds. *Journal of Colloid and Interface Science*, *450*, 213-223.

05-4506832 pustaka.upsi.edu.my Perpustakaan Tuanku Bainun Kampus Sultan Abdul Jalil Shah PustakaTBainun ptbupsi

05-4506832 pustaka.upsi.edu.my Perpustakaan Tuanku Bainun Kampus Sultan Abdul Jalil Shah PustakaTBainun ptbupsi

Subramaniam, M. N., Goh, P. S., Abdullah, N., Lau, W. J., Ng, B. C. & Ismail, A. F. (2017). Adsorption and photocatalytic degradation of methylene blue using high surface area titanate nanotubes (TNT) synthesized via hydrothermal method. *Journal of Nanoparticle Research*, *19*, 1-13.

Sun, H., Dong, B., Song, L., Du, J., Gao, R., Su, G., et al. (2017). High photodegradation ability of dyes by Fe(III)-tartrate/TiO_2 nanotubular photocatalyst supported via photo-Fenton reaction. *Journal of Photochemistry and Photobiology A: Chemistry*, *334*, 20-25.

Sun, B., Yu, X., Wang, L., Feng, L. J. & Li, C. H. (2016). Enhanced visible light photocatalytic oxidative desulfurization by BiOBr-graphene composite. *Journal of Fuel Chemistry and Technology*, *44*(9), 1074-1081.

Szczepanik, B. (2017). Photocatalytic degradation of organic contaminants over clay-TiO_2 nanocomposites: A review. *Applied Clay Science*, *141*, 227–239.

Torrent, J. O. S. E. & Barrón, V. (2008). Diffuse reflectance spectroscopy. *Methods of Soil Analysis Part 5—Mineralogical Methods*, *5*, 367-385.

Verma, A., Kar, M. & Agnihotry, S. A. (2007). Aging effect of diethanolamine stabilized sol on different properties of TiO_2 films: Electrochromic applications. *Solar energy materials and solar cells*, *91*(14), 1305-1312.

Wang, X. J., Li, F. T., Liu, J. X., Kou, C. G., Zhao, Y., Hao, Y., et al. (2012). Preparation of TiO_2 in Ionic Liquid via Microwave Radiation and in Situ Photocatalytic Oxidative Desulfurization of Diesel Oil. *Energy & Fuels*, *26*(11), 6777−6782.

Wang, C., Zhu, W., Xu, Y., Xu, H., Zhang, M., Chao, Y., et al. (2014). Preparation of TiO_2/g-C_3N_4 composites and their application in photocatalytic oxidative desulfurization. *Ceramics International*, *40*(8), 11627-11635.

Wei, H., McMaster, W. A., Tan, J. Z., Cao, L., Chen, D. & Caruso, R. A. (2017). Mesoporous TiO_2/g-C_3N_4 microspheres with enhanced visible-light photocatalytic activity. *The Journal of Physical Chemistry C*, *121*(40), 22114-22122.

05-4506832 pustaka.upsi.edu.my Perpustakaan Tuanku Bainun Kampus Sultan Abdul Jalil Shah PustakaTBainun ptbupsi

05-4506832 pustaka.upsi.edu.my Perpustakaan Tuanku Bainun Kampus Sultan Abdul Jalil Shah PustakaTBainun ptbupsi

Wu, Z., Chen, X., Liu, X., Yang, X. & Yang, Y. (2019). A ternary magnetic recyclable $ZnO/Fe_3O_4/g\text{-}C_3N_4$ composite photocatalyst for efficient photodegradation of monoazo dye. *Nanoscale research letters*, *14*(1), 1-14.

Wu, J., Li, J., Liu, J., Bai, J. & Yang, L. (2017). A novel Nb_2O_5/Bi_2WO_6 heterojunction photocatalytic oxidative desulfurization catalyst with high visible light-induced photocatalytic activity. *RSC Advances*, *7*(81), 51046-51054.

Xu, J., Zhang, T. & Zhang, J. (2020). Photocatalytic degradation of methylene blue with spent FCC catalyst loaded with ferric oxide and titanium dioxide. *Scientific Reports*, *10*(1), 1-10.

Xue, X., Ji, W., Mao, Z., Mao, H., Wang, Y., Wang, X., et al. (2012). Raman investigation of nanosized TiO_2: Effect of crystallite size and quantum confinement. *The Journal of Physical Chemistry C*, *116*(15), 8792-8797.

Yang, H., Han, C. & Xue, X. (2014). Photocatalytic activity of Fe-doped $CaTiO_3$ under UV–visible light. *Journal of Environmental Sciences*, *26*(7), 1489-1495.

05-4506832 pustaka.upsi.edu.my Perpustakaan Tuanku Bainun Kampus Sultan Abdul Jalil Shah PustakaTBainun ptbupsi

Yazici, M., Comakli, O., Yetim, T., Yetim, A. F. & Celik, A. (2016). Effect of sol aging time on the wear properties of $TiO_2 – SiO_2$ composite films prepared by a sol-gel method. *Tribiology International*, *104*, 175-182.

Yu, F., Liu, C., Yuan, B., Xie, P., Xie, C. & Yu, S. (2016). Energy-efficient extractive desulfurization of gasoline by polyether-based ionic liquids. *Fuel*, *177*, 39-45.

Yu, J. H., Nam, S. H., Lee, J. W., Kim, D. I. & Boo, J. H. (2018). Oxidation state and structural studies of vanadium-doped titania particles for the visible light-driven photocatalytic activity. *Applied Surface Science*, *472*, 46-53.

Zaid, H., Kait, C. & Mutalib, M. (2016). Preparation and characterization of Cu-Fe/TiO_2 photocatalyst for visible light deep desulfurization. *Malaysian Journal of Analytical Sciences*, *20*(4), 713-725.

Zarrabi, M., Entezari, M. H. & Goharshadi, E. K. (2015). Photocatalytic oxidative desulfurization of dibenzothiophene by C/TiO_2@MCM-41 nanoparticles under visible light and mild conditions. *RSC Advances*, *5*(44), 34652-34662.

05-4506832 pustaka.upsi.edu.my Perpustakaan Tuanku Bainun Kampus Sultan Abdul Jalil Shah PustakaTBainun ptbupsi

05-4506832 pustaka.upsi.edu.my Perpustakaan Tuanku Bainun Kampus Sultan Abdul Jalil Shah PustakaTBainun ptbupsi

Zeelani, G. G., Ashrafi, A., Dhakad, A., Gupta, G. & Pal, S. L. (2016). Catalytic Oxidative desulfurization of liquid fuels: A review. *International Research Journal of Engineering and Technology*, *3*(5), 331-336.

Zeng, G., Zhang, Q., Liu, Y., Zhang, S. & Guo, J. (2019). Preparation of TiO_2 and Fe-TiO_2 with an impinging stream-rotating packed bed by the precipitation method for the photodegradation of gaseous toluene. *Nanomaterials*, *9*(8), 1-17.

Zhang, F., Cheng, Z., Kang, L., Cui, L., Liu, W., Xu, X., et al. (2015). A novel preparation of Ag-doped TiO_2 nanofibers with enhanced stability of photocatalytic activity. *RSC Advances*, *5*(41), 32088-32091.

Zhang, L., Zhang, Q., Xie, H., Guo, J., Lyu, H., Li, Y., et al. (2017). Electrospun titania nanofibers segregated by graphene oxide for improved visible light photocatalysis. *Applied Catalysis B: Environmental*, *201*, 470-478.

Zhang, Y., Hu, H., Chang, M., Chen, D., Zhang, M., Wu, L., et al. (2017). Non-uniform doping outperforms uniform doping for enhancing the photocatalytic efficiency of Au-doped TiO_2 nanotubes in organic dye degradation. *Ceramics International*, *43*(12), 9053-9059.

Zhang, Z., Li, X., Chen, H., Shao, G., Zhang, R. & Lu, H. (2018). Synthesis and properties of Ag/ZnO/g-C_3N_4 ternary micro/nano composites by microwave-assisted method. *Materials Research Express*, *5*(1), 15-21.

Zhang, W., Tian, Y., He, H., Xu, L., Li, W. & Zhao, D. (2020). Recent advances in the synthesis of hierarchically mesoporous TiO_2 materials for energy and environmental applications. *National Science Review*, *7*(11), 1–24.

Zhao, H. & Baker, G. A. (2015). Oxidative desulfurization of fuels using ionic liquids: A review. *Frontiers of Chemical Science and Engineering*, *9*(3), 262-279.

Zhao, D., Zhang, J., Wang, J., Liang, W. & Li, H. (2009). Photocatalytic oxidation desulfurization of diesel oil using Ti-containing Zeolite. *Petroleum Science and Technology*, *27*(1), 1-11.

05-4506832 pustaka.upsi.edu.my Perpustakaan Tuanku Bainun Kampus Sultan Abdul Jalil Shah PustakaTBainun ptbupsi

05-4506832 pustaka.upsi.edu.my Perpustakaan Tuanku Bainun Kampus Sultan Abdul Jalil Shah PustakaTBainun ptbupsi

Zhiming, S., Rui, M., Xiyu, Z., Lina, W. & Xiaohuan, W. (2017). Effects of pre-annealing atmosphere on microstructure and photocatalytic activities of Fe-doped titania nanotubes. *Rare Metal Materials and Engineering*, *46*(11), 3244-3252.

Zhou, D., Chen, Z., Yang, Q., Dong, X., Zhang, J. & Qin, L. (2016). In-situ construction of all-solid-state Z-scheme g-C_3N_4/TiO_2 nanotube arrays photocatalyst with enhanced visible-light-induced properties. *Solar Energy Materials and Solar Cells*, *157*, 399-405.

Zhu, W., Xu, Y., Li, H., Dai, B., Xu, H., Wang, C., et al. (2014). Photocatalytic oxidative desulfurization of dibenzothiophene catalyzed by amorphous TiO_2 in ionic liquid. *Korean Journal of Chemical Engineering*, *31*(2), 211-217.

Zhu, Y., Li, X. & Zhu, M. (2016). Mesoporous graphitic carbon nitride as photo-catalyst for oxidative desulfurization with oxygen. *Catalysis Communications*, *85*, 5-8.

Zhu, Z., Murugananthan, M., Gu, J. & Zhang, Y. (2018). Fabrication of a Z-scheme g-C_3N_4/Fe-TiO_2 photocatalytic composite with enhanced photocatalytic activity under visible light irradiation. *Catalysts*, *8*(3), 1-16.

Zieba, M., Wojtasik, K., Tyszkiewicz, C., Gondek, E., Niziol, J., Suchanek, K., et al. (2021). High refractive index silica-titania films fabricated via the sol–gel method and dip-coating technique—physical and chemical characterization. *Materials*, *14*(23), 7125-7129.

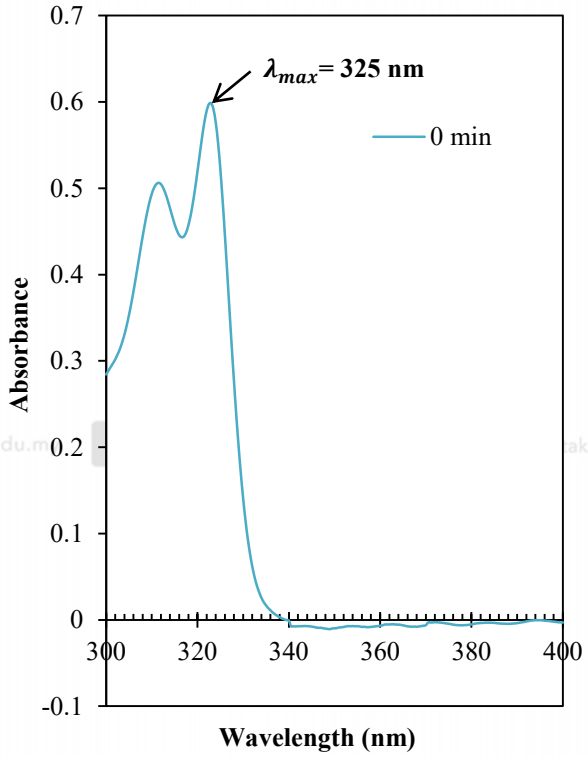
Zou, M., Xiong, F., Ganeshraja, A. S., Feng, X., Wang, C., Thomas, T., et al. (2017). Visible light photocatalysts (Fe, N):TiO_2 from ammonothermally processed, solvothermal self-assembly derived Fe-TiO_2 mesoporous microspheres. *Materials Chemistry and Physics*, *195*, 259-267.

05-4506832 pustaka.upsi.edu.my Perpustakaan Tuanku Bainun Kampus Sultan Abdul Jalil Shah PustakaTBainun ptbupsi

05-4506832 pustaka.upsi.edu.my Perpustakaan Tuanku Bainun Kampus Sultan Abdul Jalil Shah PustakaTBainun ptbupsi

APPENDIX A

UV-Vis absorption spectra of DBT solution at initial time

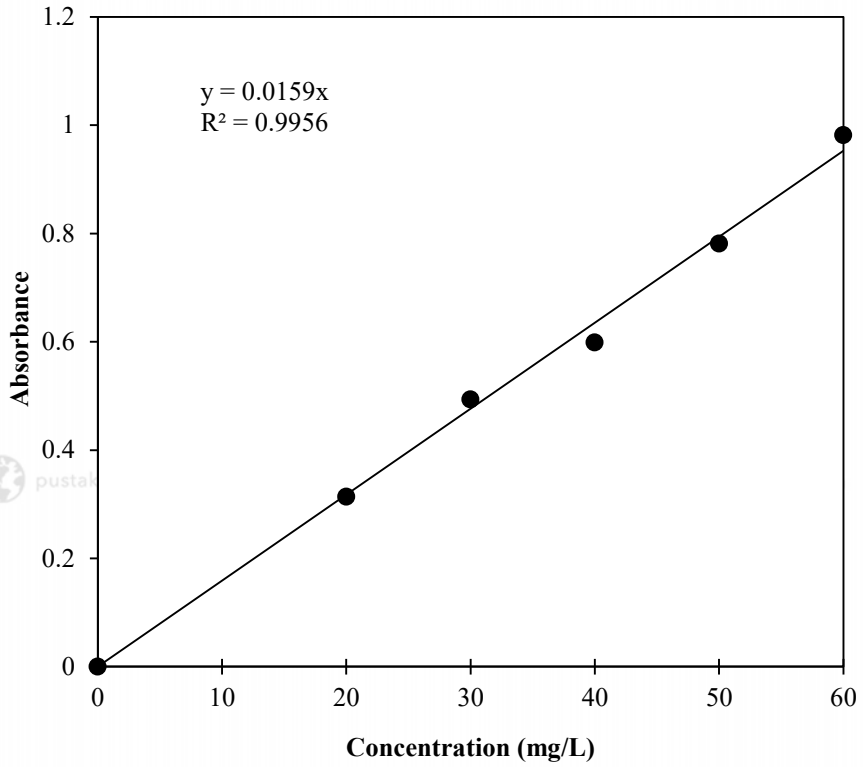


05-4506832 pustaka.upsi.edu.my Perpustakaan Tuanku Bainun Kampus Sultan Abdul Jalil Shah PustakaTBainun ptbupsi

05-4506832 pustaka.upsi.edu.my Perpustakaan Tuanku Bainun Kampus Sultan Abdul Jalil Shah PustakaTBainun ptbupsi

APPENDIX B

Calibration curve of the standard DBT in acetonitrile solution



05-4506832 pustaka.upsi.edu.my Perpustakaan Tuanku Bainun Kampus Sultan Abdul Jalil Shah PustakaTBainun ptbupsi

05-4506832 pustaka.upsi.edu.my Perpustakaan Tuanku Bainun Kampus Sultan Abdul Jalil Shah PustakaTBainun ptbupsi

APPENDIX C

List of Publications

Title	:	Advancement of TiO_2-Based Photocatalyst for Photodegradation of Organic Pollutants in Wastewater
Authors	:	Nurul Adilah Mohd Noor, Siti Munirah Sidik, Mohamad Saufi Rosmi, Che Ku Nor Liana Che Ku Hitam, Nur Farhana Jaafar
Journal	:	*Central Asia & the Caucasus*
Year	:	2022
Status	:	Published

Title	:	Effect of aging time on the formation of Mesoporous Titania Nanoparticles via sol-gel method
Authors	:	Nurul Adilah Mohd Noor, Siti Munirah Sidik, Mohamad Saufi Rosmi, Nur Farhana Jaafar, Norhayati Hashim and Maizatul Najwa Jajuli
Journal	:	*Malaysian Journal of Microscopy*
Year	:	2024
Status	:	Published

05-4506832 pustaka.upsi.edu.my Perpustakaan Tuanku Bainun Kampus Sultan Abdul Jalil Shah PustakaTBainun ptbupsi

05-4506832 pustaka.upsi.edu.my Perpustakaan Tuanku Bainun Kampus Sultan Abdul Jalil Shah PustakaTBainun ptbupsi

APPENDIX D

List of Conferences

Conference	:	International Conference on Science, Technology, Engineering & Mathematics 2021 (ICSTEM2021) in conjunction with 9th International Postgraduate Conference on Science & Mathematics 2021 (IPCSM2021)
Venue	:	Universiti Pendidikan Sultan Idris (UPSI)
Date	:	7 August 2021
Title	:	Improvement of Titania-Based Photocatalyst for Photodegradation of Organic Pollutants in Wastewater
Authors	:	Nurul Adilah Mohd Noor, Siti Munirah Sidik, Mohamad Saufi Rosmi, Che Ku Nor Liana Che Ku Hitam, Nur Farhana Jaafar

Conference	:	International Conference on Research Advancements in Chemistry 2021
Venue	:	National University of Sciences and Technology (NUST)
Date	:	10-11 March 2021

05-4506832 pustaka.upsi.edu.my Perpustakaan Tuanku Bainun Kampus Sultan Abdul Jalil Shah PustakaTBainun ptbupsi


ICSTEM 2021
in conjunction with
9th IPCSM 2021
INTERNATIONAL CONFERENCE ON SCIENCE, TECHNOLOGY, ENGINEERING & MATHEMATICS
9TH INTERNATIONAL POSTGRADUATE CONFERENCE ON SCIENCE & MATHEMATICS
WEBSITE
http://ipcsm2021.upsi.edu.my
FACEBOOK
ICSTEM2021 & IPCSM2021
DATE
7 AUGUST 2021
VIRTUAL PRESENTATION
THEME
EMPOWERING AND TRANSFORMING INNOVATION
DR. WAN MOHD NUZUL HAKIMI W. SALLEH
Chairperson
ICSTEM 2021 in conjunction with 9th IPCSM 2021
7 AUGUST 2021
VIRTUAL PRESENTATION
FACULTY OF SCIENCE AND MATHEMATICS
CERTIFICATE OF PARTICIPATION
This certificate is awarded to
Ms. Nurul Adilah Mohd Noor
as
PRESENTER
in INTERNATIONAL CONFERENCE ON SCIENCE, TECHNOLOGY, ENGINEERING & MATHEMATICS (ICSTEM2021)
in conjunction with
9th INTERNATIONAL POSTGRADUATE CONFERENCE ON SCIENCE & MATHEMATICS 2021 (IPCSM2021)
held on
7 AUGUST 2021



National University of Sciences and Technology

Certificate

This certificate is presented to

NURUL ADILAH BINTI MOHD NOOR

For participating in the first online

International Conference on Research Advancements in Chemistry 2021

Organized by

Department of Chemistry, School of Natural Sciences, NUST, Islamabad, Pakistan

Held on March 10-11, 2021.

Dr. Rashid Farooq	Dr. Azhar Mahmood	Dr. Manzar Sohail	Dr. Adil Mansoor
Chief Patron/Principal,	Patron/	Conference Organizer/	Conference Secretory/
School of Natural Sciences, NUST	Head of Department (Chemistry)	Associate Professor	Assistant Professor